



Universitat
de les Illes Balears

MASTER'S THESIS

SURFACE OCEAN CURRENTS BY USING DRIFTING SEABIRDS IN THE BALEARIC SEA (WESTERN MEDITERRANEAN)

Noemí Calafat Hernández

Master's Degree in Master's in Advanced Physics and Applied

Mathematics

(Specialisation/Pathway *Oceanography*)

Centre for Postgraduate Studies

University of the Balearic Islands

Academic Year 2019-20

SURFACE OCEAN CURRENTS BY USING DRIFTING SEABIRDS IN THE BALEARIC SEA (WESTERN MEDITERRANEAN)

Noemí Calafat Hernández

Master's Thesis

Centre for Postgraduate Studies

University of the Balearic Islands

Academic Year 2019-20

Key words:

Surface ocean currents, Balearic Sea, local wind, animal tracking, mesoscale variability.

Thesis Supervisor's Name Simón Ruiz Valero

Tutor's Name (if applicable) Antonio Sánchez Román

Tutor's Name (if applicable) Romualdo Romero March

Acknowledgments

The seabird fieldwork was conducted by SEO/BirdLife in the frame of Projects Important Bird Areas for seabirds in Spain (LIFE04NAT/ES/00049) and LIFE + INDEMARES. We would like to thank Jose Manuel Arcos for providing us the seabird data and thank all people helping in the fieldwork campaigns used in this study, particularly Beneharo Rodriguez, Juan Becares, Asuncion Ruiz, Santiago Bateman, Javier Blasco, Albert Cama, Raul Escandell, David Garcia, Meritxell Genovart, Marcel Gil, Jose Manuel Igual, Eli Miralles and Blanca Sarzo. We also would like to thank Dr. Giacomo Tavecchia and Dra. Maite Louzano for the fruitful discussions. The study was partially supported by a fellowship from ICTS SOCIB. Altimetry and IBI ocean model data used here were generated, processed and freely distributed by CMEMS ([http:// marine.copernicus.eu](http://marine.copernicus.eu)). The in situ surface buoy data used to validate both the wind product and altimetry data was provided by Puertos del Estado (www.puertos.es). ERA5 are freely produced by the European Center for Medium-Range Weather Forecast (ECMWF).

Contents

1	Introduction	9
1.1	Motivation and background	9
1.2	Surface circulation in the Balearic Sea	10
2	Data	13
2.1	Animal-borne GPS data	13
2.2	Altimetry	14
2.3	Oceanographic buoy	15
2.4	ERA5 atmospheric reanalysis	16
2.5	IBI-MFC numerical ocean model	18
3	Methods	19
3.1	Seabird data	19
3.2	Altimetry and oceanographic buoy data	20
3.3	ERA5 and IBI	20
3.3.1	Interpolation of wind and current data to birds trajectories	21
3.3.2	Statistics parameters	21
4	Results	22
4.1	Validation of local winds and geostrophic surface currents	22
4.2	Case studies. Wind and surface current during seabird campaigns	23
4.2.1	Wind driving examples	24
4.2.2	Sea Surface Current driving examples	29
4.2.3	Wind and Current driving example	33
4.2.4	Other trajectories with no influence of neither, wind or current	37
5	Discussion and Conclusions	40
6	Supplementary Information about all the seabird trajectories	44
	Bibliography	45

List of Figures

1.1	Map of the Balearic Sea study region in the Western Mediterranean Sea, showing the main circulation in the Balearic Sub-basin. Mean locations of the Northern (NC) and Balearic (BC) currents are depicted in solid black line. Inflow to the Balearic Sea and outflow through the Ibiza and Mallorca channels is indicated by dashed arrows. Catalan and Balearic fronts are represented by dots and dashed line respectively (from <i>Ruiz et al. [2009]</i>). Note that there are also outflows towards the Algerian Basin through both channels. Inflow is prevalent but there are also outflows in the Ibiza and Mallorca Channels.	11
2.1	Puffinus Mauretanicus tagged with GPS logger. Figure from [<i>Louzano, 2016</i>]	13
2.2	Altimetry measurement principle	15
2.3	SeaWatch buoy operating schema.	15
2.4	Location of the oceanographic buoys of Valencia (V), Tarragona (T), Cabo de Begur (B) and Dragonera Island (D) from Puertos del Estado in the WMED.	16
2.5	Example of ERA5 reanalysis data assimilation schema.	17
2.6	Area covered by the IBI Service Domain on its native model grid (magenta) and the full native model domain, used to run the simulation (black). Figure from http://resources.marine.copernicus.eu/documents/QUID/CMEMS-IBI-QUID-005-002.pdf	18
3.1	Rafting behaviour (red dots) and foraging trips (blue lines) of each individual seabirds tracked during the three campaigns, according to the criterions described in the text. Gray lines show the 200 m and 500 m isobaths that delimit the continental shelf-slope.	19
3.2	Comparison of seabird tracks and oceanographic buoy data. The bottom left panel displays all the seabird trajectories obtained in the ConiGPS201205 campaign and the location of the Tarragona buoy, whilst the trajectory used to compare with the buoy data (inside the black circle) is displayed in the magenta dotted line. The time series of the magnitude (black line) and direction (green line) of surface wind, surface currents, and wave data collected by the buoy are displayed respectively in the upper, middle and lower panels on the right side. the Magenta line stands for the interpolated seabird data.	20
4.1	Validation of velocity (m/s) and direction (degrees) time series for wind data from ERA5 and Geostrophic currents derived from satellite-altimetry (green lines) with in situ measurements from Valencia’s oceanographic buoy (orange dots).	22
4.2	Surface wind (black arrow), sea surface current (white arrow) and surface temperature field (background colour) corresponding to the median time snapshot of the seabird trajectory ConiGPS201405_29 (pink dots), the beginning of the trajectory is marked with an asterisk. Left: General view; right: zoom on the seabird trajectory zone. The circle on the seabird trajectory of the right panel indicates the moment (May 29 at 01:30 for surface current and temperature fields, and 29 May at 02:00 for wind data) that correspond to wind, current and temperature data plotted in this figure.	24
4.3	The same as Figure 4.2 but for six hourly snapshots: from June 2, at 21:30h to June 3, at 02:20h	25
4.4	Time series of directions (degree) of the original seabird trajectory ConiGPS201405_29, (black line) and the smoothed one (pale-blue line),together with the local wind (red line) and surface current (blue line) data interpolated to the bird positions and time. The orange box indicates the time instant of the Figure 4.2	26

4.5	The same as explained in Figure 4.2, now for this example from ConiGPS201405, trajectory 17, and the surface current, temperature and wind data corresponding to this seabird track analyzed here.	27
4.6	The same as Figure 4.4 but for the ConiGPS201405_17 seabird trajectory.	28
4.7	Hourly snapshots of wind, surface current and surface temperature fields during the ConiGPS201405 trajectory 17. The magenta dotted line stands for the seabird track.	28
4.8	The same as Figure 4.2 but for the seabird trajectory ConiGPS201205_13.	30
4.9	The same as Figure 4.4 but for the seabird trajectory ConiGPS201205_13.	30
4.10	The same as Figure 4.3 but for nine hourly snapshots from trajectory ConiGPS201205_13.	31
4.11	The same as Figure 4.2 but for the seabird trajectory ConiGPS201205_2.	32
4.12	The same as Figure 4.11 but for ten hourly snapshots spanning from May 27 at 30:30h to May 28 at 05:30h	32
4.13	The same as Figure 4.4 but for the ConiGPS201205_2 seabird trajectory.	33
4.14	The same as Figure 4.2 but for the seabird trajectory ConiGPS201405_21.	34
4.15	The same as Figure 4.14 but for five hourly snapshots on May 31 from 01:30h to 05:20h	34
4.16	The same as Figure 4.4 but for the ConiGPS201405_21 seabird trajectory.	35
4.17	The same as Figure 4.2 but for the seabird trajectory ConiGPS201405_27.	36
4.18	The same as Figure 4.4 but for the ConiGPS201405_27 seabird trajectory.	37
4.19	The same as Figure 4.2 but for the seabird trajectory ConiGPS201205_3.	38
4.20	The same as Figure 4.2 but for the seabird trajectory ConiGPS201305_18.	38
4.21	The same as Figure 4.4 but for the ConiGPS201205_3 seabird trajectory.	39
4.22	The same as Figure 4.4 but for the ConiGPS201305_18 seabird trajectory.	39

List of Tables

2.1	Incidence of rafting. Number of tracked birds, tracked birds providing data and time period analysed for the three campaigns conducted in the breeding colony of Sa Conillera included in this study. The number of rafting GPS fixes used in each campaign is also included.	13
2.2	Oceanographic buoy variables used to conduct this study. The time interval (min) and units of the different measurements are provided.	16
4.1	Validation of the ERA5 dataset against the oceanographic buoy data in terms of correlation coefficient, rmse and standard deviation of time series.	23
4.2	The same as Table 4.1 but for the altimetry dataset.	23
4.3	Trajectories analysed from the three campaigns investigated. These trajectories were split into full trajectories and partial trajectories according to the procedure described in the text. The total number of seabird trajectories is also provided.	24
4.4	Statistics for the comparison between the wind and surface currents time series and the ConiGPS201405_29 seabird track. The statistical parameters displayed are: linear correlation coefficient, significance, rmse (degrees), mean and SD of direction (degrees) of both wind and surface currents; and also for the seabird track; and the difference in direction (degrees) of the two former with the latter. .	26
4.5	The same as Table 4.4 but for the Section 1 of the seabird track.	27
4.6	The same as Table 4.4 but for the Section 2 of the seabird track.	27
4.7	The same as Table 4.4 but for the Coni2014GPS-17 seabird track.	29
4.8	The same as Table 4.7 but for the Section 1 of the seabird track.	29
4.9	The same as Table 4.7 but for the Section 2 of the seabird track.	29
4.10	The same as Table 4.7 but for the Section 3 of the seabird track.	29
4.11	The same as 4.4 but for the ConiGPS201405_21 seabird track.	31
4.12	The same as Table 4.4 but for the Coni2012GPS-2 seabird track.	33
4.13	The same as Table 4.4 but for the ConiGPS201405_21 seabird track.	35
4.14	The same as Table 4.4 but for the Coni201405GPS_27 seabird track.	36
5.1	Classification of the seabird trajectories investigated in this work for the three campaigns analysed according to the driving force acting on them. The total numbers are also provided.	41

Chapter 1

Introduction

1.1 Motivation and background

Ocean currents strongly sway marine ecosystems affecting primary production and contribute to determine the ocean spatial distribution of productive areas that concentrate top predators such as fish and birds. These productive areas are known to be associated with mesoscale currents [Ribic *et al.*, 1997].

Nowadays ocean currents can be measured with different instruments, thanks to the latest technological advantages such as the use of remote sensing techniques of satellites, drifters, coastal High-Frequency (HF) radars, Autonomous Underwater Vehicles (AUVs) or Acoustic Doppler Currentmeter Profilers (ADCP) at fix stations or mounted on vessels. On the other hand, models help us to understand how our oceans behave providing objective tools. A numerical ocean prediction model is a simulation tool based on mathematical equations and numerical calculations to evaluate and understand, among others, the dynamics of physical processes in the marine environment. Operational models simulate the daily state of the ocean (e.g. temperature, salinity, currents, etc) at global and regional scales (see for instance, Copernicus Marine Environmental Monitoring Services (CMEMS) portal <http://marine.copernicus.eu/>), for public and private users.

There is a continuous effort to assess and improve the ocean currents from models (Mason *et al.*, 2019) that have allowed to provide a good representation of the large scale ocean currents. However, at meso and submesoscale (spatial scales of 1-100 km; time scales from few days to several months), models still need further validation with in situ measurements and/or remote sensing data to improve forecast.

A common way to measure the near-surface ocean currents in the last century, has been the use of satellite-tracked drifters with a 15-m drogue [Lumpkin and Pazos, 2007]. However, we have also learnt that all drifters (with and without drogue) are affected by the direct wind and surface waves, so they can not be precise perfect Lagrangian instruments. One of the principal physical aspect to investigate in relation with the effect of winds on drifters is the wind-driven Ekman currents [Poulain *et al.*, 2009] that produce a theoretical change of the current direction in the water column. Other physical aspect is the direct action of wind and waves on the surface parts of the drifter, inducing a relative motion with respect the water that is referred to as slippage.

In this context, the present study uses precision global positioning system (GPS) tracking dataset of Puffinus Mauretanicus (Balearic shearwater) while resting at the sea surface (i.e. it can be considered as a surface drifter), as an innovative way to measure ocean currents in areas where is difficult to have in-situ data (e.g. coastal and shelf zones). During rafting, while the individuals are settled on the sea surface, they act as a passive drifters that are carried by ocean surface currents, geostrophic and ageostrophic flows [Sánchez-Román *et al.*, 2019]. The latter are driven by direct stress imparted by the local wind (i.e. Ekman and/or Stokes drifts), as shown by [Yoda *et al.*, 2014]. These authors used individuals of the species Calonectris leucomelas as Lagrangian instruments acting like drifting buoys to investigate the Oyashio - Tsugaru Warm Current near Japan. They compared currents estimated by seabird drift movements with ocean surface currents derived from satellite data and in-situ observations. They proved that animal-borne data can be an advantageous tool to deduce ocean surface currents. This fact was recently proved by [Sánchez-Román *et al.*, 2019] in the Western Mediterranean Sea

(WMED) by analysing the rafting behaviour of individuals of the species *Calonectris diomedea* in the Balearic Sea.

This master's thesis aims to investigate the relationships between seabirds rafting and ocean surface currents in the Balearic Sea. Previous studies in this area and in other areas of the global ocean have shown qualitative analysis of the surface currents derived from bird's trajectories. A novel contribution of this Master work is the extensive statistic analysis performed to assess the influence of winds and currents on surface ocean velocities estimated from seabird drifting.

Results contribute to improve our knowledge on the surface circulation in coastal areas using GPS tracking data set of seabirds. Moreover, understanding relationships between seabirds rafting and ocean currents may yield further information for the conservation of marine ecosystems, for defining protected areas at sea and efficient management of ecosystem-based fisheries [Carter *et al.*, 2016].

The document is organized as follows, first a short description of the surface circulation in the Balearic Sea is given for people who are not familiar with the dominant ocean surface currents and oceanographic conditions of the study area. Chapter 2 describes the data used in this master's while chapter 3 is devoted to methods, results are presented in chapter 4. Discussion and concluding remarks are presented in chapter 5 and finally, future work is given in chapter 6. An annex with additional information is included at the end of the document.

1.2 Surface circulation in the Balearic Sea

The Balearic Basin, relatively shallow at < 2500 m, is a wide region of the WMED located in between the Liguro-Provençal Basin in the north and the Algerian Basin in the south [García *et al.*, 1994]. It is bounded by the northern slopes of the Balearic Islands, and the Valencian and Catalan slopes. Zonal exchange of water between the basin and the adjacent Liguro-Provençal Basin takes place through the open eastern margin, while meridional exchange is mediated by the island channels [Pinot *et al.*, 2002; Testor *et al.*, 2005; Heslop *et al.*, 2012]. The Algerian Basin to the south is deeper (>2500 m), bigger and less restricted than the Balearic Basin [Mason and Pascual, 2013].

The cyclonic circulation pattern within the Balearic Basin is mainly density driven, and strongly constrained by steep bottom topography [Pinot *et al.*, 1999]. The Northern Corrent (NC) enters the domain from the east along the Liguro-Provençal slope. It presents a marked seasonal variability being stronger in winter and weaker in spring-summertime [Castellón *et al.*, 1990; Pinot *et al.*, 2002; Birol *et al.*, 2010; Poulain *et al.*, 2012].

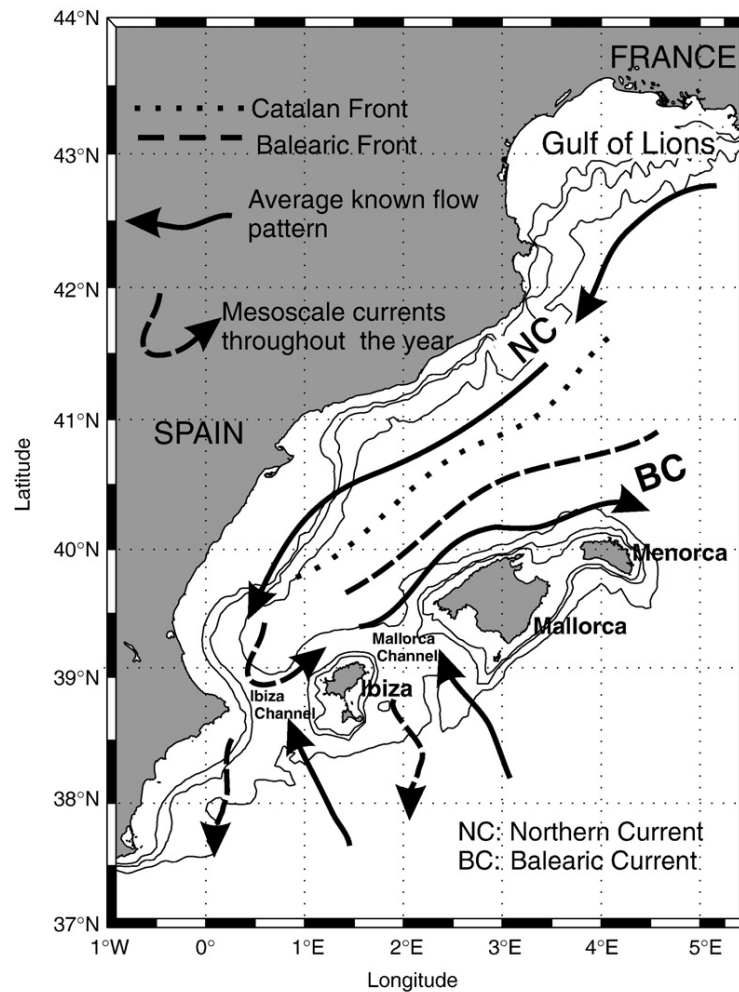


Figure 1.1: Map of the Balearic Sea study region in the Western Mediterranean Sea, showing the main circulation in the Balearic Sub-basin. Mean locations of the Northern (NC) and Balearic (BC) currents are depicted in solid black line. Inflow to the Balearic Sea and outflow through the Ibiza and Mallorca channels is indicated by dashed arrows. Catalan and Balearic fronts are represented by dots and dashed line respectively (from Ruiz *et al.* [2009]). Note that there are also outflows towards the Algerian Basin through both channels. Inflow is prevalent but there are also outflows in the Ibiza and Mallorca Channels.

The NC is associated with a slope front known as the Catalan front, which is mainly marked by a change in salinity. It separates boundary (lighter) and interior (denser and older) varieties of the so-called old Atlantic Water (AW) with salinity of around 38 [Font *et al.*, 1988], which enters the domain from the Gulf of Lions to the north and is found throughout the Balearic Basin. [Mason and Pascual, 2013]; see Fig. 1.1. The NC flows along the Iberian Peninsula slope, with a mean surface velocity of about 20 cm/s. The Catalan Front intersects the seabed at depths of nearly 400 m and intersects the surface at 15 - 20 Km of the shelf break [García *et al.*, 1994] being discernible offshore of the Catalan coast to as far south as 41°N [LaViolette, 1990].

At the Ibiza channel, characteristic NC modes have been identified, [Pinot *et al.*, 1999, 2002; Heslop *et al.*, 2012] that can be associated with Western Intermediate Water (WIW) presence or absence. When is present, these waters temporarily block the channel, forcing the NC eastward to feed into the Balearic Current (BC), which flows along the northern insular slope. In the absence of WIW, the NC continues southward through the channel [Pinot *et al.*, 2002; Monserrat *et al.*, 2008].

The BC is associated with a frontal region, known as the Balearic Front, that marks the division between the old Modified Atlantic Water (MAW), located in the center of the Balearic Basin, and the lighter recent MAW flowing from the south through the Balearic channels [García *et al.*, 1994]. Its vertical structure reveals a frontal zone well defined in the surface layer [Ruiz *et al.*, 2009], with isolines bending to the horizontal on the southern side of the front at depths of 100 - 150 m [Font *et al.*, 1988]. The salinity gradient across the Balearic front has

been implicated in mesoscale eddy generation within the basin [Bouffard *et al.*, 2012].

On the other hand, wind stress patterns over the WMED are strongly influenced by the episodic Mistral and Tramuntana winds, with the Gulf of Lions having the highest probability of high wind speeds (> 10 m/s in the Mediterranean sea [Jansa, 1987; Zecchetto and De Biasio, 2007; Chronis *et al.*, 2011]). In the adjacent Balearic Sea, winds are less intense and more variable, with slight dominance of westerly winds in winter and spring, easterly winds in summer, and easterly/northeasterly winds in autumn [Dorman *et al.*, 1995; Palomares Losada, 2001; Chronis *et al.*, 2011]. The differing wind stress characteristics between the Balearic Sea and the Gulf of Lions lead to the generation of significant anticyclonic wind stress curl over the eastern part of the Balearic Sea.

Chapter 2

Data

2.1 Animal-borne GPS data

Puffinus Mauretanicus is an endemic seabird of the Mediterranean Sea, it breeds in the Balearic Islands, but in its displacements can reach the Atlantic and the Cantabrian, either to the Bay of Biscay or further north, or to north-west Africa. It is a strictly marine specie and outside the colonies remains mostly on the continental shelf. The Balearic shearwater is characterized by having an average body length of 34 - 38 cm and an average wingspan of 83 - 93 cm [Ruffino *et al.*, 2008]. This specie feeds in water near the archipelagos or in the shallow waters on the continental shelf of the Mediterranean margins.

GPS data used in this work comes from seabirds tagged in the frame of INDEMARES project, between end of May and beginning of June for years 2012, 2013 and 2014. A total of 63 birds were fitted with GPS loggers to monitor their foraging trips, see Table 2.1. Adult birds were captured when they flew back to the colony. GPS loggers were attached to the back plumage using Tesa tape.



Figure 2.1: *Puffinus Mauretanicus* tagged with GPS logger. Figure from [Louzano, 2016]

Breeding colony: Sa Conillera. Lon: 1° 12' 38". Lat: 38° 58' 58"				
CAMPAING	Traked birds	Traked birds providing data	No. GPS fixes (rafting)	Period analized
ConiGPS201205	21	7	812	25/05 - 03/06 2012
ConiGPS201305	13	9	935	23/05 - 30/05 2013
ConiGPS201405	12	8	2274	26/05 - 07/06 2014
TOTAL	63	32	4437	

Table 2.1: Incidence of rafting. Number of tracked birds, tracked birds providing data and time period analysed for the three campaigns conducted in the breeding colony of Sa Conillera included in this study. The number of rafting GPS fixes used in each campaign is also included.

Birds were recaptured two weeks after fixing GPS to take out the loggers and recover the data. No sign of damage was shown in any individual after release, and any birds that were not caught would lose the device within a few weeks due to moulting. 32 of those tracked birds were providing data during the three campaigns Fig: 3.1. Most of them located near Ibiza and the northeast coast of the Iberian Peninsula. The loggers were programmed to obtain a GPS position every 5 minutes for all the campaigns. Although it was not the original aim of the field campaigns, taking advantage of the information collected in this fieldwork, like in [Sánchez-

[Román *et al.*, 2019]. It was possible to evaluate the tracks when seabirds are settled on the sea surface and act as drifting buoys driven by local winds, sea surface currents or both.

2.2 Altimetry

Satellite altimetry has been providing accurate measurements of sea surface height (SSH) for the last 28 years. The altimetric satellites determine the height of the ocean surface with respect to a reference ellipsoid. Estimations of the Sea Level Anomaly (SLA) are obtained subtracting a SSH reference mean (based on the time period 1993-2019). Fig. 2.2 sketches the altimetry measurement principle: an altimeter is an active radar that sends a microwave pulse towards the ocean surface. A very precise on-board clock measures the return time of the pulse from which the distance or range between the satellite and the sea surface is derived. The range precision is a few centimeters for a distance of 800 to 1300 km [Le Traon, 2013].

Altimeter missions provide along-track 1 Hz measurements every 7 km along repetitive tracks. Since the satellite usually repeats over exactly the same ground track pattern every cycle, it observes the same geoid signal and the dynamic topography, which is time varying. This allows a precise estimation of the sea level or dynamic topography anomaly even if the geoid is not known [Le Traon, 2013]. Gridded SLA data, obtained from the along-track measurements, are commonly used for, among others, assimilation into models, signal analysis or comparison with in situ measurements [Le Traon *et al.*, 1998].

In this work, Absolute Dynamic Topography (ADT) obtained from the SSALTO/DUACS multi-mission (Saral, Cryosat-2, Jason-3 and Sentinel - 3A) specific reprocessed gridded merged product (level 4) for the Mediterranean Sea is used. ADT is computed as the sum of the SLA measured by the satellite and a Mean Dynamic Topography (MDT) [Rio *et al.*, 2014]. The MDT represents the stationary component of the ocean dynamic topography and describes the long-term average circulation [Aulicino *et al.*, 2017]. The ADT product is available in the website of the Copernicus Marine Environment Monitoring Service (CMEMS), <http://marine.copernicus.eu>. A comprehensive description of SSALTO/DUACS multi-mission processing is given in [Pujol, 2013; Pujol *et al.*, 2016; Taburet *et al.*, 2019].

The spatial resolution of the dataset is $1/8 \times 1/8$ degree and the time period used in this work spans from May 2012 - 2014. Data are available on a daily basis.

The precise knowledge of the ocean's MDT is a fundamental point for a number of oceanographic applications and may be calculated as the filtered difference between an altimeter mean sea surface and a geoid model [Rio *et al.*, 2014]. Sea surface variability can be accurately characterized from satellite altimetry and this approach provides surface geostrophic velocity at large spatial scales [Pascual *et al.*, 2013]. Geostrophic velocity (u_g, v_g) is obtained as:

$$u_g = \frac{-g}{f} \frac{\partial H}{\partial y}; v_g = \frac{g}{f} \frac{\partial H}{\partial x} \quad (2.1)$$

where g is the gravitational acceleration, f the local Coriolis parameter and H is the sea surface height derived from altimetry.

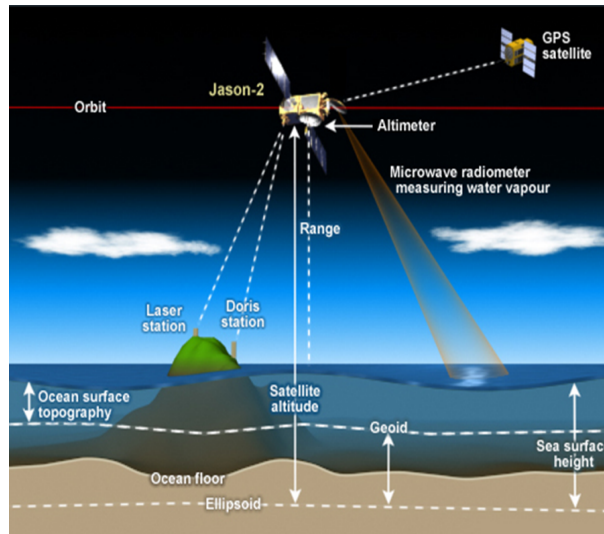


Figure 2.2: Altimetry measurement principle

Daily altimetry data was used to compare with seabird trajectories, so it was first identified and separate the available seabird data corresponding to each day for campaign. Trajectories obtained from seabird drifts were then compared with altimetry data (ADT, u_g and v_g and) to establish relationships between the seabird drift data and the sea surface geostrophic currents. [Sánchez-Román *et al.*, 2019].

2.3 Oceanographic buoy

These buoys are oceanographic devices floating on the sea surface and anchored to the seabed which collect ocean and weather data, measuring temperature, salinity, wind and current velocity, sea level or air pressure, among others, depending on the sensors arranged on the buoy.

Oceanographic buoy data used in this study come from four devices deployed by Puertos del Estado (PE) in the study area. PE is a public body under the Ministry of Public Works of Spain, with global responsibilities over the entire state-owned port system. PE has developed and maintains systems for measuring and forecasting the marine environment, like REDEX. The data set used here consists in measurements from the deep buoys network, Red de Boyas profundas (Red Exterior) <http://www.puertos.es/es-es/oceanografia/Paginas/portus.aspx>.

These buoys are characterized by being anchored away from the coastline, so that the wave measurements of these sensors are not disturbed by local effects, providing representative observations of large coastal areas.

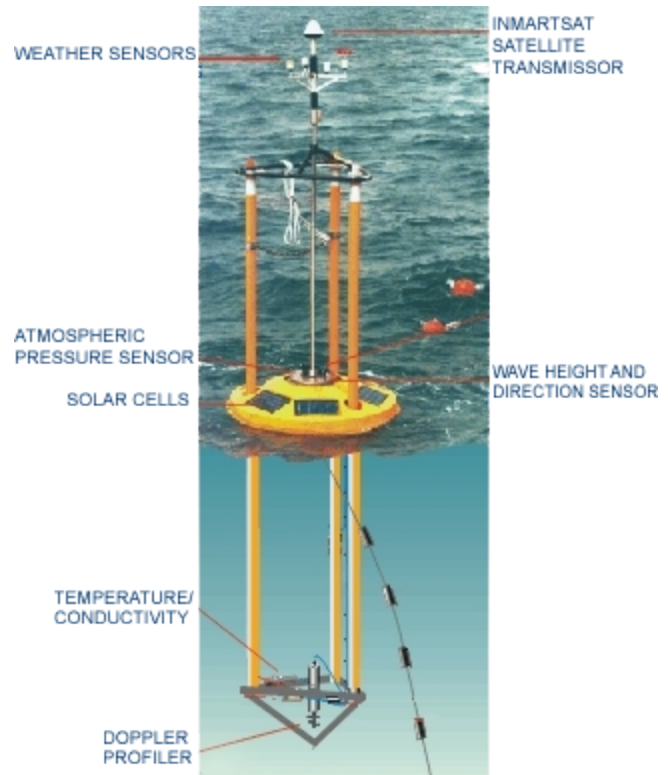


Figure 2.3: SeaWatch buoy operating schema.

Red Exterior network has two types of buoys depending on the measurements performed: Wavescan (waves

Oceanographic buoy data by Puertos del Estado			
Data	Variable	Time interval*	Units
Wave	Spectral Significant Height	26 min	m
	Average direction	26 min	Degrees (0=N,90=E)
Wind	Average velocity	10 min	m/s
	Average direction	10 min	Degrees (0=N,90=E)
Current	Average velocity	10 min	cm/s
	Average direction	10 min	Degrees (0=N,90=E)

Table 2.2: Oceanographic buoy variables used to conduct this study. The time interval (min) and units of the different measurements are provided.

and atmospheric variables) and SeaWatch (waves, atmospheric and oceanographic parameters. The buoys selected for this work are SeaWatch buoys Fig. 2.3 located in the WMED: Tarragona, Valencia, Cabo Begur and Dragonera island, see Fig. 2.4, providing averaged hourly data from measurements of wind and current every 10 minutes, and wave data collected with a time interval of 26 minutes. The variables chosen to conduct this study are shown in Table. 2.2.

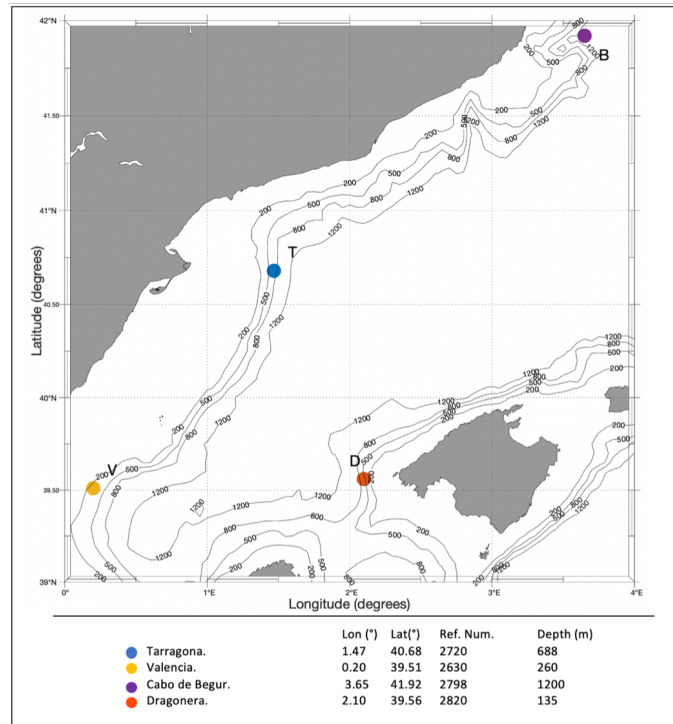


Figure 2.4: Location of the oceanographic buoys of Valencia (V), Tarragona (T), Cabo de Begur (B) and Dragonera Island (D) from Puertos del Estado in the WMED.

2.4 ERA5 atmospheric reanalysis

A few decades ago, almost all ocean wind measurements came from merchant ships. Nowadays, operational numerical weather prediction (NWP) based on models also gives wind information [Liu and Xie, 2014]. Models are essential tools for studying atmospheric and ocean processes. Model simulations are typically driven by external data from meteorological reanalysis or operational forecast [Hoffmann et al., 2019]. Reanalysis is a method for developing a large register of how weather and climate change over time. Observations and a numerical model that simulates one or more aspects of the Earth system are combined to estimate the state of the system. Reanalysis products are used in climate research and services, including for monitoring and comparing current climate conditions, identifying the causes of climate variations and change, and preparing climate predictions [Carton and Giese, 2008].

Data assimilation for numerical weather prediction

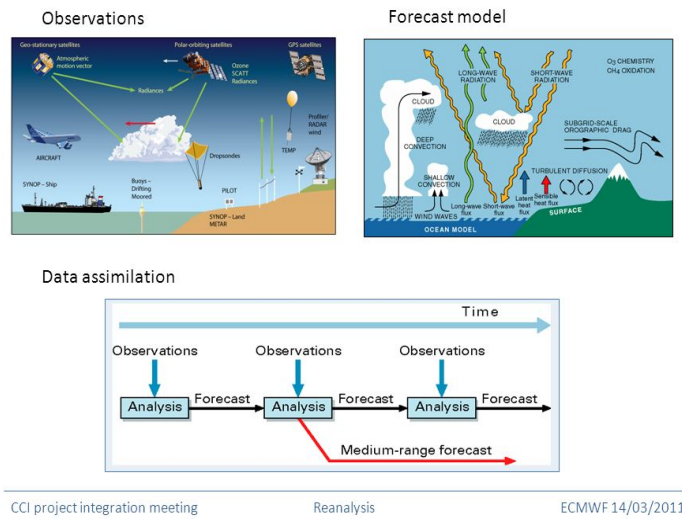


Figure 2.5: Example of ERA5 reanalysis data assimilation schema.

ERA5 is the last version available at the time climate reanalysis produced by the European Center for Medium-Range Weather Forecast (ECMWF). It combines a weather model with historical observations from satellites and ground sensors. Many ocean models in marine forecasting centers use ECMWF-based wind inputs for ocean forcing. ERA5 was produced using 4D-Var data assimilation of ECMWF’s Integrated Forecast System (IFS), with 137 hybrid sigma/pressure (model) levels in the vertical, with the top level at 0.01 hPa. This dataset covers the period from 1979 to a few months before the present and provides hourly estimates of many atmospheric, land and ocean climate parameters. Data is available in the Climate Data Store (<https://cds.climate.copernicus.eu/>) and also at the ECMWF webpage <https://www.ecmwf.int/en/forecasts/datasets/reanalysis-datasets/era5>. on regular latitude-longitude grids at $0.25^\circ \times 0.25^\circ$ spatial resolution, with atmospheric parameters interpolated to 37 pressure levels.

ERA winds are characterized by extreme mean zonal winds (westerlies) with too feeble mean poleward flows in the middle latitudes and too-weak mean meridional winds (trades) in the tropics. ERA stress curl is too cyclonic in middle and high latitudes, with implications for Ekman upwelling estimates. It is conjectured that large-scale mean wind biases in ERA are related to their lack of high-frequency (transient wind) variability, which should be promoting residual meridional circulations in the Ferrel and Hadley cells. Surface wind data from ERA5 is used in this work to estimate the effect of wind on seabird trajectories.

On the other hand, this product was used to compute the wind stress (not shown). The aim is to have an accurate estimation of the influence of surface winds in ocean surface currents. Ocean surface wind stress and the associates heat and momentum fluxes play an important role in driving surface and deep ocean circulation. Surface wind stress adjusts the amount of energy available for the ocean gyres in terms of Ekman transport and pumping, ocean stirring by vertical turbulent mixing and deep convection responses [Belmonte Rivas and Stoffelen, 2019].

Wind-induced stress drives ocean surface current as ageostrophic component. Stress affects directly the turbulent transfer of heat, moisture and gases between the ocean and the atmosphere. Ocean surface stress, τ , is the turbulent transfer of momentum generated by atmospheric instability caused both by wind shear (difference between wind and current) and buoyancy (vertical density stratification resulting from temperature and humidity gradients) [Liu and Xie, 2014].

2.5 IBI-MFC numerical ocean model

The Iberia Biscay Irish Monitoring Forecasting Centre (IBI MFC) provides an operational marine monitoring and forecasting service for the European Atlantic cover (the Iberia-Biscay-Ireland zone). Its principal task bases on efficient operation of an accurate marine service and the production of high quality products (delivered by CMEMS in [http:// marine.copernicus.eu](http://marine.copernicus.eu)).

Monthly, daily and hourly ocean fields for surface variables, such as temperature, salinity, sea level and currents, are given by IBI Ocean Reanalysis system. IBI system is based on NEMO3.6 model and includes data assimilation. Observations (altimeter data, in situ temperature and salinity vertical profiles and satellite sea surface temperature) are used to estimate the initial conditions for numerical ocean forecasting. This product is a L4 processing level, with a spatial resolution of $0.0083^\circ \times 0.0083^\circ$, time coverage from 1992 to 2018, and vertical coverage of 50 levels (from -500 to 0).

Find additional details in the Quality information document, available at

<http://resources.marine.copernicus.eu/documents/QUID/CMEMS-IBI-QUID-005-002.pdf>.

In this work, Sea Surface Temperature (SST) and surface velocity current (hourly data) from IBI was used to analyse current direction from U (zonal) and V (meridional) components; and to compare with seabird trajectories while resting at the sea surface. Mesoscale structures such as eddies, fronts and filaments reproduced by the IBI model can influence such trajectories.

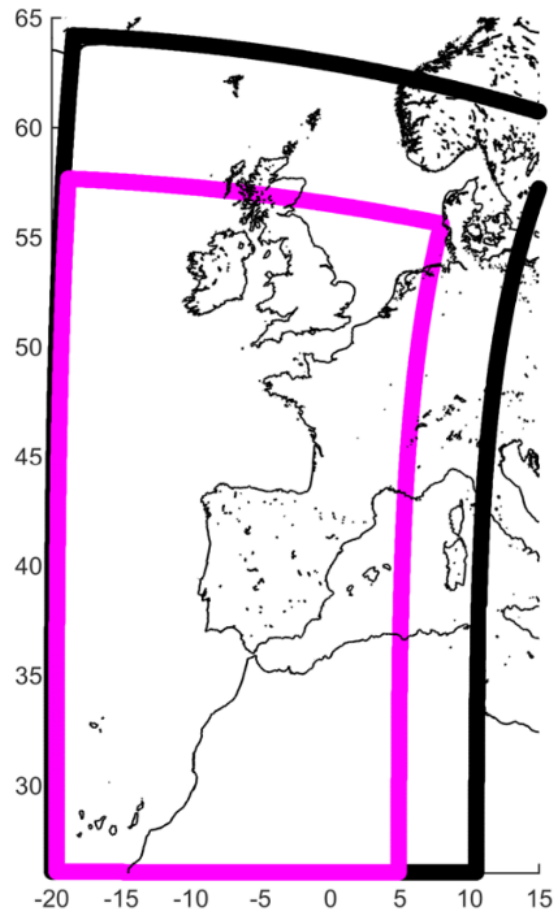


Figure 2.6: Area covered by the IBI Service Domain on its native model grid (magenta) and the full native model domain, used to run the simulation (black). Figure from <http://resources.marine.copernicus.eu/documents/QUID/CMEMS-IBI-QUID-005-002.pdf>

Chapter 3

Methods

This Chapter provides an explanation of the data processing and methods used in this study, including animal-borne GPS data.

3.1 Seabird data

As mentioned in the previous chapter, GPS fixes from seabirds are obtained every 5 minutes, so firstly distances between contiguous fixes were computed. Then the birds ground speed and distance to the colonies were estimated.

The criteria used here to identify the rafting behaviour of shearwaters has been described by [Louzao *et al.*, 2009]. According to this criterion, rafting is defined as two or more consecutive GPS fixes under a speed threshold of 0.5 m/s, when birds are likely to be resting at the sea surface. To avoid spurious data collected when seabirds return to their colony, an additional selection criterion was imposed: only data collected at least 5 km away from the colony was used.

Longer rafting duration per trip provide more complete datasets for the purposes of mesoscale current pattern detection; therefore, all resting trajectories shorter than 3 hours (36 consecutive GPS fixes) were removed. In this way, the tracks analysed here were long enough to properly compare with local sea surface velocity mesoscale patterns and wind fields in order to assess the driving forces of the seabird trajectories in the Balearic Sea. These criteria have been applied following the methodology described in [Sánchez-Román *et al.*, 2019].

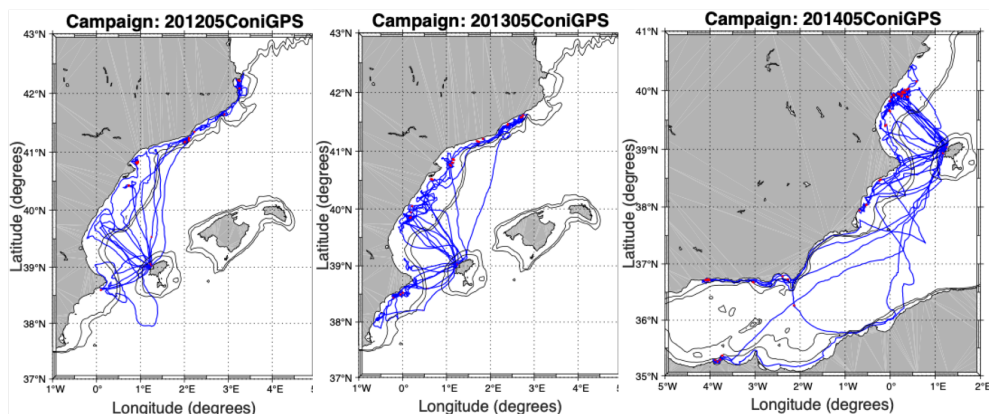


Figure 3.1: Rafting behaviour (red dots) and foraging trips (blue lines) of each individual seabirds tracked during the three campaigns, according to the criteria described in the text. Gray lines show the 200 m and 500 m isobaths that delimit the continental shelf-slope.

The variables taken from GPS animal-borne are position (longitude and latitude) from each GPS fix, time and velocity from the trajectories that fulfill all the criteria. Finally, a total sample of 60 Balearic Shearwater drift trajectories were used to estimate surface currents in the Balearic Sea.

3.2 Altimetry and oceanographic buoy data

Daily altimetry data provides a general context of the geostrophic circulation in the vicinity of the bird tracks, however it has not enough spatial and temporal resolution to compare with the higher temporal resolution of bird tracks data. Moreover, after selection of bird trajectories, most of them are located near the coast, where altimetric data are absent or of low quality, so the potential comparison with altimetry data is significantly reduced. To overcome this limitation of altimetry, IBI model is considered in the data analysis. Altimetry information is therefore incorporated in the analysis through its assimilation in the model.

Concerning the comparison with oceanographic buoy data, the first step was to calculate the distance between each trajectory to the four oceanographic buoy positions, see Fig: 2.3, then select the trajectories with a radius of one degree from each buoy, so as to compare them to the nearest one. Once this criterion is applied, the number of samples (drifting trajectories) decreases considerably to a total of 37 paths, just over half of all the trajectories. If a shorter distance criterion were used, the number of samples decreases so much that would no longer be significant in terms of number of selected trajectories.

The next step was to collocate in time buoy and trajectories data, this is, to find the corresponding buoy data of the same time as the seabirds were drifting at the sea surface. Finally, the buoy measurements were compared with each bird trajectory to analyse the role of the surface currents and wind on the birds tracks.

After that, data described in Tab:2.2 from each oceanographic buoy was compared with the trajectories near to them. Fig: 3.2 shows an example of this comparison by displaying, on the left side: all the trajectories from ConiGPS201205 campaign, within one degree of distance to the buoy (down left) indicating the trajectory that is being analysed (magenta dotted line). On the right side, time series of velocity, direction and spectral significant height from buoy data, corresponding to the time period of all campaigns, are shown.

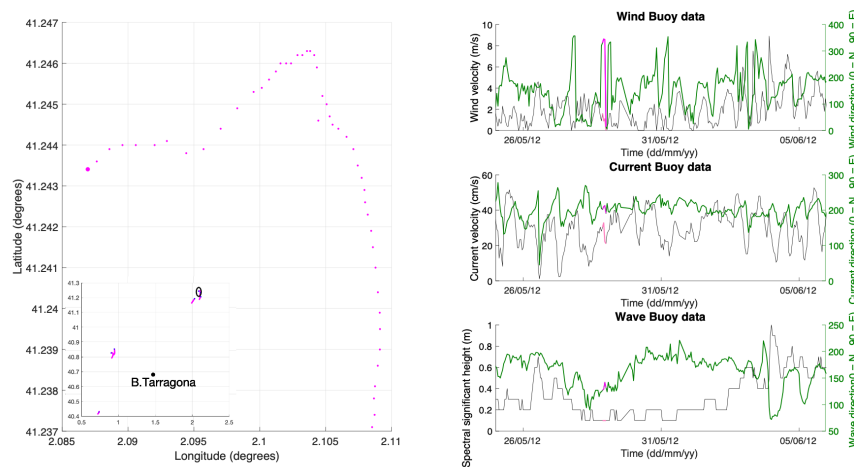


Figure 3.2: Comparison of seabird tracks and oceanographic buoy data. The bottom left panel displays all the seabird trajectories obtained in the ConiGPS201205 campaign and the location of the Tarragona buoy, whilst the trajectory used to compare with the buoy data (inside the black circle) is displayed in the magenta dotted line. The time series of the magnitude (black line) and direction (green line) of surface wind, surface currents, and wave data collected by the buoy are displayed respectively in the upper, middle and lower panels on the right side. The Magenta line stands for the interpolated seabird data.

3.3 ERA5 and IBI

Hourly data from ERA5 and IBI have been used as follows: first, they are interpolated in time and space to the position of every fix of the trajectory under consideration. Then, once the interpolation was computed, the direction of each bird's trajectory and the direction, either wind or current, were calculated from its velocity components.

The following section is dedicated to better explain the interpolation of wind and current data from ERA5 and IBI models.

3.3.1 Interpolation of wind and current data to birds trajectories

A linear interpolation method is used¹, so the interpolated value at a given point is based on values at neighboring grid points in each respective dimension. The scheme used for the three dimension interpolation considers time and position (longitude and latitude) of the variables. Routine `interp3` interpolates to find the zonal and meridional components of wind or current, of the underlying 3-D function at the given points in longitude, latitude and time arrays.

3.3.2 Statistics parameters

In order to complement the analysis of the influence of wind (ERA5) and surface current (IBI) products on the trajectories of the seabirds, a set of statistical parameters are estimated for all the campaigns: linear correlation coefficient (R), P value, root mean square error (RMSE), mean, standard deviation (SD) and difference between the product (wind or current) and bird directions.

A brief explanation of the statistic parameters, estimated using matlab functions is given below.

Correlation coefficient and P-value: This function returns the matrices of correlation coefficients and p-values for testing the hypothesis that there is no relationship between the observed phenomena (null hypothesis). If an off-diagonal element of P is smaller than the significance level (default is 0.05), then the corresponding correlation in R is considered significant.

Root Mean Square Error: Is the standard deviation of the residuals errors. Residuals are a measure of how far from the regression line data points are. RMSE is a measure of how spread out these residuals are, it tells you how concentrated the data is around the line of best fit.

Mean: The arithmetic mean, also called the mathematical expectation or average, is the central value of a discrete set of numbers: specifically, the sum of the values divided by the number of values.

Standard Deviation: Is the square root of the variance, a measure of the amount of variation or dispersion of a set of values. A low SD indicates that the values tend to be close to the mean (also called the expected value) of the set, while a high standard deviation indicates that the values are spread out over a wider range.

Due to the errors in data from the products, or the lack of data near the coast, the statistical analysis could be affected by incomplete data series. To avoid that, data series analysed must keep the condition of not having absent values (NaN). Thus, the results presented in the next chapter were obtained by considering only the cases in which data are not absent in both products (wind and current).

A low-pass Butterworth filter, with a cut-off frequency of $1/100 \text{ min}^{-1}$ and a pass-band of $1/200 \text{ min}^{-1}$, was applied in order to filter-out high-frequency variability of seabird trajectories.

¹Interp3 routine from Matlab

Chapter 4

Results

4.1 Validation of local winds and geostrophic surface currents

Before conducting the comparison of seabird drift trajectories with both, local wind patterns and sea surface geostrophic currents, the wind product and altimetry data were validated. Altimetry observations have been assimilated in the IBI model so it was not necessary to validate the IBI product. The objective was to obtain reliable spatial patterns. To do that, the methodology described in [Sánchez-Román *et al.*, 2019] has been followed, using in-situ current and wind data from the oceanographic buoys of Valencia, Tarragona, and Dragonera collected during the campaign, see Appendix. The oceanographic buoy of Cabo Begur was not considered due to its abnormal functioning during this period.

Wind and current fields were interpolated to the position and time of the in-situ measurements. Then, correlation coefficient and RMSE for both altimetry and wind product data were computed with respect to the in-situ observations. Fig. 4.1 displays an example of the comparison between wind speed and direction from ERA5 and also surface current velocity and direction from altimetry with wind data and total currents measured by the Valencia buoy, located at 39.52° N 0.21° E. In-situ wind velocities collected by this buoy show daily fluctuations, with maximum values larger than 11 m/s. Wind speed from ERA5 presents a similar temporal pattern, tending to give higher values, see Fig. 4.1.

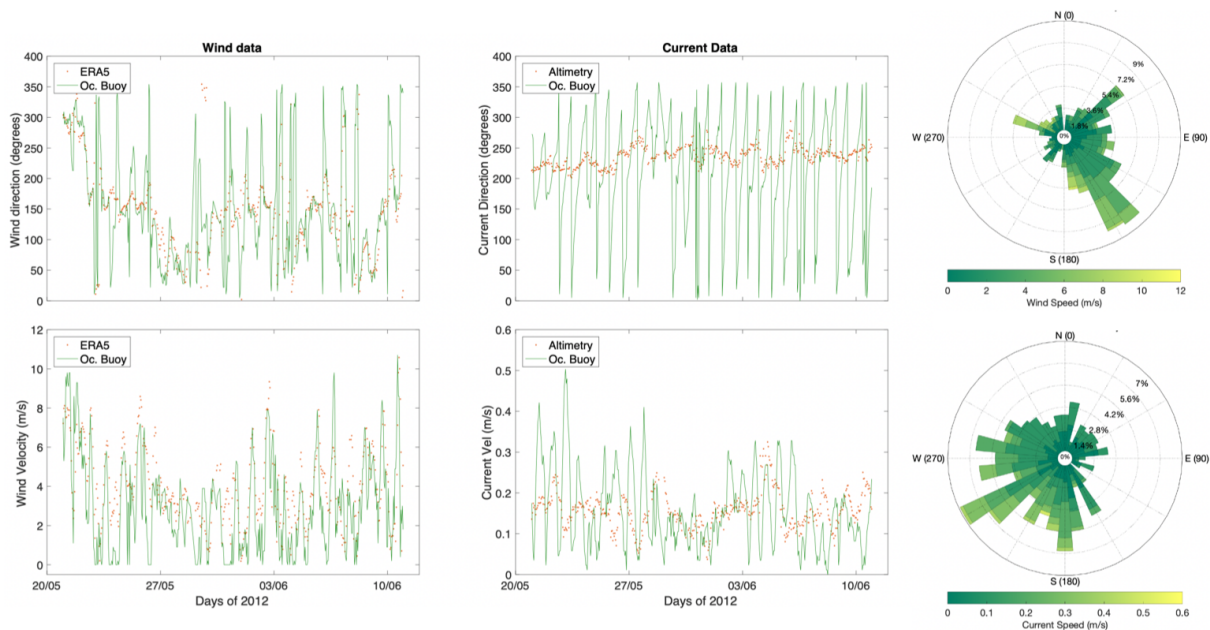


Figure 4.1: Validation of velocity (m/s) and direction (degrees) time series for wind data from ERA5 and Geostrophic currents derived from satellite-altimetry (green lines) with in situ measurements from Valencia's oceanographic buoy (orange dots).

As a consequence, the wind product has a standard deviation of 2.02 m/s, a bit lower than that obtained for the in-situ measurements (2.45 m/s). Furthermore, the spatial resolution of the wind product ($0.25^\circ \times 0.25^\circ$) means that the wind variability is also degraded, this translating into larger discrepancies with the in-situ buoy measurements, see [Table 4.1](#). These factors also apply to the wind direction comparison.

	Velocity (m/s)	Direction (degrees)
Corr.Coef	0,67	0,48
RMSE	2,10	84,13
SD_BUOY	2,45	91,29
SD_ERA5	2,02	70,57

Table 4.1: Validation of the ERA5 dataset against the oceanographic buoy data in terms of correlation coefficient, rmse and standard deviation of time series.

In-situ winds mainly blew from the south-east (approximately ranging between 130 and 155 degrees). Directions of the wind product match with the in-situ wind measurements showing origins ranging between 180 and 285 degrees. Thus, winds at the sea surface flew mainly from the south south-west, see wind rose [Fig: 4.1](#) on the right side. As a result, see [Table 4.1](#), the RMSE obtained for the wind speed (direction) is 2.10 m/s (84.13 degrees). The correlation coefficients are 0.67 and 0.48, respectively. Moreover, the SD of the in-situ direction measurements is 91.29 degrees, whilst for the wind product is 70.57 degrees, thus indicating a more dispersion for the buoy measurements with respect to the ERA5 product.

	Velocity (m/s)	Direction (degrees)
Corr.Coef	0,92	0,34
RMSE	0,11	96,58
SD_BUOY	0,09	91,84
SD_ALT	0,05	15,69

Table 4.2: The same as [Table 4.1](#) but for the altimetry dataset.

Overall, satellite derived geostrophic currents present lower values than those reported by the in-situ velocities. It is due to the oceanographic buoys measuring the ageostrophic components of the velocity field that are not measured by altimetry. [Table 4.2](#) summarizes the results. RMSE obtained for the current velocity and direction is lower than that found for the wind validation: 0.11 m/s and 96.58 degrees, respectively. The correlation coefficients are 0.92 and 0.34, respectively. The SD obtained for velocities from both datasets (oceanographic buoy and altimetry) are 0.09 m/s and 0.05 m/s respectively while directions show a SD of 91.84 degrees for in-situ measurements and 15.69 degrees for altimetry, this highlighting again more dispersion for the former with respect to the latter, see [Tab:4.2](#). According to Sanchez-Roman et al., (2019), this is due to the high-frequency variability of the surface currents which is captured by the buoy (hourly interval measurement), whilst these fluctuations are not observed in the geostrophic currents derived from altimetry since they are obtained from daily data.

4.2 Case studies. Wind and surface current during seabird campaigns

In this section the wind and surface current conditions are analysed to evaluate their effects on the seabird trajectories and classify them according to the driving forces. As described in the previous chapter, the approach followed is based on the analysis of wind and currents maps together with an additional statistical analysis, which refines the classification of bird trajectories and complements the qualitative qualification approach followed in [[Sánchez-Román et al., 2019](#)]. As was aforementioned, 60 drifting seabird trajectories are available (see [Tab:4.3](#)). A selection of these trajectories and analysis are presented in this section while the rest of results have been included in [Appendix](#).

Some considerations should be stated for the sake of clarity:

- In general, only one map of wind speed and surface current vectors is showed, corresponding to the mean time snapshot of the duration of each bird trajectory.
- In some cases, where wind and currents showed higher variability, a set of 6 hourly maps are displayed together with the bird trajectory.
- Some bird trajectories were split in 2 o 3 partial tracks to better assess the driving forces acting on retrieved seabird tracks.

Campaigns	Trajectories analysed	full trajectories	partial trajectories
ConiGPS201205	13	5	8
ConiGPS201305	18	10	8
ConiGPS201405	29	11	18
Total	60	26	34

Table 4.3: Trajectories analysed from the three campaigns investigated. These trajectories were split into full trajectories and partial trajectories according to the procedure described in the text. The total number of seabird trajectories is also provided.

Table 4.3 summarizes the final classification of the 60 trajectories investigated in this work. They can be split into 39 partial trajectories due to changes in direction of the trajectory and 21 full trajectories.

Some examples of trajectories driven by surface wind, current, both or other forces, are provided hereunder.

4.2.1 Wind driving examples

Campaign ConiGPS201405 Trajectory 29

The first example, see Fig. 4.2, represents a seabird trajectory driven by the local wind. This trajectory consists of 67 GPS fix points, time elapse of five hours and a half, from 02 June at 21:19:13 to 03 June at 02:42:36 of an individual while resting at the sea surface as a drifter.

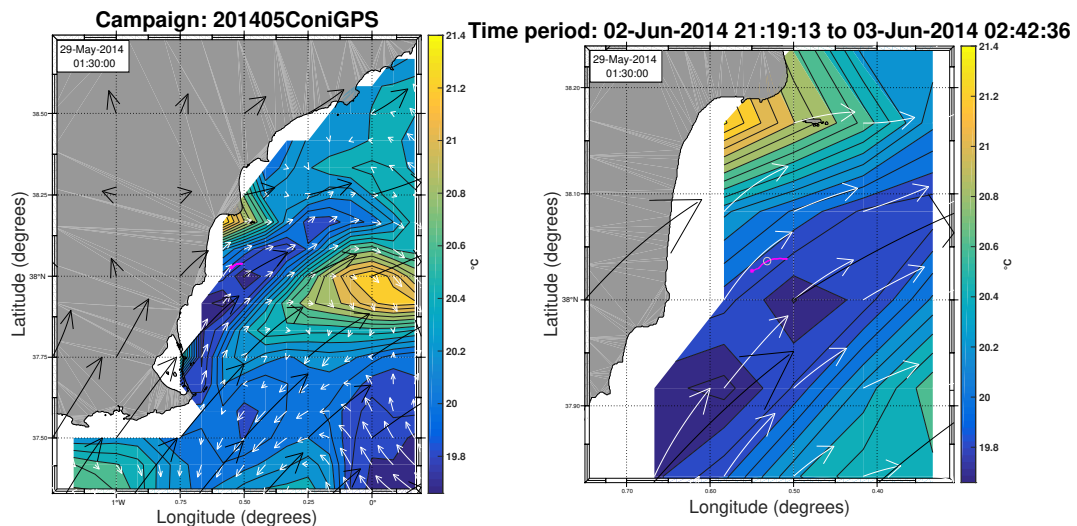


Figure 4.2: Surface wind (black arrow), sea surface current (white arrow) and surface temperature field (background colour) corresponding to the median time snapshot of the seabird trajectory ConiGPS201405_29 (pink dots), the beginning of the trajectory is marked with an asterisk. Left: General view; right: zoom on the seabird trajectory zone. The circle on the seabird trajectory of the right panel indicates the moment (May 29 at 01:30 for surface current and temperature fields, and 29 May at 02:00 for wind data) that correspond to wind, current and temperature data plotted in this figure.

Current and SST data represented in Fig. 4.2 correspond to the snapshot 01:30:00 am whilst wind data corresponds to 02:00:00 am.

At first sight, from maps of this figure it could state that the seabird track is driven by both the local wind and surface current. However, taking a look at the six hourly snapshots of this trajectory shown in Fig. 4.3, it reveals that the surface current was flowing towards the east south-east during the first three hours of the seabird track and then shifted towards the north-east. On the contrary, persistent south-west winds flowed during the whole seabird drift driving this individual towards the north-east. This fact can be observed in Fig. 4.4 that shows the time series of directions of the original seabird trajectory (black line) and the smoothed one (pale-blue line), together with the local wind (red line) and surface current (blue line) data interpolated to the bird positions and time. The orange box indicates the time instant of Fig. 4.2.

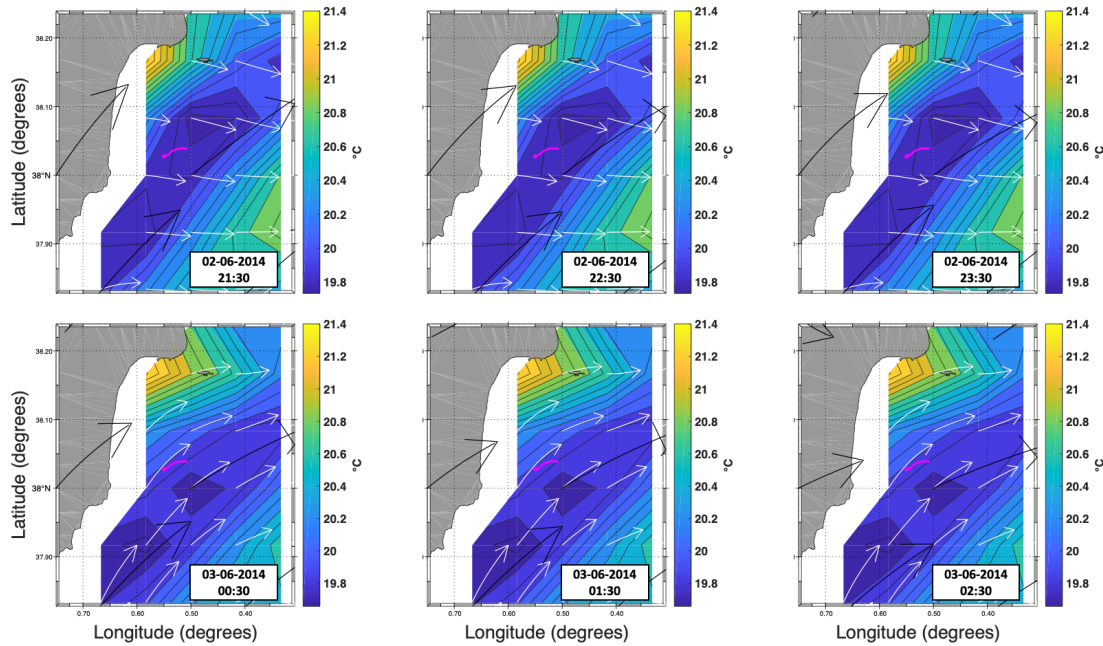


Figure 4.3: The same as Figure 4.2 but for six hourly snapshots: from June 2, at 21:30h to June 3, at 02:20h

Fig. 4.4 depicts that wind and bird directions present a similar behaviour, while sea surface current shifts drastically from almost 100 degrees to 60 degrees. The statistics for this seabird trajectory shown in Tab. 4.4 confirm the aforementioned related to the driving force acting on this seabird track. The correlation coefficient between wind and seabird time series is 0.90 (significant at the 95% confidence level). The RMSE between both time series is 16.85 degrees whilst the mean direction of the seabird is 13.91 degrees larger than that obtained for the local wind, that is, almost 14 degrees towards the east. This fact is in accordance with the angles reported by Poulain *et al.* [2009, 2012] for drogue-less drifters in the Mediterranean Sea.

	R	p-value	RMSE	mean	std	mean_B	std_B	dif
Wind	0.90	6.66e-25	16.85	64.10	4.99	78.00	13.85	13.91
Current	-0.90	1.04e-25	31.31	79.11	18.43	78.00	13.85	1.11

Table 4.4: Statistics for the comparison between the wind and surface currents time series and the ConiGPS201405_29 seabird track. The statistical parameters displayed are: linear correlation coefficient, significance, rmse (degrees), mean and SD of direction (degrees) of both wind and surface currents; and also for the seabird track; and the difference in direction (degrees) of the two former with the latter.

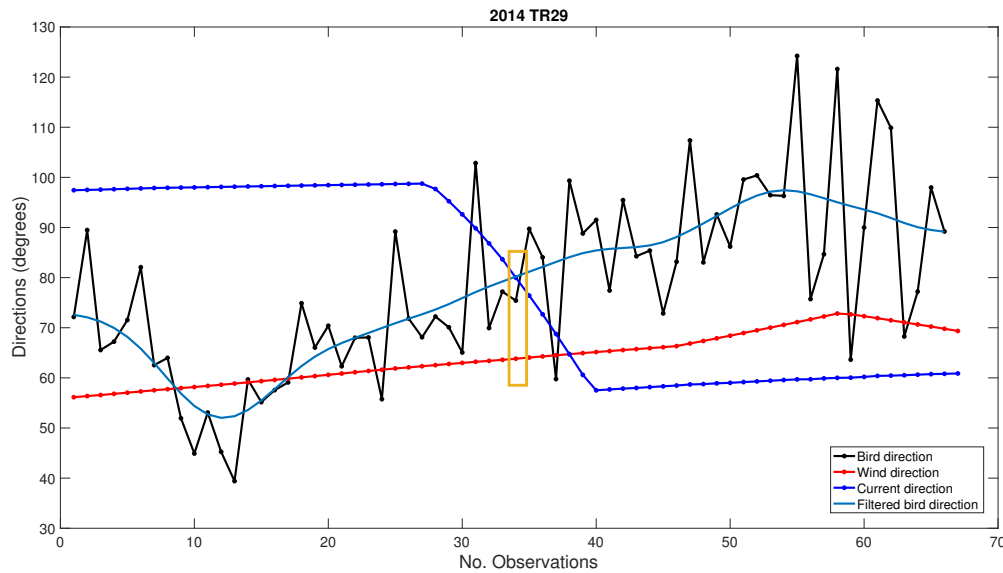


Figure 4.4: Time series of directions (degree) of the original seabird trajectory ConiGPS201405_29, (black line) and the smoothed one (pale-blue line), together with the local wind (red line) and surface current (blue line) data interpolated to the bird positions and time. The orange box indicates the time instant of the Figure 4.2

On the other hand, the statistics computed for the sea surface current time series [Tab: 4.4](#) exhibit a negative correlation with the seabird track, this indicating an opposite behaviour in time. Actually, seabird track direction hardly rotates in a clockwise sense whereas the surface current remains almost stable and suddenly rotates in an anti-clockwise sense to become stable again. The RMSE between both datasets is 31.31 degrees, the mean direction of the individual is 78.00 degrees. The difference between the mean direction of the surface current interpolated data and the mean direction of the seabird is 1.12 degrees.

Due to the slight discrepancy between the qualitative analysis done it from interpreting [Fig: 4.3](#) and the difference obtained for the statistical analysis comparing surface current and seabird directions for the whole trajectory, it was decided to analyse this track as a partial trajectory and calculate the statistical parameters for each one. The first part of the trajectory consists of the first three hours of the track; the second part, the other three hours.

[Tab:4.5](#) shows the statistical parameters for the first part of this track, with a correlation coefficient between wind and seabird direction of 0.40 while the correlation coefficient for current and bird direction is -0.43, this indicates a negligible effect of the current over the seabird trajectory.

The two correlation coefficient results are significant at 95% confident level, with a p-value of 0.02 for wind and 0.01 for current comparison. RMSE and difference between wind and seabird direction are 8.96 and 5.54 respectively, revealing that direction of the seabird and wind during this first part of the trajectory are quite similar. Whilst, RMSE (33.52) and differences (32.41) between surface current and seabird direction, for this first part of the track, reveal that surface current are not affecting as the wind does. Differences between surface current and seabird track directions larger than 30 degrees are obtained, this strongly limits the effects of the current driving force over the seabird trajectory.

For the second part of the track, [Tab:4.6](#) still shows a strong influence of wind over the seabird drift with a correlation coefficient of 0.89, a RMSE of 21.38 degrees and difference of 21.11 degrees. The statistical results

between surface current and seabird direction for this section also reveal that the influence of surface wind was stronger than current with a negative correlation coefficient of -0.74. Here, RMSE (28.89) and difference (25.52) results were similar to those found for the comparison with wind, approximately 30 degrees. This means that they are almost at the edge of exercising an influence on the seabird trajectory.

Section 1	R	p-value	RMSE	mean	std	mean_B	std_B	dif
Wind	0.41	0.02	8.955	59.65	2.17	65.20	7.75	5.54
Current	-0.43	0.01	33.52	97.60	1.85	65.20	7.75	32.41

Table 4.5: The same as Table 4.4 but for the Section 1 of the seabird track.

Section 2	R	p-value	RMSE	mean	std	mean_B	std_B	dif
Wind	0.89	5.22e-13	21.38	67.90	3.17	89.10	5.90	21.11
Current	-0.74	3.21e-07	28.89	63.49	8.78	89.10	5.90	25.53

Table 4.6: The same as Table 4.4 but for the Section 2 of the seabird track.

Campaign ConiGPS201405 Trajectory 17

This second example presented in Fig. 4.5), consists on 113 GPS fixes, almost nine and a half hours, from 26 of May 2014 at 18:04:00 to 27 of May 2014 at 03:38:18. Sea surface current and temperature data plotted in Fig. 4.5 correspond to May 26 2014 at 23:30 while surface wind data correspond to May 27 2014 at 00:00 .

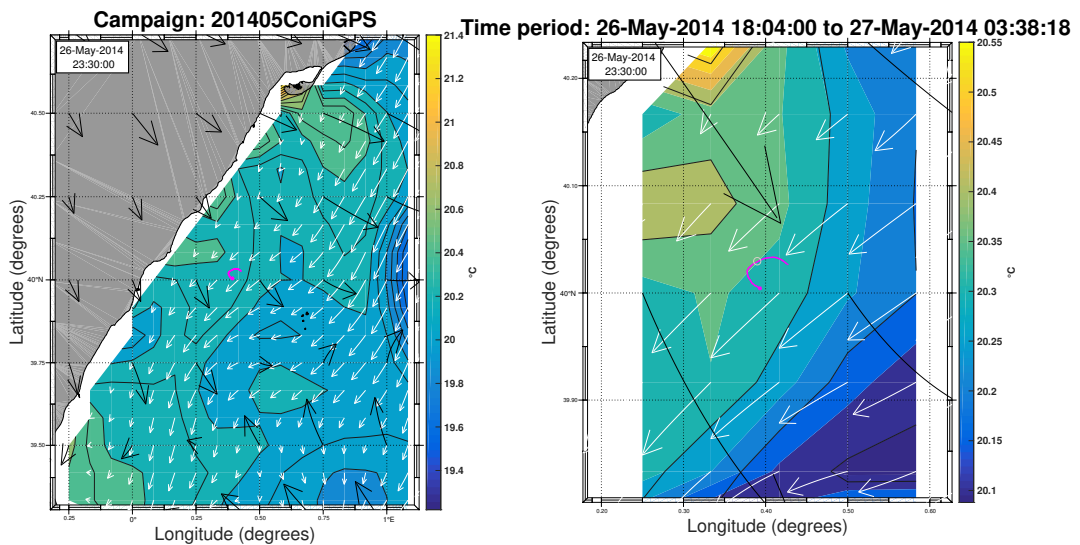


Figure 4.5: The same as explained in Figure 4.2, now for this example from ConiGPS201405, trajectory 17, and the surface current, temperature and wind data corresponding to this seabird track analyzed here.

Fig. 4.6 shows significant changes in the direction of wind, surface current and seabird trajectory. The overall pattern of the change in direction of the wind and seabird trajectory is quite similar, so it was proceeded to analyse the maps corresponding to each time laps of wind and current data, see Fig. 4.7.

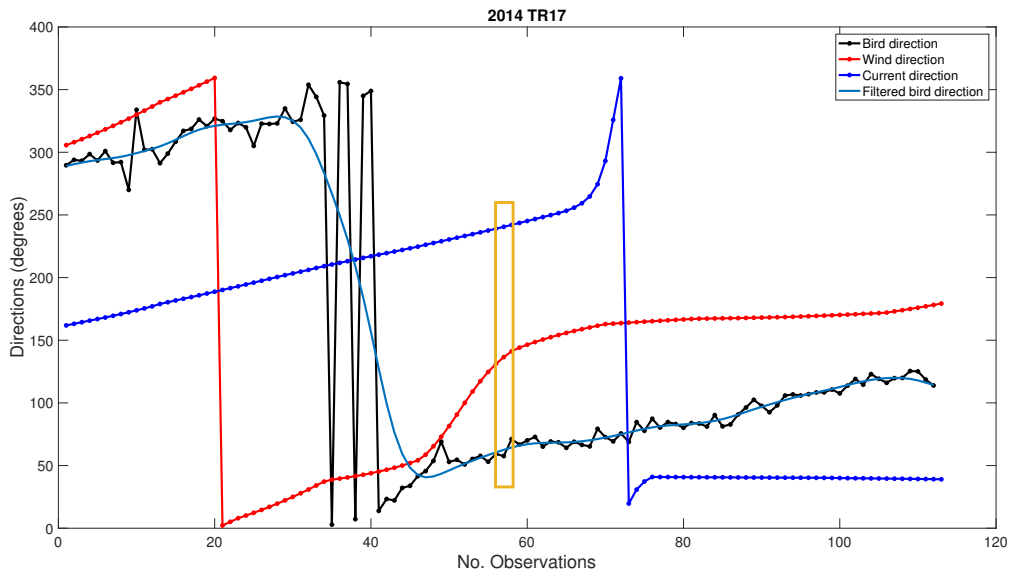


Figure 4.6: The same as Figure 4.4 but for the ConiGPS201405_17 seabird trajectory.

Each panel in Fig. 4.7 shows the corresponding snapshot of hourly wind and current data for the duration of the seabird drift. There were two more snapshots added, in order to better understand the wind and current patterns for this example.

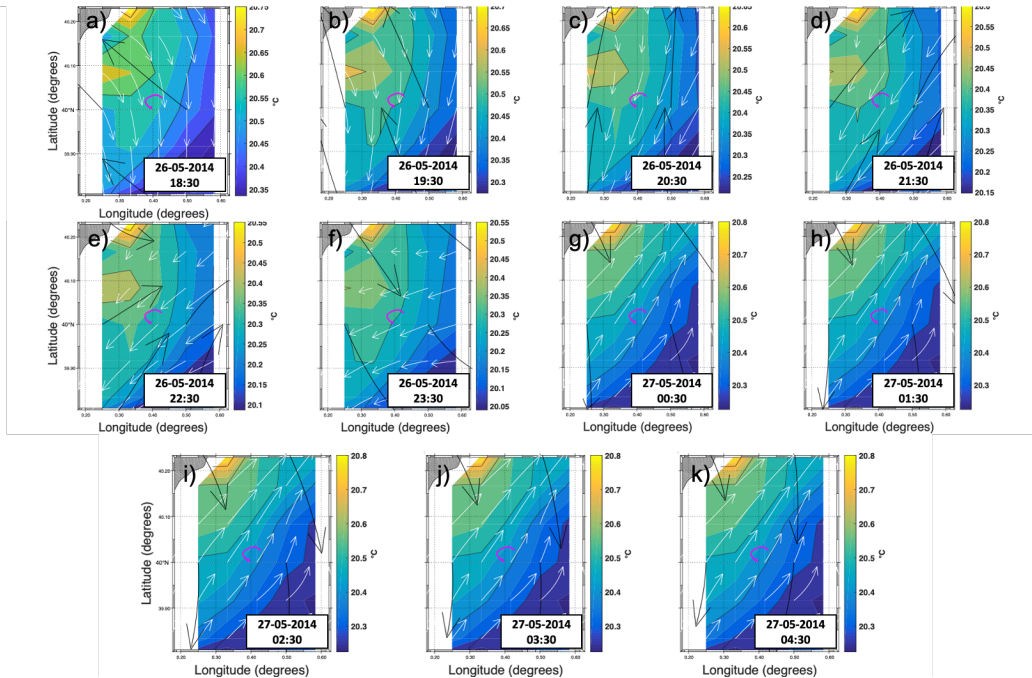


Figure 4.7: Hourly snapshots of wind, surface current and surface temperature fields during the ConiGPS201405 trajectory 17. The magenta dotted line stands for the seabird track.

A qualitative assessment suggests that wind is influencing the entire path described by the bird. To confirm this fact, the statistical analysis has been done for the full trajectory (see Tab: 4.7 and Tab: 4.7) and for partial sections. In this case study, the trajectory was divided in three sections.

	R	p-value	RMSE	mean	std	mean_B	std_B	dif
Wind	0.22	0.02	127.61	157.38	98.96	159.61	106.04	2.24
Current	0.17	0.08	126.67	152.32	89.69	159.61	106.04	7.29

Table 4.7: The same as Table 4.4 but for the Coni2014GPS-17 seabird track.

Section 1	R	p-value	RMSE	mean	std	mean_B	std_B	dif
Wind	0.20	0.02	190.25	175.52	155.27	291.34	46.58	115.83
Current	-0.45	0.00	115.58	190.14	17.25	291.34	46.58	101.21

Table 4.8: The same as Table 4.7 but for the Section 1 of the seabird track.

Section 2	R	p-value	RMSE	mean	std	mean_B	std_B	dif
Wind	0.16	0.04	69.55	118.65	44.35	64.99	16.88	53.65
Current	-0.07	0.07	180.47	234.06	60.62	64.99	16.88	169.06

Table 4.9: The same as Table 4.7 but for the Section 2 of the seabird track.

Section 3	R	p-value	RMSE	mean	std	mean_B	std_B	dif
Wind	0.86	3.88e-12	69.72	169.38	3.31	100.69	14.82	68.68
Current	0.04	0.09	62.55	39.88	1.64	100.69	14.82	60.81

Table 4.10: The same as Table 4.7 but for the Section 3 of the seabird track.

For the first section, [Tab: 4.8](#), the correlation Coefficient between wind and seabird direction is 0.20, with a RMSE of 190.25 (degrees) and with a difference of 115.83 degrees, while between surface current and seabird, the correlation coefficient is -0.45, the RMSE and difference are 115.58 and 101.21 degrees. These results reveal that the surface wind is driving the seabird trajectory.

For the second section, [Tab: 4.9](#) shows the Correlation coefficient, RMSE and difference between surface wind and seabird directions, that are 0.16, 69.55 and 53.65, respectively. For the comparison between surface current and seabird direction, the correlation coefficient is -0.72, whilst the RMSE is 180.47 and the difference in direction 169.06 degrees. These results also reveal the influence of wind on the seabird drift.

Finally, for the third section, the statistical outcomes demonstrate that surface wind is affecting to this section of the seabird trajectory, see [Tab: 4.10](#). The correlation coefficient, RMSE and difference between wind and seabird direction are 0.86, 69.72 degrees and 68.69 degrees, respectively; while for surface current are 0.04, 62.55 degrees and 60.81 degrees.

4.2.2 Sea Surface Current driving examples

Following the same methodology, the next examples represent two trajectories driven by sea surface currents.

Campaign ConiGPS201205 Trajectory 13

The trajectory shown in [Fig: 4.8](#) is an example of a trajectory driven by surface currents. It consists on 100 GPS fixes, approximately 8h of this seabird drifting on the sea surface, that starts on May 27 at 21:03:18 until May 28 at 05:17:08.

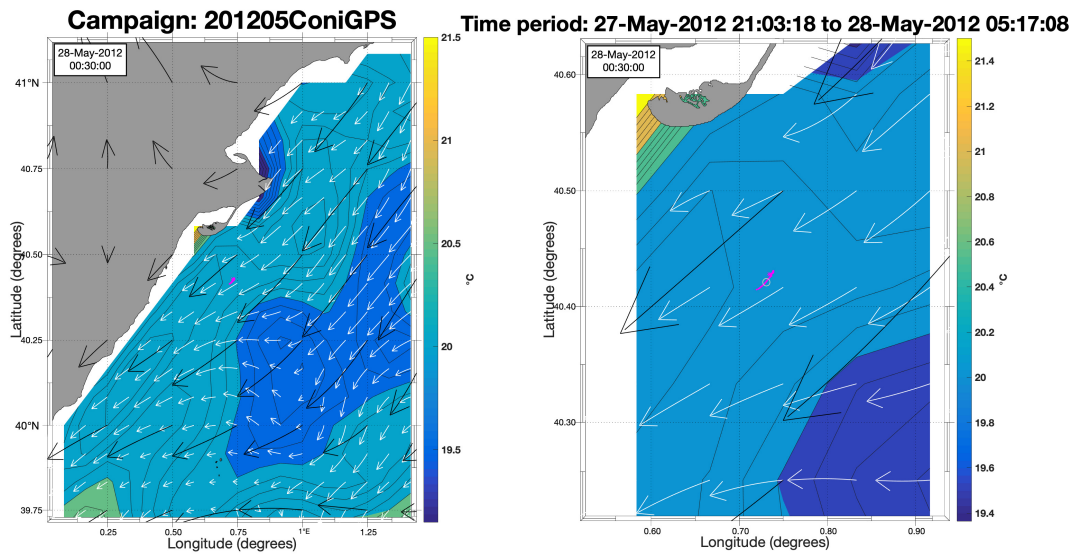


Figure 4.8: The same as Figure 4.2 but for the seabird trajectory ConiGPS201205_13.

In Fig: 4.8, data from IBI (sea surface current and temperature) correspond to 00:30 whilst wind data from ERA5, to 01:00.

As seen in Fig: 4.8, the direction of this seabird trajectory follows a roughly straight line, even at the beginning that shows some chaotic path, so this trajectory is analysed as a full trajectory. Fig: 4.9 shows that surface current direction is slightly more than 150 degrees, constant during the first 30 GPS fixes of the seabird trajectory, then changes to 250 degrees until the end of the track. Wind direction gradually changes in an anti-clockwise sense towards the south-west from near 300 to 200 degrees.

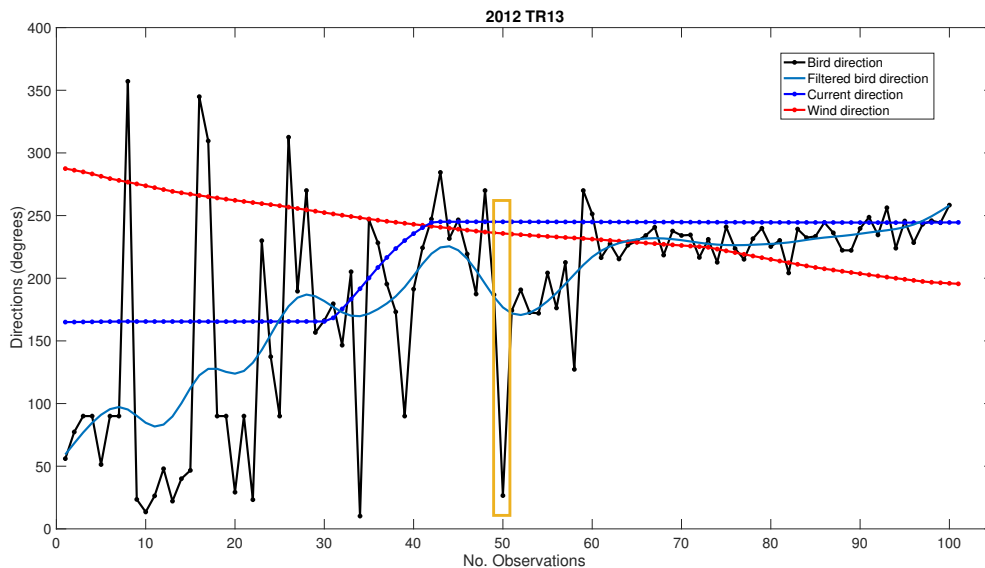


Figure 4.9: The same as Figure 4.4 but for the seabird trajectory ConiGPS201205_13.

As a consequence of the aforementioned behaviour, nine hourly snapshots corresponding to this example were produced, see Fig: 4.10.

	R	p-value	RMSE	mean	std	mean_B	std_B	dif
Wind	-0.92	8.93e-43	91.74	238.02	24.59	186.69	53.12	51.33
Current	0.85	5.12e-30	41.51	216.75	36.59	186.69	53.12	30.05

Table 4.11: The same as 4.4 but for the ConiGPS201405_21 seabird track.

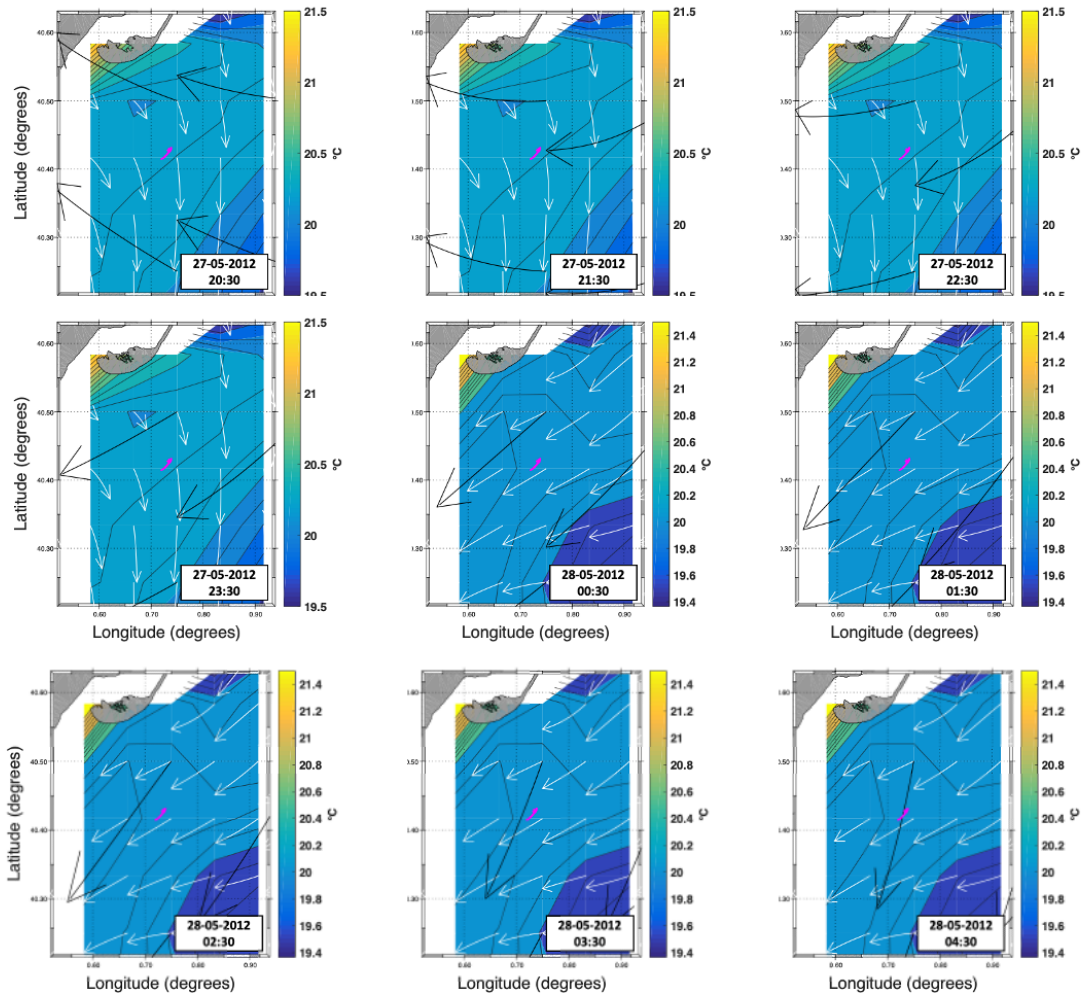


Figure 4.10: The same as Figure 4.3 but for nine hourly snapshots from trajectory ConiGPS201205_13.

Fig: 4.10 shows the aforementioned changes and reinforce what Fig: 4.9 reveals; that is: sea surface current seems to follow the same direction as the seabird especially from the shift of direction of the former.

Campaign ConiGPS201205 Trajectory 2

Fig: 4.11 displays other example of a seabird trajectory driven by sea surface current. It consists of 96 GPS fix points, 8 hours drifting trajectory, from 27 May 2012 at 20:52:22 to 28 May 2012 at 05:04:36. Temperature and current data represented in Fig: 4.11 correspond to 28 May at 01:30 and wind data to that day at 02:00.

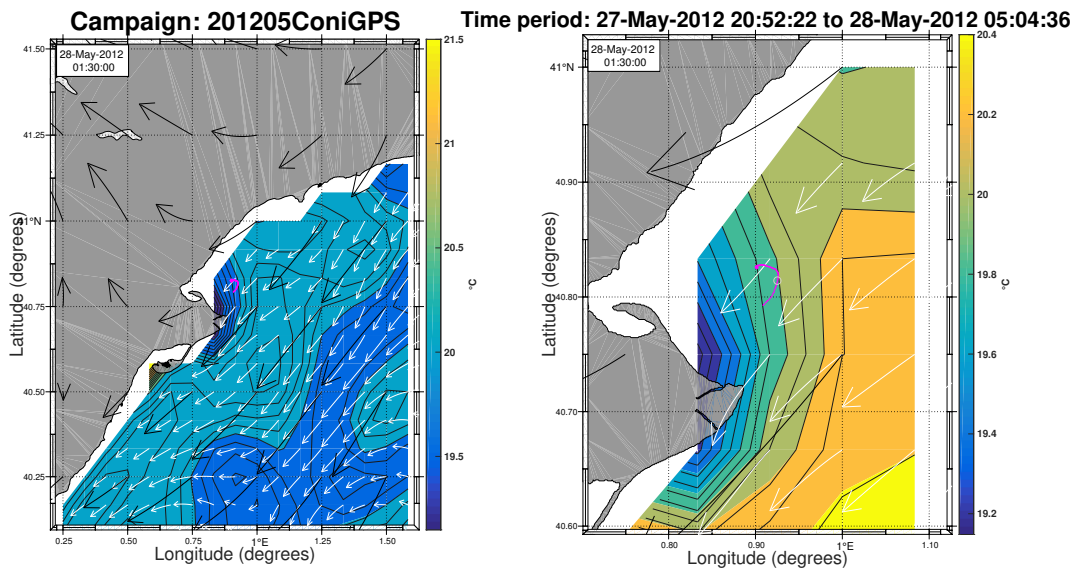


Figure 4.11: The same as Figure 4.2 but for the seabird trajectory ConiGPS201205_2.

In this case, the driving force affecting the bird trajectory is, a priori, unclear. It seems that neither wind or current have a dominant effect on the bird path (Fig: 4.11). However, investigating the different snapshots of the track (see Fig: 4.12), and the statistical parameters calculated for this trajectory (see Table 4.12 it can be seen that surface currents have an impact on the whole trajectory. Seabird direction changes clockwise in the same way than surface currents do, this can be observed in Fig: 4.13, where bird and current directions change simultaneously from south-east to south-west. Due to this reasons, it was not necessary to split this trajectory.

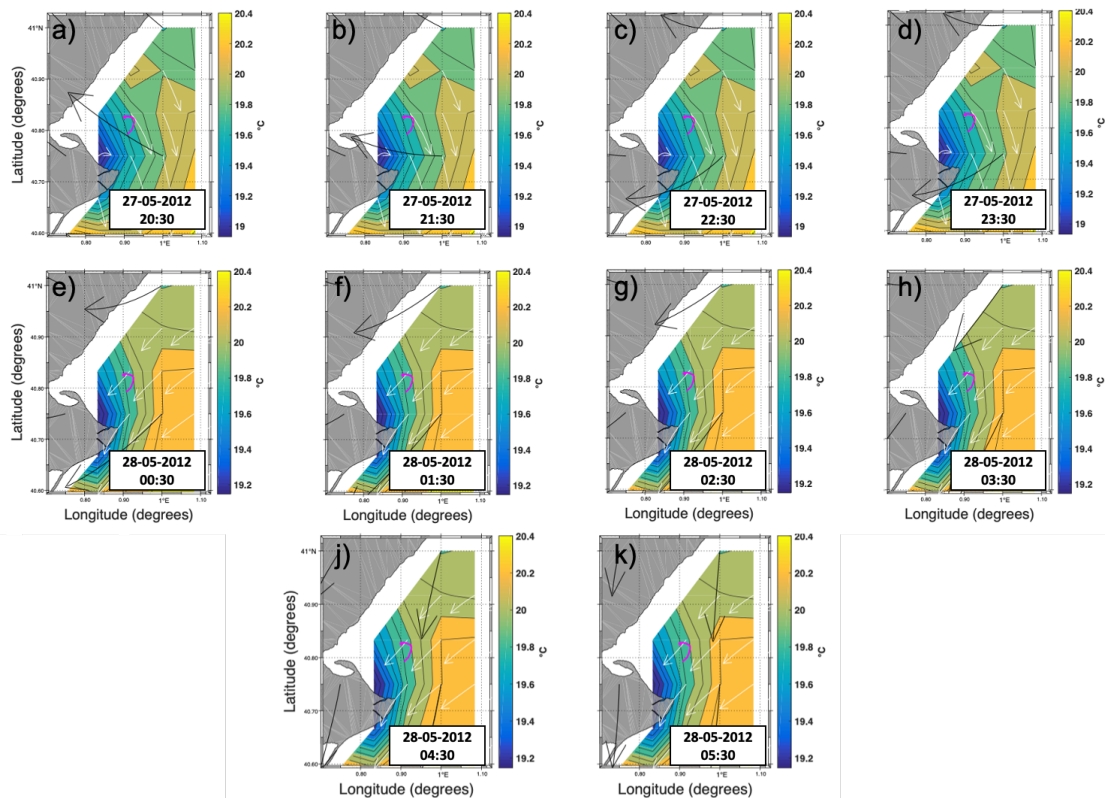


Figure 4.12: The same as Figure 4.11 but for ten hourly snapshots spanning from May 27 at 30:30h to May 28 at 05:30h

	R	p-value	RMSE	mean	std	mean_B	std_B	dif
Wind	-0.91	3.21e-36	114.53	233.02	26.28	148.01	52.56	85.01
Current	0.75	1.62e-18	55.76	191.58	44.29	148.01	52.56	43.57

Table 4.12: The same as Table 4.4 but for the Coni2012GPS-2 seabird track.

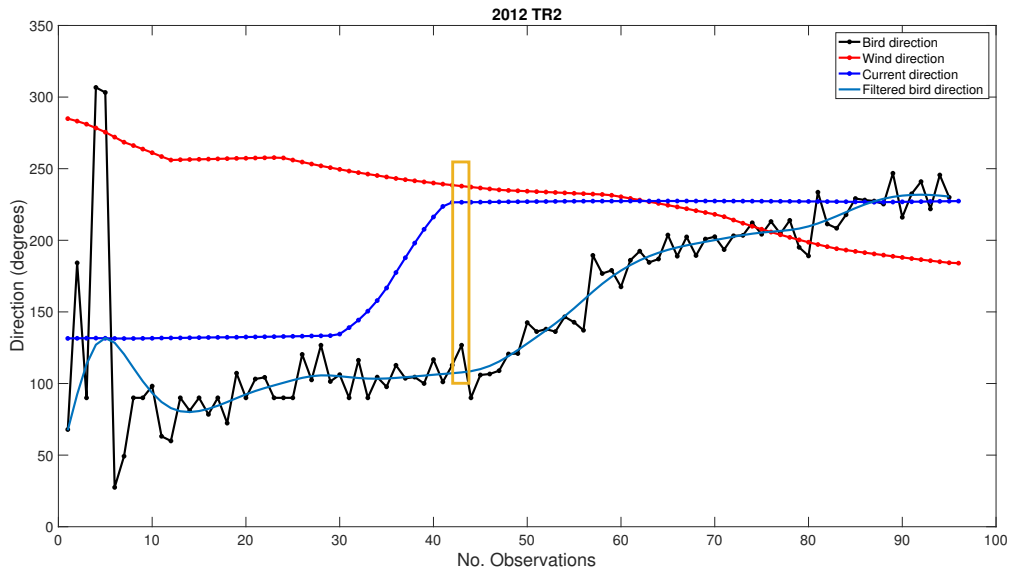


Figure 4.13: The same as Figure 4.4 but for the ConiGPS201205_2 seabird trajectory.

As a result, the statistical parameters were calculated for the whole trajectory (not by sections). Outcomes for the comparison between surface current and seabird for this example (trajectory 2) are shown in Table 4.12. The correlation coefficient is 0.75, significant at the 95% confidence level, the RMSE is almost 56 degrees, and the difference between mean directions is 43.57 degrees.

On the other hand, Table 4.12 shows the statistical parameters between surface wind and the seabird trajectory. A negative correlation coefficient of -0.90 is observed, whilst a RMSE of 114.53 degrees and a difference between the mean directions of 85 degrees are obtained. As a consequence, a negligible impact of surface winds on the seabird track is observed. The statistical results corroborate that sea surface currents are driving the whole drifting trajectory of the individual while resting at the sea surface.

4.2.3 Wind and Current driving example

The following examples shows a seabird trajectory driven by both, surface wind and currents.

Campaign201405 Trajectory 21

The trajectory represented in Fig: 4.14, is formed by 60 fixes GPS, so this seabird was drifting on the sea surface for over 5 hours on 31 May 2014 from 01:08:54 to 06:05:04. Surface current and temperature data correspond to 03:30 am; and wind data to 04:00 am.

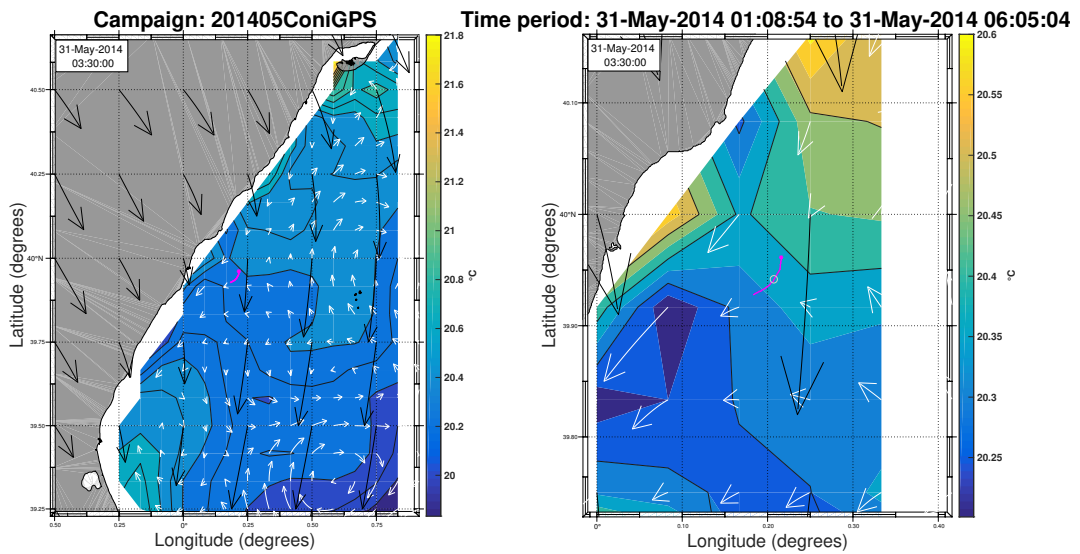


Figure 4.14: The same as Figure 4.2 but for the seabird trajectory ConiGPS201405_21.

This trajectory has not been split because it hardly changes direction, which ranges between 180 and 270 degrees all the time.

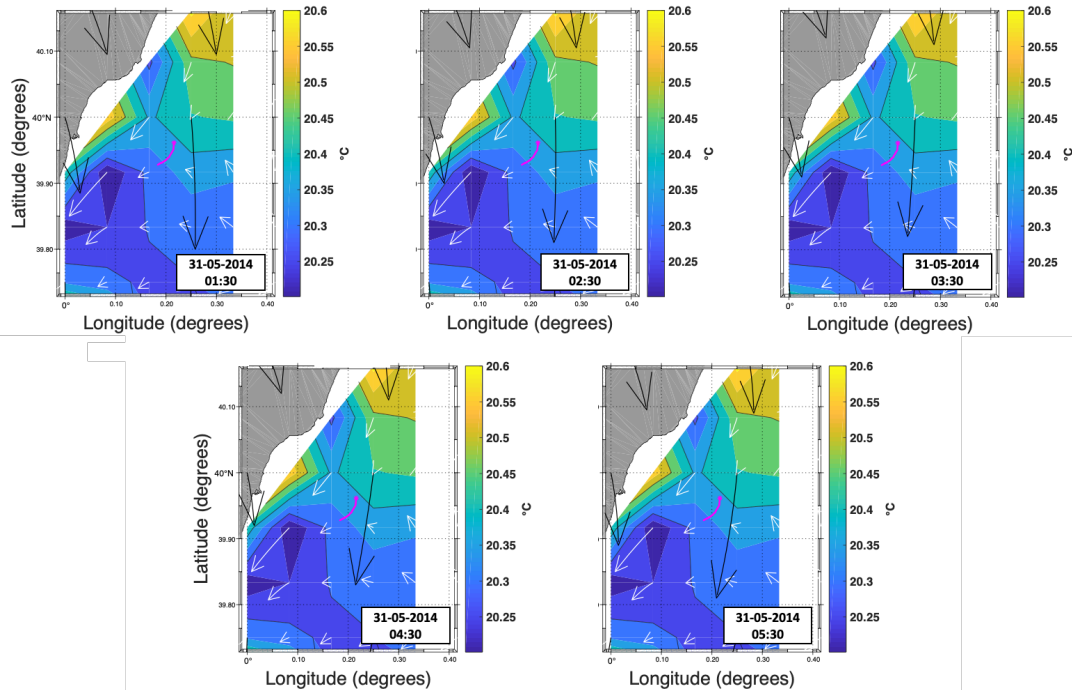


Figure 4.15: The same as Figure 4.14 but for five hourly snapshots on May 31 from 01:30h to 05:20h

As a first estimation, Fig: 4.14 right panel reveals a strong influence of surface currents and local wind on the seabird track. The two nearest white arrows (current data), above and underneath the seabird drift trajectory, seem to align with the direction of the trajectory drawing almost the same path. The nearest black arrow (wind data) turns gradually from south- southeast to south-southwest like the bird trajectory.

Fig: 4.15 displays five hourly snapshots in order to better understand the driving forces acting over the whole trajectory. Analysing Fig: 4.15, sea surface current follows the same direction as the seabird path. Also, wind

	R	p-value	RMSE	mean	std	mean_B	std_B	dif
Wind	0.97	2.04e-37	42.44	181.28	5.95	220.04	23.16	38.76
Current	0.92	1.53e-25	38.60	252.93	3.02	220.04	23.16	32.88

Table 4.13: The same as Table 4.4 but for the ConiGPS201405_21 seabird track.

direction shifts westward and could affect the seabird drift direction.

Fig: 4.16 reveals that the surface current and wind directions are almost the same during the whole track, as observed in the seabird one. It is important to keep in mind that wind and current data are interpolated into the bird GPS fixes in Fig: 4.16 whilst in Fig: 4.15 hourly data are plotted.

For the interpretation of these results, the statistical parameters reported in Tab: 4.13 will be used, for wind and surface current.

Tab: 4.13 reveals a strong positive correlation between surface current and the seabird track direction (0.92) significant at the 95% confidence level. RMSE (38.61 degrees) and the difference (32.88 degrees) between the mean value of current and bird direction is approximately the same.

On the other hand, there is a really good correlation (0.97) between wind and the seabird trajectory. The RMSE (42.44 degrees) and difference (38.76 degrees), both approximately 40 degrees. This slightly high value could be promoted by the high variance of bird data, but even so, it seems that the wind exerts a huge influence on this track.

The statistical results reinforce the hypothesis that both, surface current and local wind are the main drivers of the seabird drift.

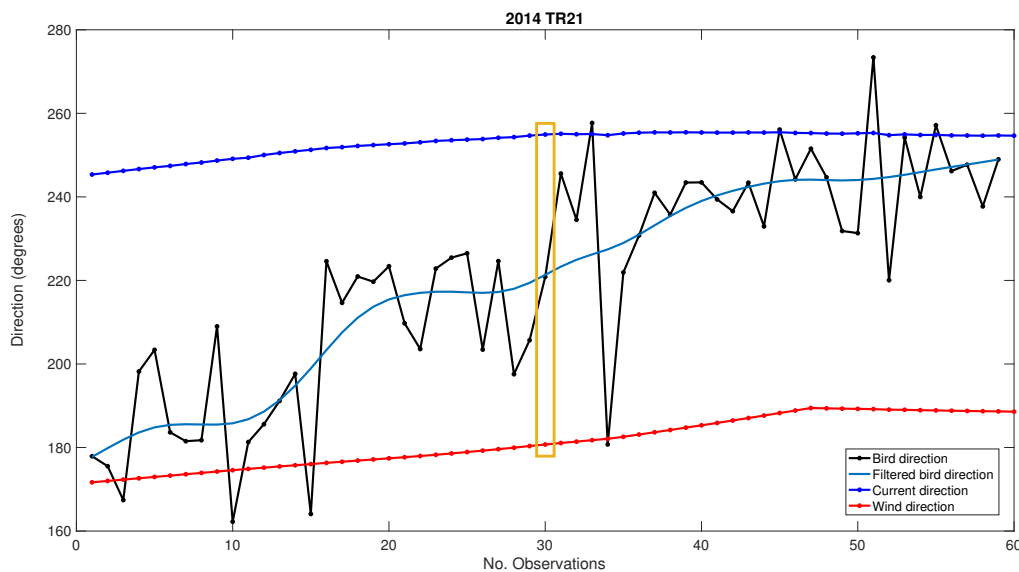


Figure 4.16: The same as Figure 4.4 but for the ConiGPS201405_21 seabird trajectory.

Campaing ConiGPS201405 Trajectory 27

This example consists in a seabird trajectory of 94 GPS fixes, a time elapse of almost 8 hours, from 28 May 2014 at 21:43:13 to 29 May 2014 at 05:23:53.

	R	p-value	RMSE	mean	std	mean_B	std_B	dif
Wind	0.12	0.26	56.70	147.75	4.24	186.03	42.33	38.29
Current	0.88	3.46e-31	74.57	120.87	6.89	186.03	42.33	65.17

Table 4.14: The same as Table 4.4 but for the Coni201405GPS_27 seabird track.

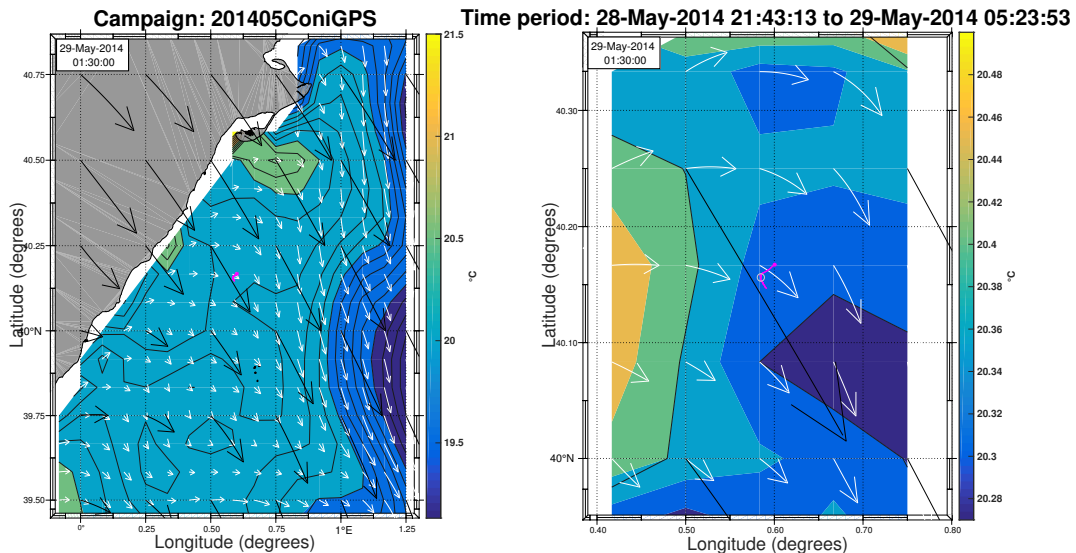


Figure 4.17: The same as Figure 4.2 but for the seabird trajectory ConiGPS201405_27.

Fig: 4.17 shows surface wind, current and temperature data corresponding to the mid-point of the seabird trajectory on 29 May at 01:30 for current and temperature, and at 02:00 for wind data. In Fig: 4.18 are displayed the time series of wind, current and bird directions. The orange box represents the mid-point time aforementioned. The bird direction changes almost 100 degrees, from nearly 250 to 150 degrees; whereas current and wind directions remain constant during all the seabird trajectory. As a consequence, it was not necessary to plot different hourly snapshots corresponding to the duration of the seabird trajectory. Furthermore, It was not necessary to analyse this example by partial trajectories because current and wind data are almost constant. Table 4.13 shows the statistic between the seabird and wind directions for the whole trajectory. Moreover, Fig: 4,15 displays the time series of both current and wind together with the bird directions. The statistical parameters reveals the influence of both, surface wind and current. Correlation coefficient result for current and bird direction is 0.88 with a RMSE of 74.56 degrees and a difference between the mean directions of 65.17. All these results are calculated with a 95% significant level. On the other hand, the correlation coefficient between wind an bird direction is nearly 0.2, whilst the RMSE is 56.70 and the difference in mean directions 38.29 degrees. Even though the correlation coefficient among wind and bird direction is smaller than that for currents and the seabird, the error and differences are lower for wind, so it can be argued that wind is influencing the seabird drift as well as the surface current, the latter showing a larger impact on the track.

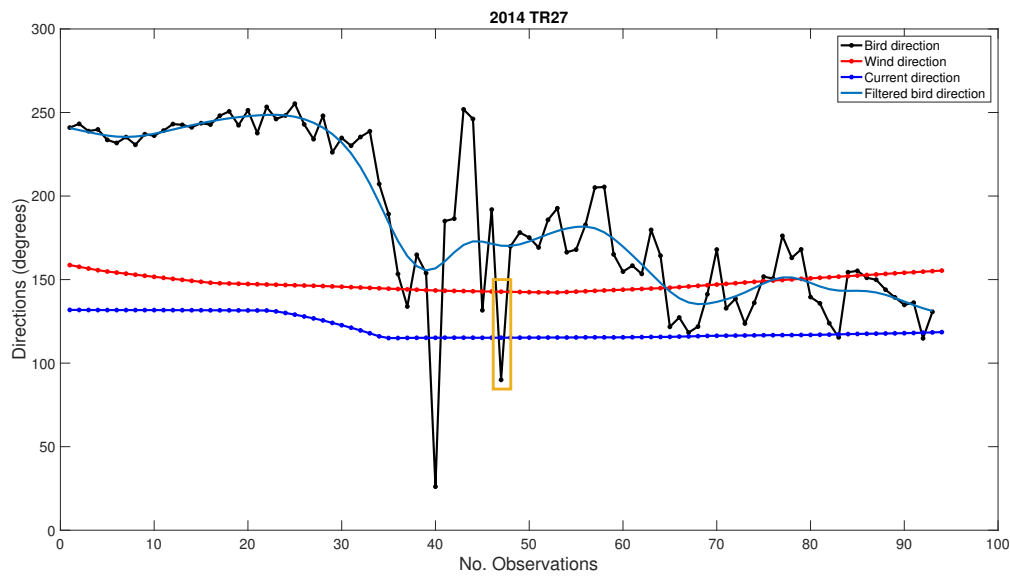


Figure 4.18: The same as Figure 4.4 but for the ConiGPS201405_27 seabird trajectory.

4.2.4 Other trajectories with no influence of neither, wind or current

Campaign ConiGPS201205 Trajectory 3 and ConiGPS201305 Trajectory 18

Fig: 4.19 and Fig: 4.20 show two trajectories as an example of tracks that don't seem to be forced by neither surface currents or winds.

Figure 4.19 shows sea surface current, wind and temperature fields, corresponding to 16:30:00 for IBI data (surface current and temperature) and to 17:00:00 for wind data, together with the seabird track of approximately five hours long on 28 May 2012 from 15:12:07 to 18:23:20. In the same way, Figure 4.20 represents a seabird trajectory drifting at the sea surface from 27 May 2013 from 00:37:35 to 05:13:55 (five hours duration). Surface current, wind and temperature data plotted in Figure 4.20 correspond to 02:00:00.

Looking over the maps (Fig: 4.19 and Fig: 4.20), it seems that both currents and winds are not affecting the bird trajectories displayed. The time series of wind, current and seabird directions, corresponding to these examples, are represented in Figure 4.21 and Figure 4.22. As can be seen, directions are practically constant, so Fig: 4.19 and Fig: 4.20 are representative for all the path time. For this reason, plotting the maps representing each time instant of current, temperature and wind data was not necessary.

The statistical analysis revealed that there is no impact of neither wind or current on these tracks since no significant outcomes were obtained. See Appendix A.1 Tab: 1 and Appendix A.1 Tab: 2 for trajectory 3, corresponding to Fig: 4.19. For trajectory 18, see Appendix A.2 Tab: 3 and Appendix A.2 Tab: 4, this example correspond to Fig: 4.20.

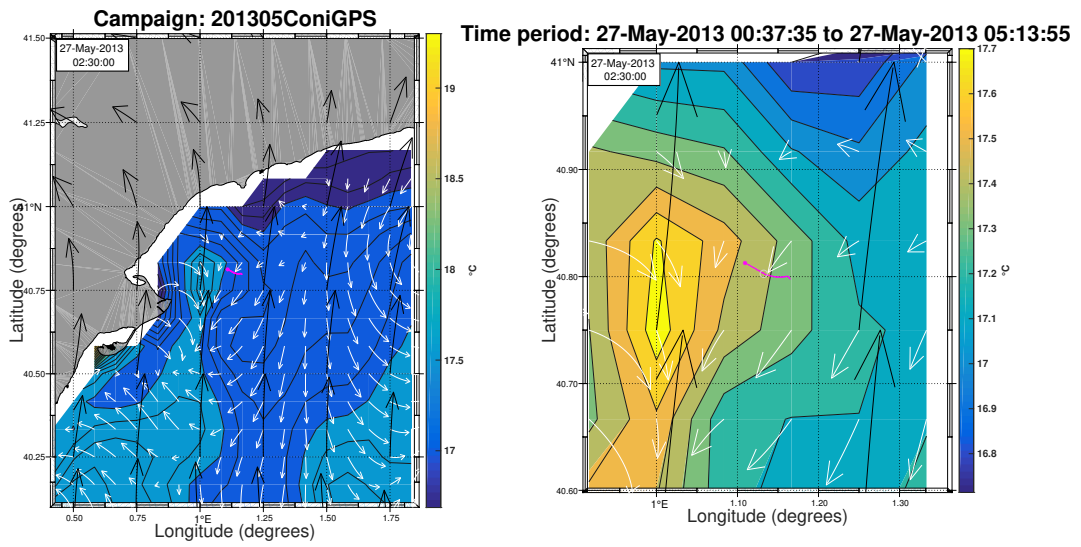


Figure 4.19: The same as Figure 4.2 but for the seabird trajectory ConiGPS201205_3.

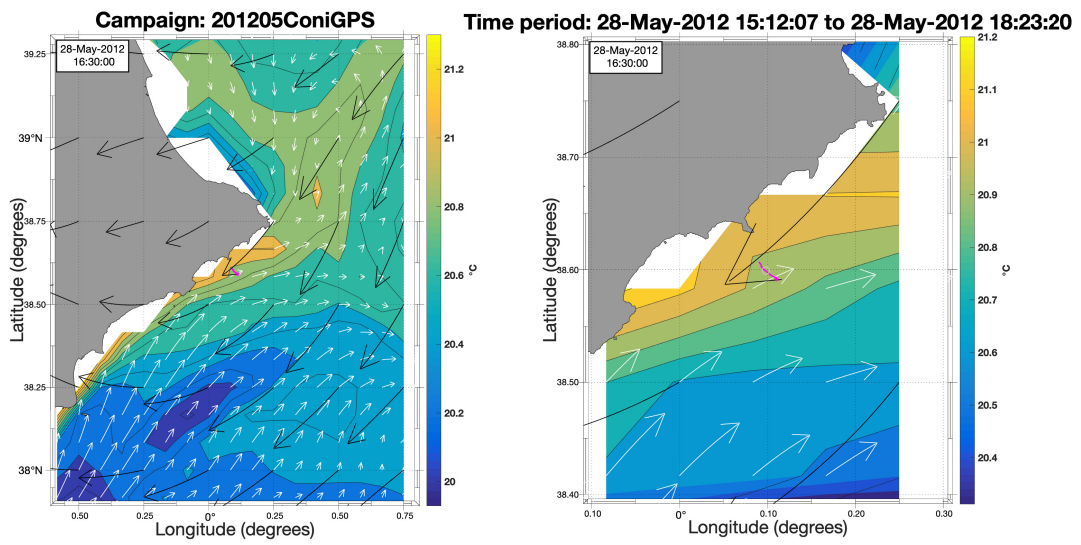


Figure 4.20: The same as Figure 4.2 but for the seabird trajectory ConiGPS201305_18.

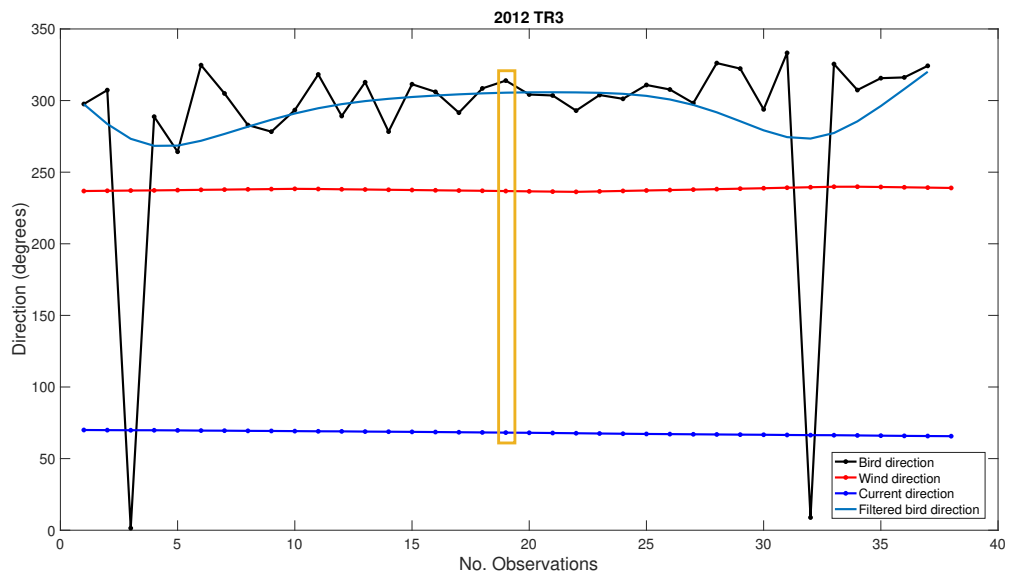


Figure 4.21: The same as Figure 4.4 but for the ConiGPS201205_3 seabird trajectory.

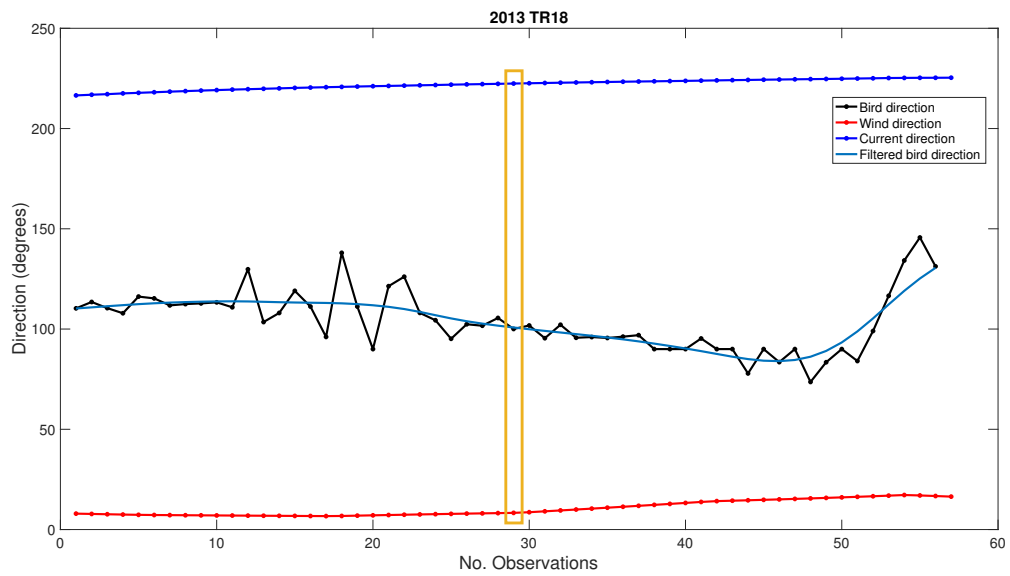


Figure 4.22: The same as Figure 4.4 but for the ConiGPS201305_18 seabird trajectory.

Chapter 5

Discussion and Conclusions

Nowadays, marine animals are more frequently equipped with different sensors to provide multiple types of oceanographic data thanks to the relatively recent development of miniaturized bio-logging devices. In this context, the present work draws on animal borne GPS data to explore the use of tracking data from *Puffinus Mauretanicus* (Balearic shearwater) as an alternative way to acquire in-situ surface velocity measurements when these seabirds rest at the sea surface acting as passive drifters. Here is presented an innovative work based on the estimation of surface currents from both a qualitative and quantitative point of view by using *Puffinus Mauretanicus* drifts in the Balearic Sea.

The engaging knowledge of the Mediterranean circulation lies on the study of the dynamical properties derived from the intense frontogenesis and the continuous input of nutrients from the entry of fresh Atlantic water through the Strait of Gibraltar. [[Zavatarielli and Mellor, 1995](#); [Juzà et al., 2013](#); [Conti et al., 2013](#); [Lana et al., 2016](#)].

Surface currents in the continental shelf and coastal areas of the Balearic sea have been evaluated using data from 32 borne GPS installed on Balearic shearwaters in the framework of the INDEMARES project. A total of 60 trajectories from seabirds were analysed: 19 trajectories were mainly driven by local wind, 13 by surface currents, 15 by both (current and wind) and 13 by other driving forces not investigated here. The results presented above contribute to improve our knowledge of the surface circulation in this area, bringing new information derived from instrumented animals, as it has been previously done in this, and other areas of the world ocean ([[Tew Kai et al., 2009](#); [Yoda et al., 2014](#); [March et al., 2019](#); [Sánchez-Román et al., 2019](#)]).

[Table 5.1](#) shows a summary of the trajectories analysed here classified according to the main driving force acting on them. Namely, surface currents, surface winds, both or other forces not investigated in this Master. Sea surface temperature from the IBI-MFC numerical ocean model was also considered as ancillary information.

Campaigns		Number of Trajectories driven by			
		Wind	Curretn	Both	Others
ConiGPS201205	Full trajectories	1	1	1	2
	Partial Trajectories	2	3	2	1
	Total	3	4	3	3
ConiGPS201305	Full trajectories	4	1	0	5
	Partial Trajectories	2	0	4	2
	Total	6	1	4	7
ConiGPS201405	Full trajectories	3	2	1	5
	Partial trajectories	5	3	5	5
	Total	8	5	6	10

Table 5.1: Classification of the seabird trajectories investigated in this work for the three campaigns analysed according to the driving force acting on them. The total numbers are also provided.

The trajectories analysed in this work can be gathered, according to the area in which they are located, in three different groups:

- The continental shelf of the Iberian Peninsula where the Northern current dominates the main circulation.
- The Ibiza Channel, between the Iberian Peninsula and Ibiza Island, where strong winds occur.
- The south of the Iberian Peninsula, near the Strait of Gibraltar, where the water exchange through the Strait of Gibraltar drives the general circulation in the area.

For those seabird trajectories located in the continental shelf of the Iberian Peninsula, the Northern Current (NC flowing from Northeast to Southwest, see Fig:1.1) may play a key role in such seabird displacements.

Moreover, the detailed analysis of these trajectories has allowed to depict a high-frequency variability of this NC, detecting significant changes in the mean direction of the Northern Current within a few hours, as shown in Fig:4.12 and Fig:4.15. However, sea surface currents obtained from the IBI model in the region do not properly reproduce such changes in direction of the Northern Current so the information obtained here for this area could be used to validate and thus improve the numerical model.

On the other hand, surface circulation in the region of the Ibiza Channel has been investigated in previous studies using conventional sources of data such as CTDs, ADCP, etc. [Pinot *et al.*, 2002; Lana *et al.*, 2016]. Results from [Lana *et al.*, 2016] revealed that local winds can drive the surface current variability in different periods of the year. All seabirds campaigns analysed in this Master began at ending May and extended until the first week of June, except the ConiGPS201305 that was conducted along the last week of May. These authors reported strong wind effects in winter time (Nov/Dec/Jan), while during summer (Jul/Aug/Sep) the wind influence was weaker, so it can be assumed that wind effects decrease during the bird campaigns, but not as much as noted by [Lana *et al.*, 2016]. Fig:4.3 Shows an example of a seabird track driven by local wind close to the Ibiza Channel, this supporting the results reported by these authors.

The third group of trajectories are located in a region out of the geographical scope of this study: the western-most part of the Mediterranean Sea. It is known that such region is mainly dominated by the oceanic circulation driven by the inflow of Atlantic Water into the Mediterranean Sea through the Strait of Gibraltar that generates strong anticyclonic eddies and jets in the Alboran Sea. However, discussion about this group of trajectories is not developed due to their remoteness location with respect to the Balearic Sea.

The mesoscale surface circulation in the Balearic Sea, of order 10-100 km, has been studied in the past by using measurements from different sources: satellite observations ([Mason and Pascual, 2013; Troupin *et al.*, 2015]), synoptic observations from oceanographic cruises by using different platforms such as (CTDs, ADCPs, drifters, etc) [Pinot *et al.*, 2002; Allen *et al.*, 2018], and more recently using autonomous underwater vehicles such as gliders [Heslop *et al.*, 2012, 2017; Aulicino *et al.*, 2017]. Moreover, the use of numerical models ([Renault *et al.*,

2012; Juzà *et al.*, 2013]), has also contributed to a better understanding of the surface circulation of the Balearic Sea.

The study presented here has shown that the use of seabird-borne GPS is an innovative approach to investigate the surface currents in the Balearic Sea that can also contribute to improve our knowledge of the surface circulation in the area. It should be noted that until recently, biologists that work on ecology and evolution, have discarded GPS data when seabirds rest at the sea surface because their investigations mainly focus on foraging trips and feeding areas located away from the breeding colonies. However, it is demonstrated here that recorded data from instrumented seabirds when they rest at sea surface can provide valuable information. Indeed, this kind of data are very useful for ocean monitoring since they allow to track sub-mesoscale features of order 0-10 km that satellite altimetry or numerical models cannot properly solve due to their spatial and temporal resolutions. Furthermore, animal-borne GPS data also contribute to fill gaps in key areas of the coastal ocean where both altimetry and numerical models have poorer accuracy due to land contamination of recorded signals from altimeters; and the difficulty of properly implement the coastal processes in the numerical models, respectively. Additionally, seabird-borne GPS data, can be used in different ways for oceanographic applications, for example being assimilated in models to improve forecasting or used (as independent data) for model validation in coastal and shelf areas.

Animal borne data analysed in this master thesis should be integrated into regional ocean observing systems ([*March et al.*, 2019]) such as SOCIB (Balearic Island Coastal Observing System). This facility has already used animal borne data from marine turtles with the aim of providing the scientific basis to support the development of risk mitigation techniques.

It is necessary to keep on working with animal-borne GPS observations for a better understanding of the relationships between seabird rafting and ocean surface currents. This may yield further information for the conservation of marine ecosystems, for defining protected areas at sea and efficient management of ecosystem based fisheries.

Future work

In this work, the impact of winds and surface currents on the rafting behaviour of seabirds while resting at the sea surface in the Balearic Sea, has been investigated. However, other driving forces or process acting on seabirds such as waves or the Ekman and Stokes drifts remained out of our scope and should be investigated in future works in order to have a more comprehensive overview of seabird's rafting. Moreover, this analysis should be extended to other regions of the Mediterranean Sea where tracked seabird data will be available.

On the other hand, a larger number of samples is needed, both in the Balearic Sea and other regions of the World Ocean, to further investigate the applications of animal borne data in coastal oceanography and how to integrate them into numerical models and observing systems in order to improve the forecast and validate the numerical outputs in the coastal region. This is a tricky point in which the synergy between biologists and physicists is crucial in order to properly design future field experiments with animal borne GPS measurements that allow us to obtain a more comprehensive view of coastal processes at finer scales.

Appendix A

Supplementary Information about all the seabird trajectories

A.1 ConiGPS201205

A1.1 IBI - ERA5

Maps

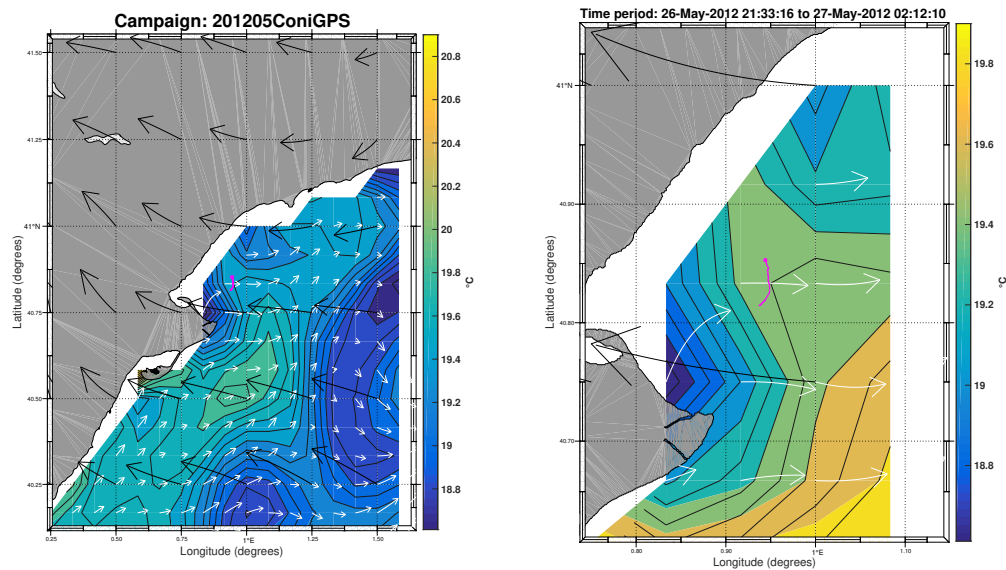


Figure 1: Surface wind (black arrow), sea surface current (white arrow) and surface temperature field (background colour) corresponding to the median time snapshot of the seabird trajectory ConiGPS201205_1 (pink dots), the beginning of the trajectory is marked with an asterisk. Left: General view; right: zoom on the seabird trajectory zone. Surface current, wind and temperature data correspond to the halfway point of the trajectory's time.

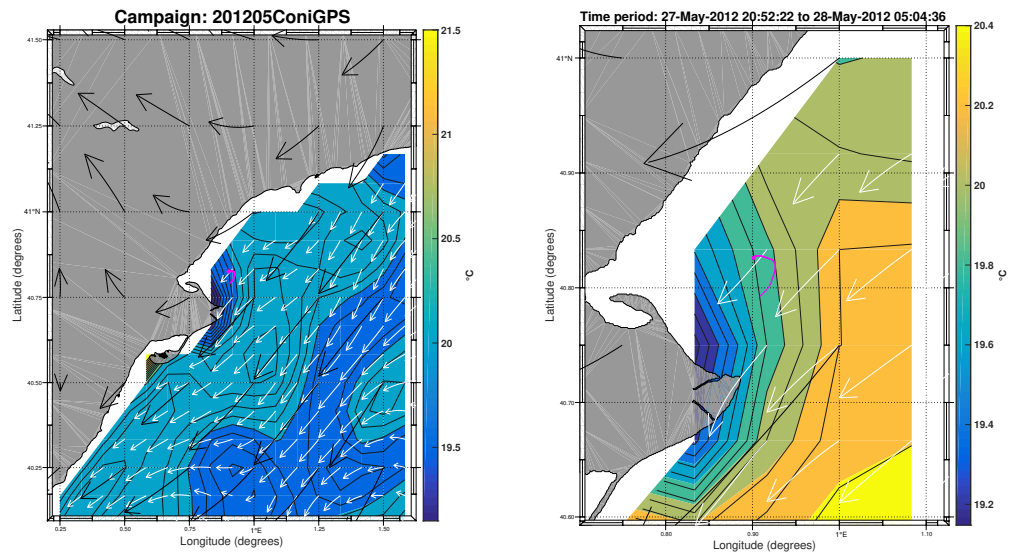


Figure 2: The same as explained in Appendix A.1 Fig. 1, now for this example from ConiGPS201205, trajectory 2, and the surface current, temperature and wind data corresponding to this seabird track analyzed here.

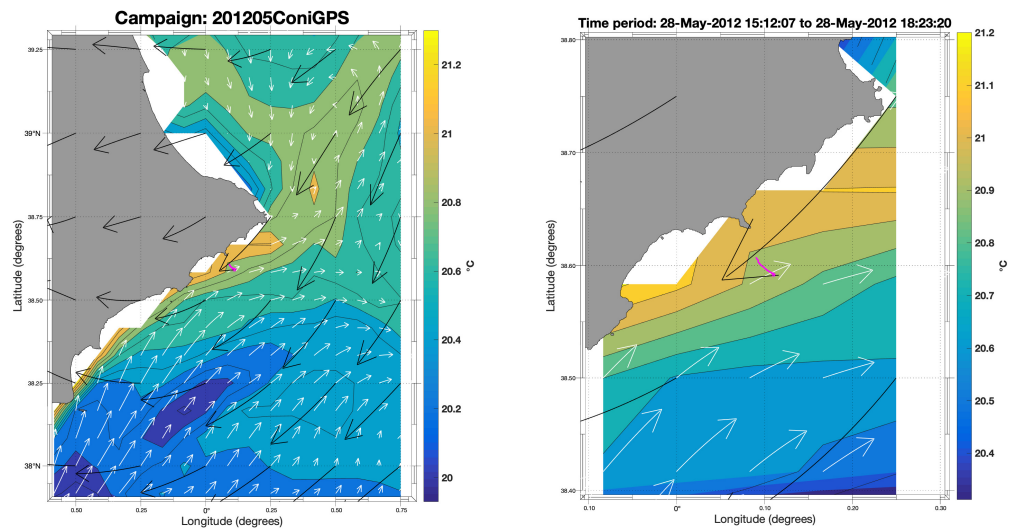


Figure 3: The same as explained in Appendix A.1 Fig. 1, now for this example from ConiGPS201205, trajectory 3, and the surface current, temperature and wind data corresponding to this seabird track analyzed here.

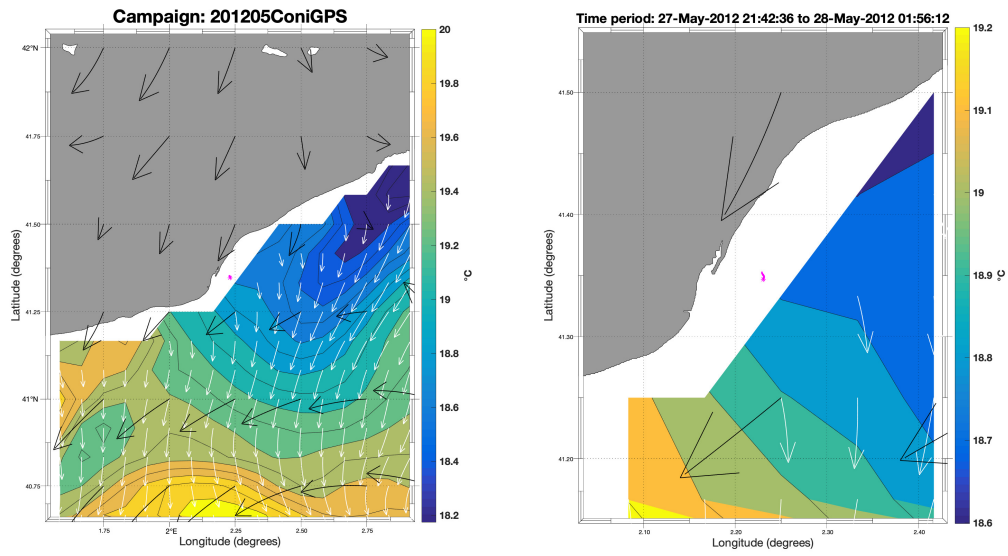


Figure 4: The same as explained in Appendix A.1 Fig. 1, now for this example from ConiGPS201205, trajectory 4, and the surface current, temperature and wind data corresponding to this seabird track analyzed here.

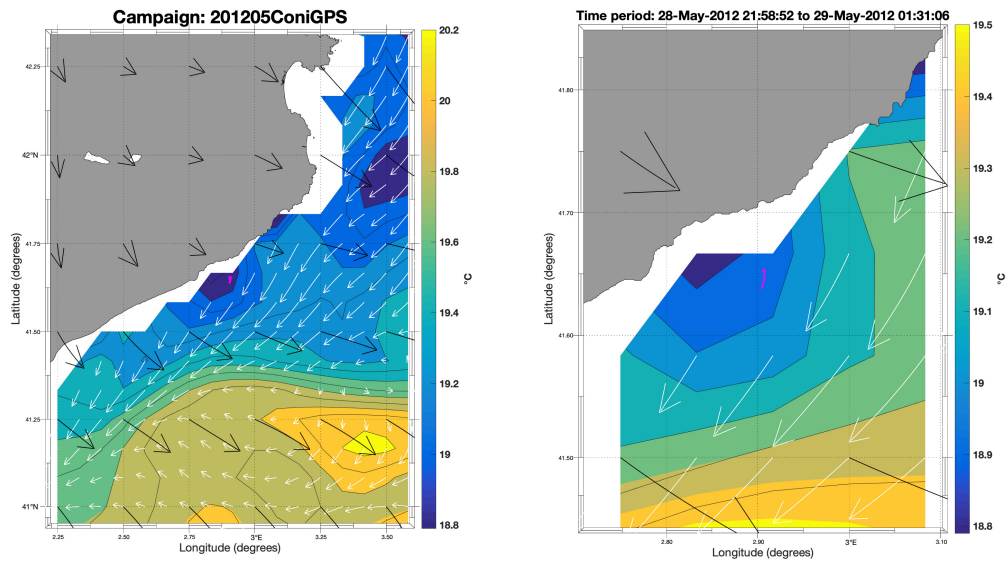


Figure 5: The same as explained in Appendix A.1 Fig. 1, now for this example from ConiGPS201205, trajectory 5, and the surface current, temperature and wind data corresponding to this seabird track analyzed here.

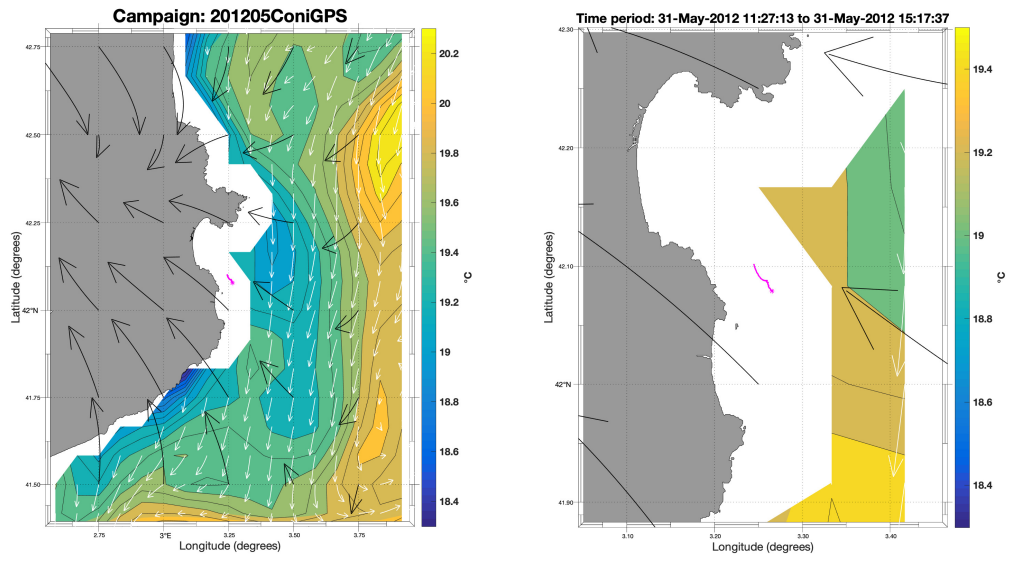


Figure 6: The same as explained in Appendix A.1 Fig: 1, now for this example from ConiGPS201205, trajectory 6, and the surface current, temperature and wind data corresponding to this seabird track analyzed here.

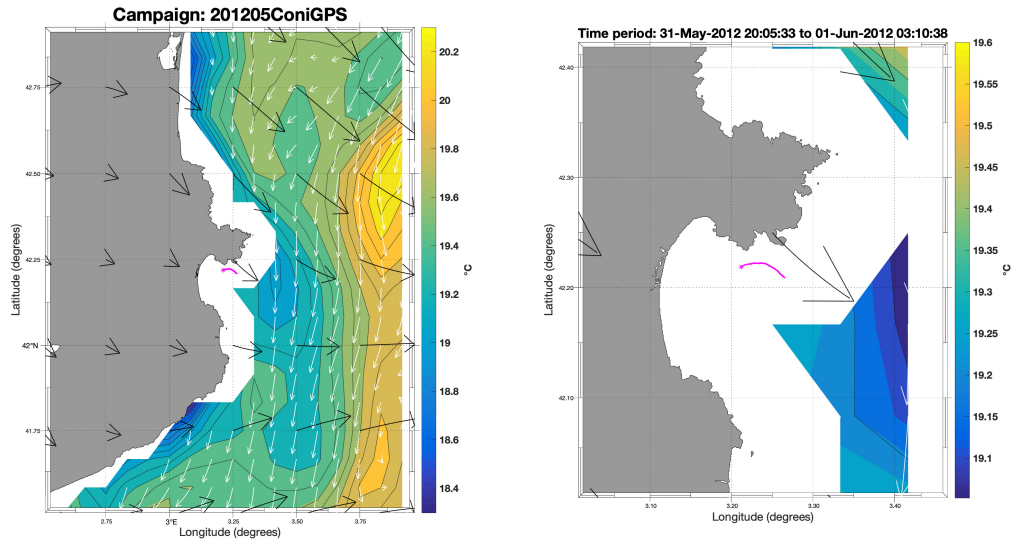


Figure 7: The same as explained in Appendix A.1 Fig: 1, now for this example from ConiGPS201205, trajectory 7, and the surface current, temperature and wind data corresponding to this seabird track analyzed here.

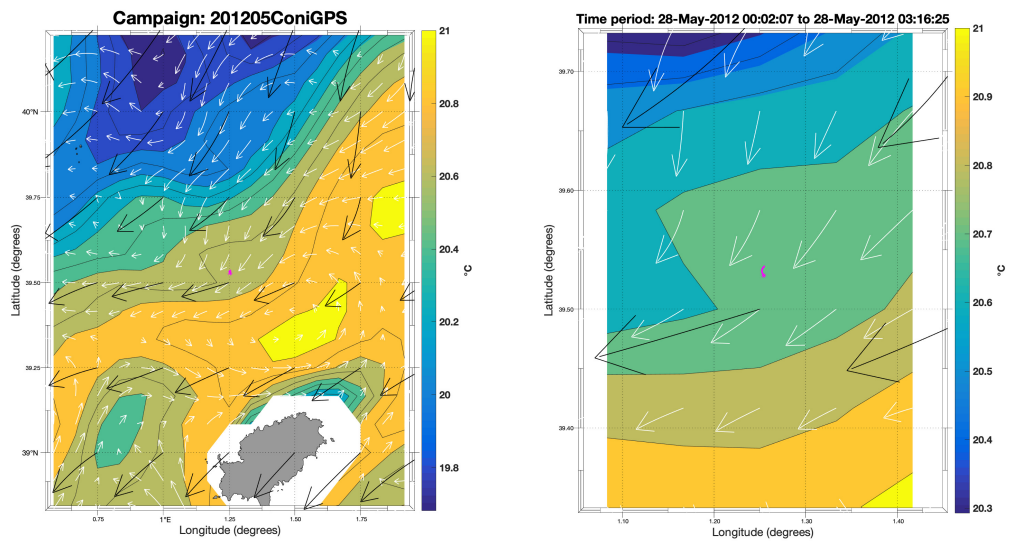


Figure 8: The same as explained in Appendix A.1 Fig: 1, now for this example from ConiGPS201205, trajectory 8, and the surface current, temperature and wind data corresponding to this seabird track analyzed here.

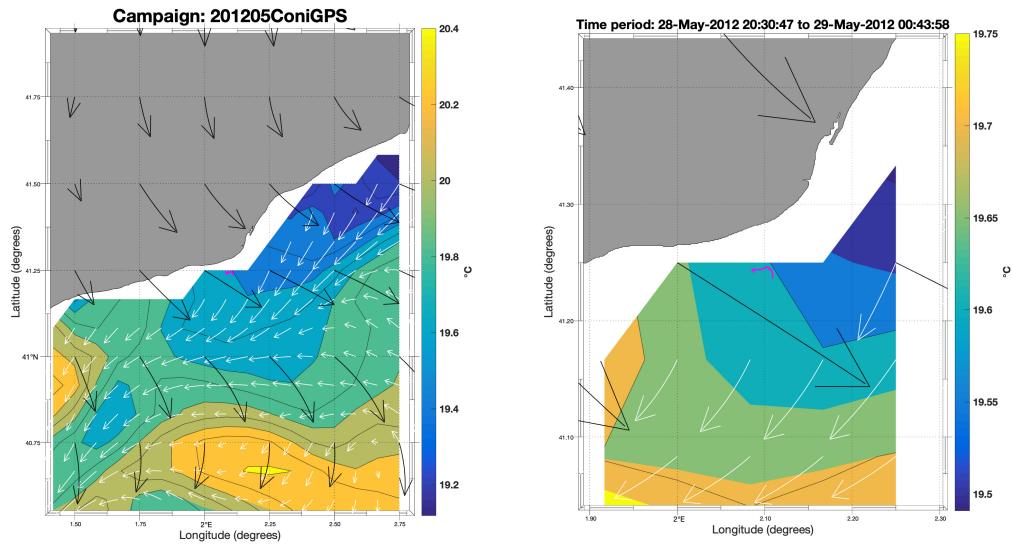


Figure 9: The same as explained in Appendix A.1 Fig: 1, now for this example from ConiGPS201205, trajectory 9, and the surface current, temperature and wind data corresponding to this seabird track analyzed here.

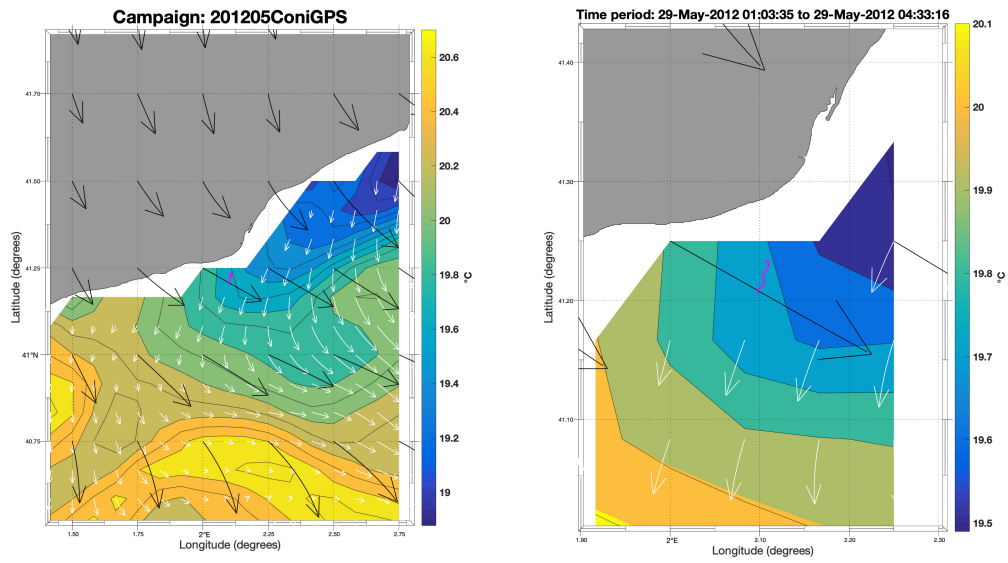


Figure 10: The same as explained in Appendix A.1 Fig: 1, now for this example from ConiGPS201205, trajectory 10, and the surface current, temperature and wind data corresponding to this seabird track analyzed here.

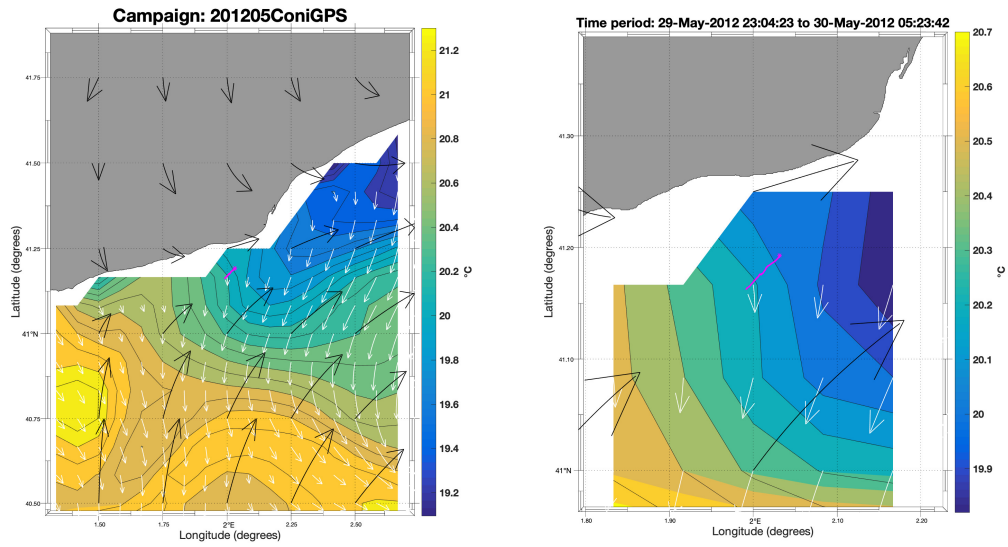


Figure 11: The same as explained in Appendix A.1 Fig: 1, now for this example from ConiGPS201205, trajectory 11, and the surface current, temperature and wind data corresponding to this seabird track analyzed here.

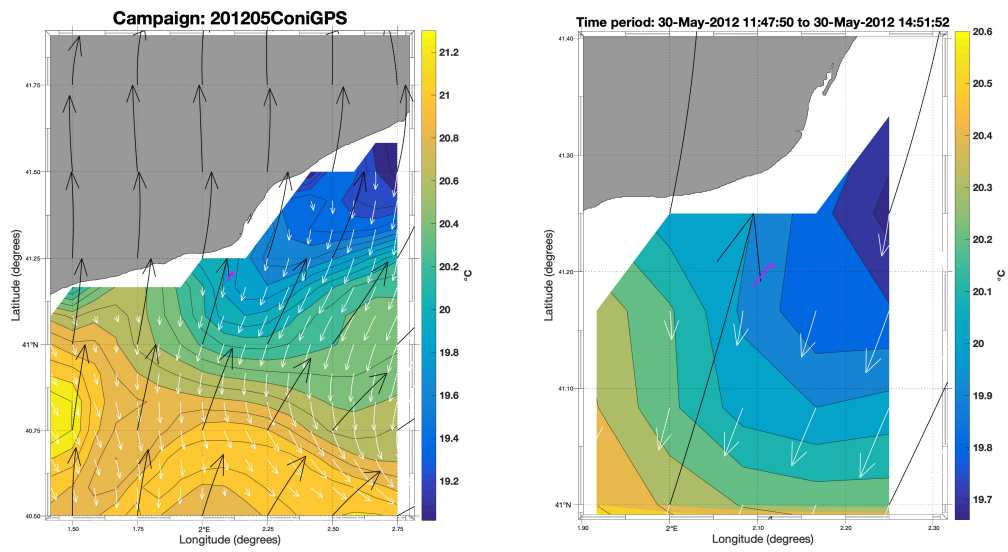


Figure 12: The same as explained in Appendix A.1 Fig: 1, now for this example from ConiGPS201205, trajectory 12, and the surface current, temperature and wind data corresponding to this seabird track analyzed here.

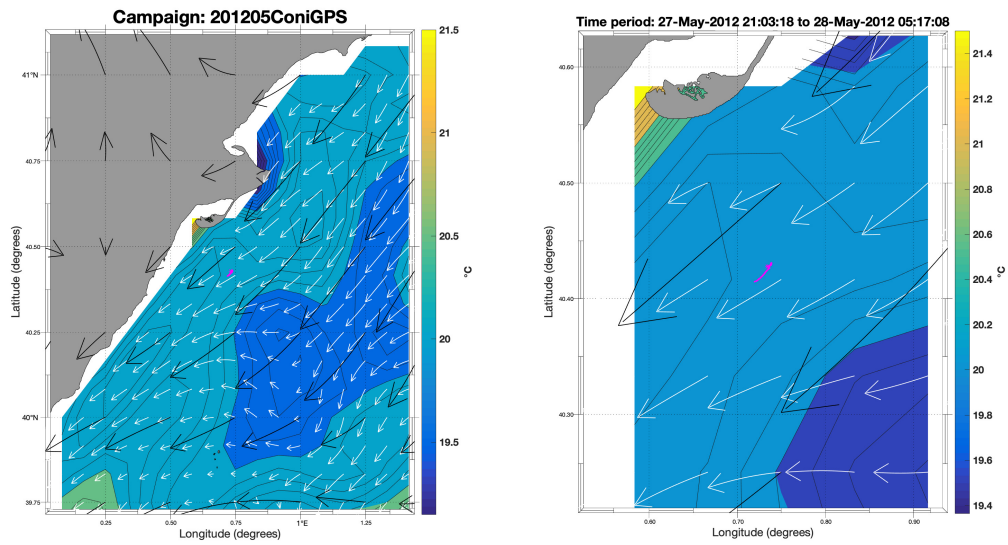


Figure 13: The same as explained in Appendix A.1 Fig: 1, now for this example from ConiGPS201205, trajectory 13, and the surface current, temperature and wind data corresponding to this seabird track analyzed here.

Temporal series

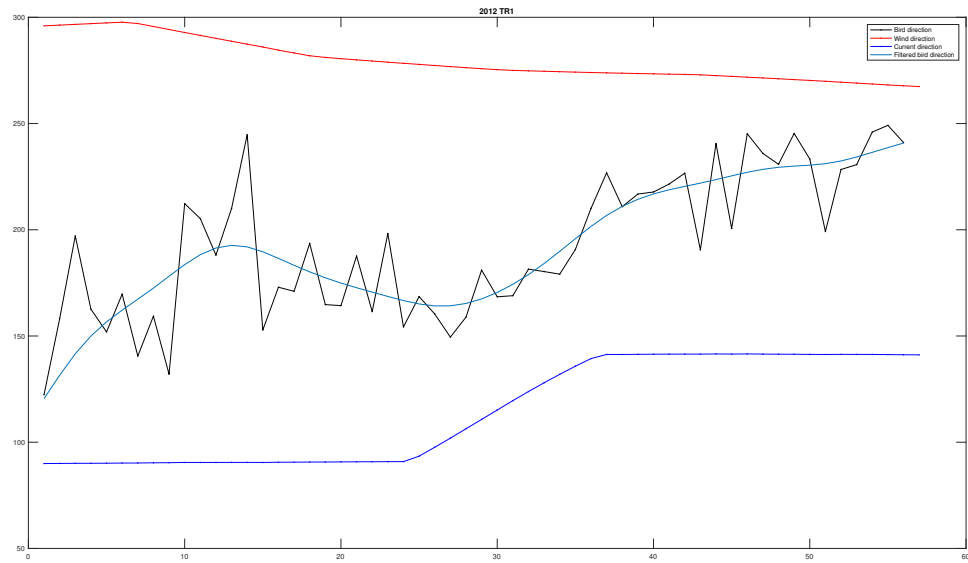


Figure 14: Time series of directions of the original seabird trajectory (blackline) and the smoothed one (pale-blue line), together with the local wind (red line) and surface current (blue line) data interpolated to the bird positions and time.

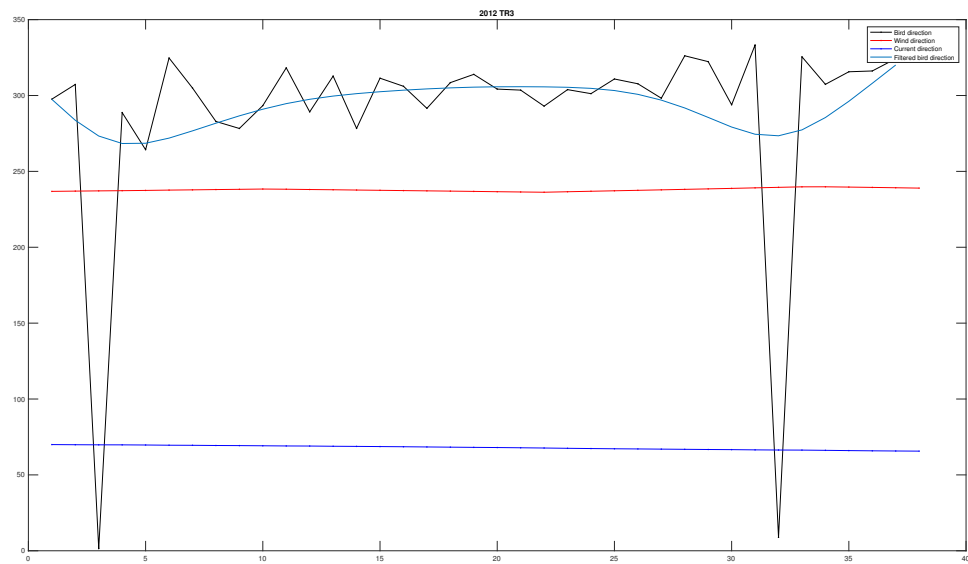


Figure 15: The same as in Appendix A.1 Fig: 14 but for the seabird trajectory 3.

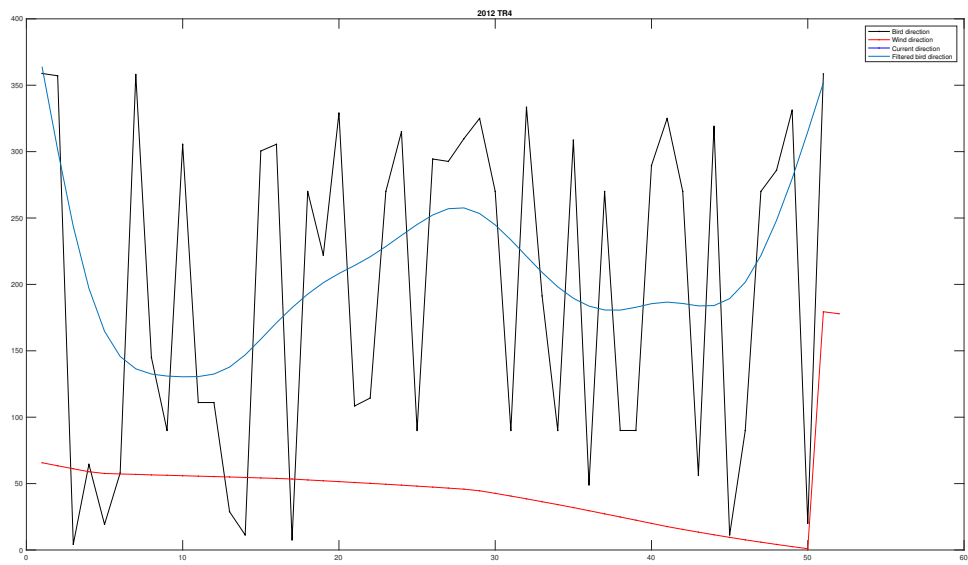


Figure 16: The same as in Appendix A.1 Fig: 14 but for the seabird trajectory 4.

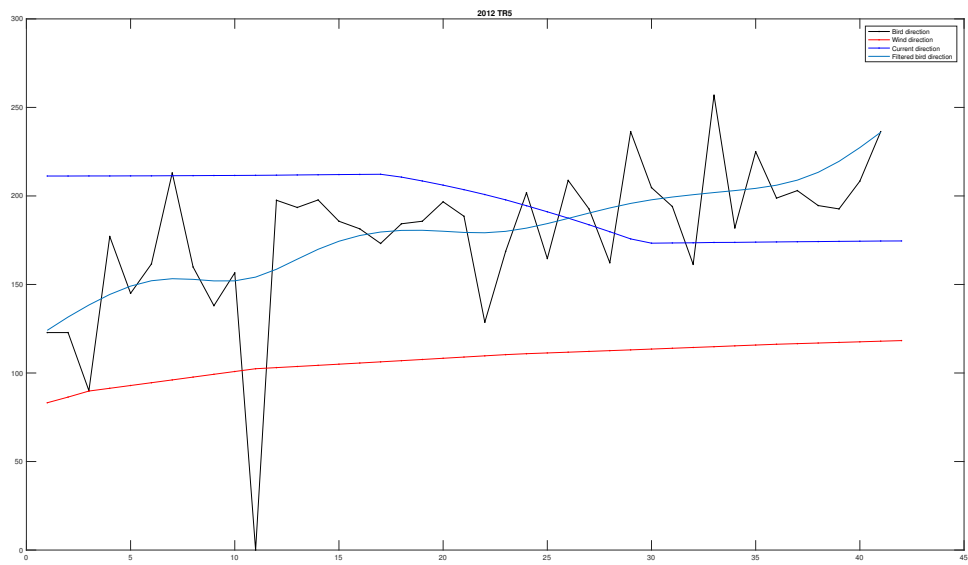


Figure 17: The same as in Appendix A.1 Fig: 14 but for the seabird trajectory 5.

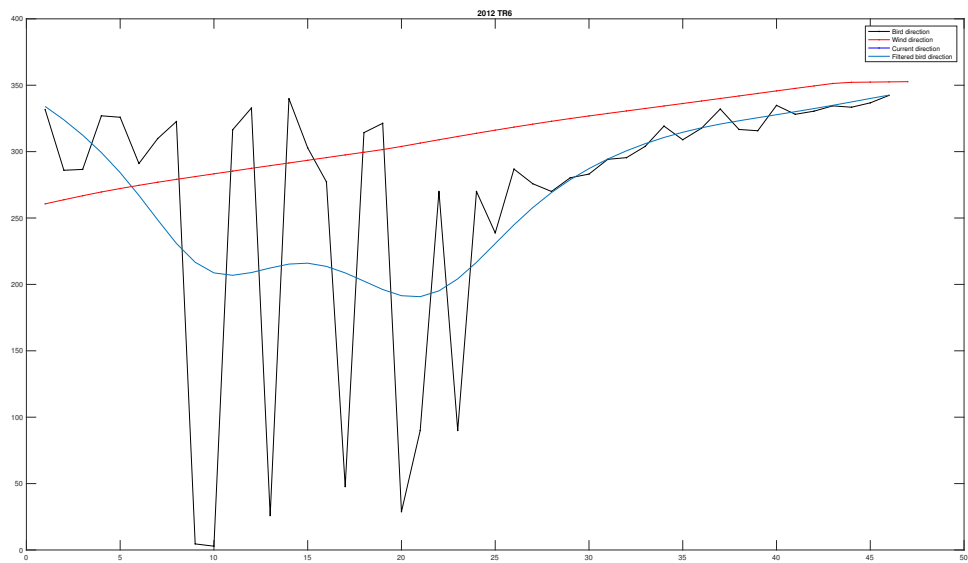


Figure 18: The same as in Appendix A.1 Fig: 14 but for the seabird trajectory 6.

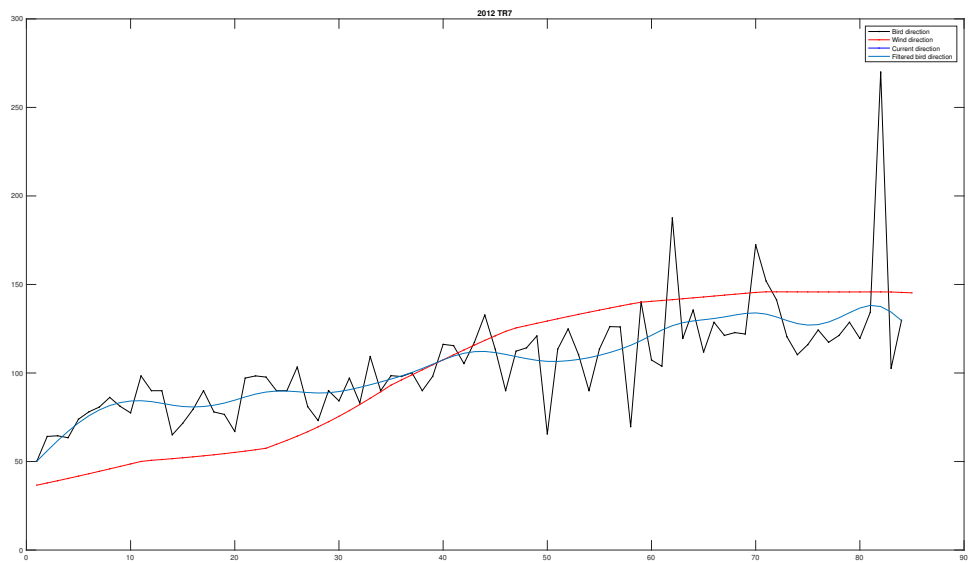


Figure 19: The same as in Appendix A.1 Fig: 14 but for the seabird trajectory 7.

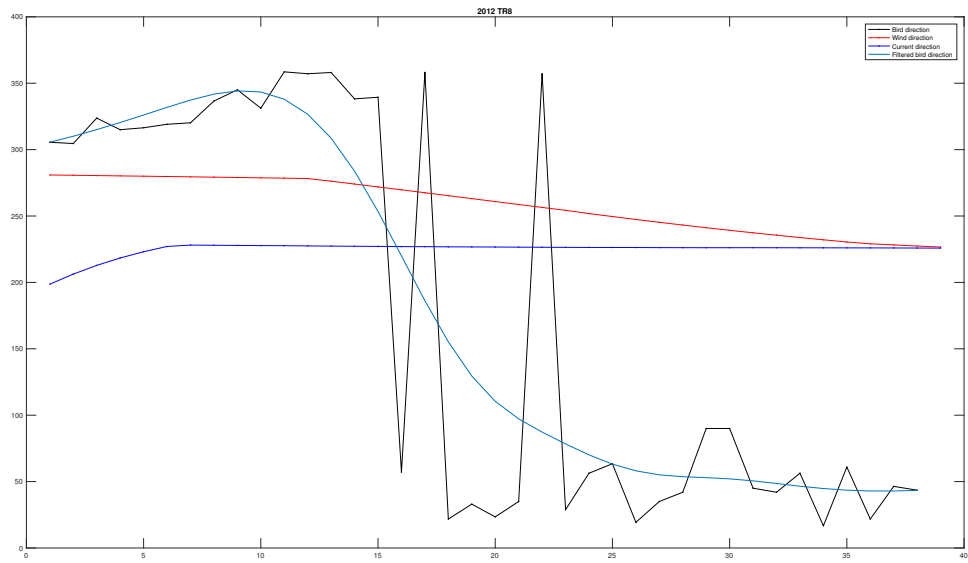


Figure 20: The same as in Appendix A.1 Fig: 14 but for the seabird trajectory 8.

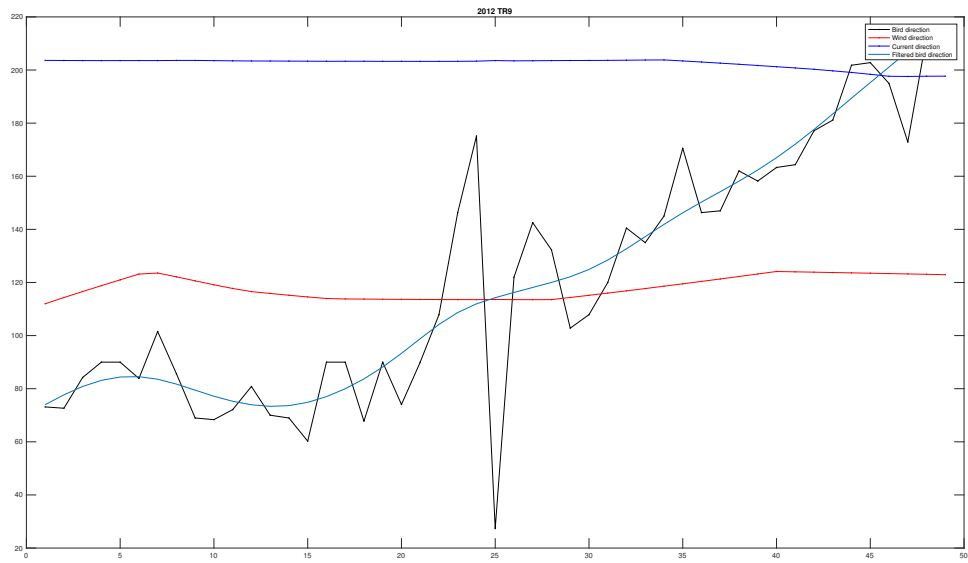


Figure 21: The same as in Appendix A.1 Fig: 14 but for the seabird trajectory 9.

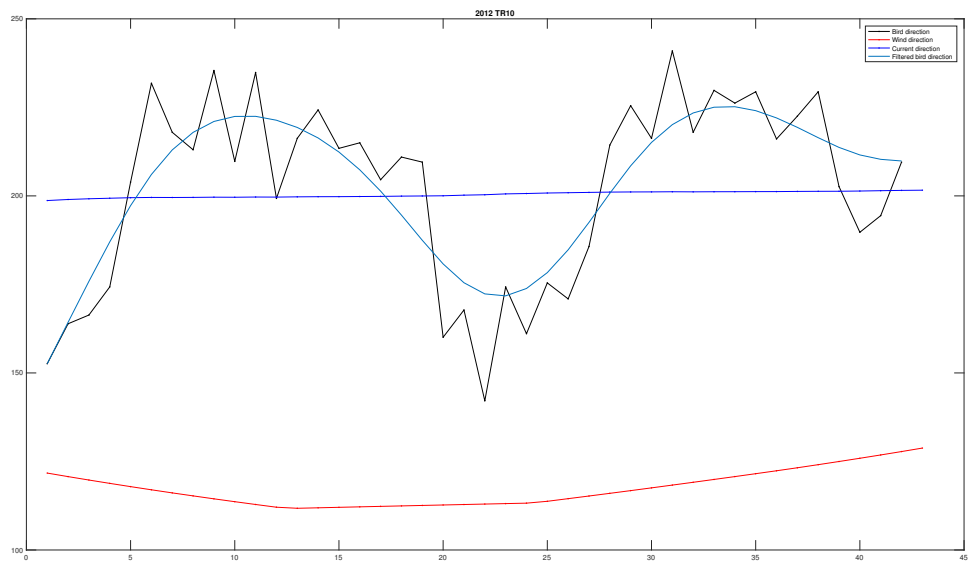


Figure 22: The same as in Appendix A.1 Fig: 14 but for the seabird trajectory 10.

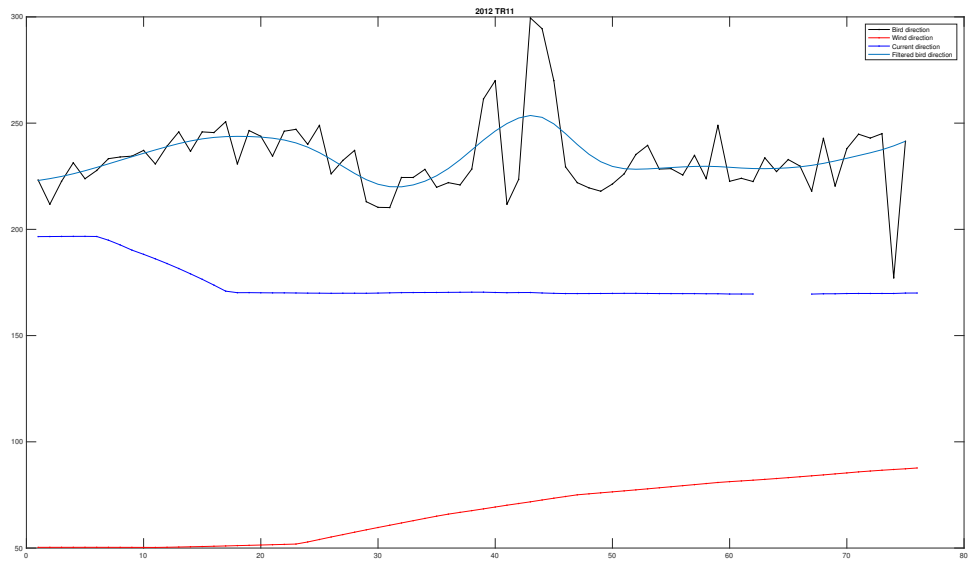


Figure 23: The same as in Appendix A.1 Fig: 14 but for the seabird trajectory 11.

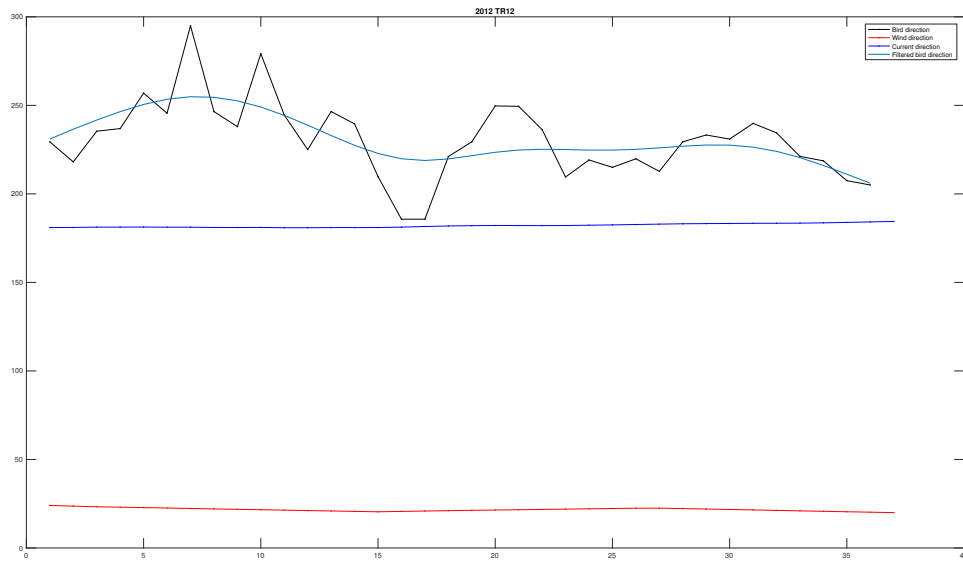


Figure 24: The same as in Appendix A.1 Fig: 14 but for the seabird trajectory 12.

Tables

Trajectory	Rw	Pw	RMSEw	meanW	stdW	meanB	sdtB	difW
1	-0,75	4,04E-11	95,43	279,74	9,42	191,75	29,71	87,99
2	-0,90	3,21E-36	114,53	233,02	26,29	148,01	52,56	85,01
3	-0,29	0,080	56,59	237,86	1,01	292,79	13,49	54,93
4	- 0,25	0,07	62,83	219,15	19,57	206,52	54,25	12,63
5	0,96	3,39E-22	74,82	106,75	9,21	179,50	26,27	72,75
6	0,51	0,00	62,61	311,33	28,16	268,08	53,16	43,25
7	0,95	1,53E-43	20,98	102,05	40,47	104,44	21,67	2,39
8	0,94	3,57E-18	136,06	259,08	19,12	174,18	125,48	84,90
9	0,63	1,71E-06	39,95	118,05	4,11	119,92	42,79	1,87
10	0,19	0,23	87,77	117,12	4,68	202,74	19,85	85,62
11	-0,07	0,55	168,10	66,77	13,57	234,38	8,35	167,32
12	0,54	0,00	209,23	21,75	0,92	230,62	12,82	208,87
13	-0,92	8,93E-43	91,74	238,02	24,59	186,69	53,12	51,32

Table 1: Statistical parameters wind-bird. ConiGPS2012

Trajectory	Rc	Pc	RMSEc	meanC	stdC	meanB	sdtB	difC
1	0,83	2,57E-15	79,15	114,33	23,73	191,75	29,71	77,42
2	0,75	1,62E-18	55,76	191,58	44,29	148,01	52,56	43,57
3	-0,28	0,092	225,18	68,03	1,33	292,79	13,49	224,76
4	NaN	NaN	NaN	NaN	NaN	206,52	54,25	NaN
5	-0,86	7,66E-13	44,28	195,72	16,92	179,50	26,27	16,22
6	NaN	NaN	NaN	NaN	NaN	268,08	53,16	NaN
7	NaN	NaN	NaN	NaN	NaN	104,44	21,67	NaN
8	-0,27	0,10	135,38	224,74	6,03	174,18	125,48	50,56
9	-0,83	2,28E-13	93,56	202,57	1,80	119,92	42,79	82,65
10	0,37	0,02	19,48	200,36	0,81	202,74	19,85	2,39
11	-0,21	0,07	61,53	174,31	8,91	234,38	8,35	60,07
12	-0,68	5,11E-06	50,39	182,03	1,04	230,62	12,82	48,59
13	0,86	5,12E-30	41,51	216,75	36,59	186,69	53,12	30,05

Table 2: Statistical parameters current-bird. ConiGPS2012

A.2 ConiGPS2013

A2.2 IBI - ERA5

Maps

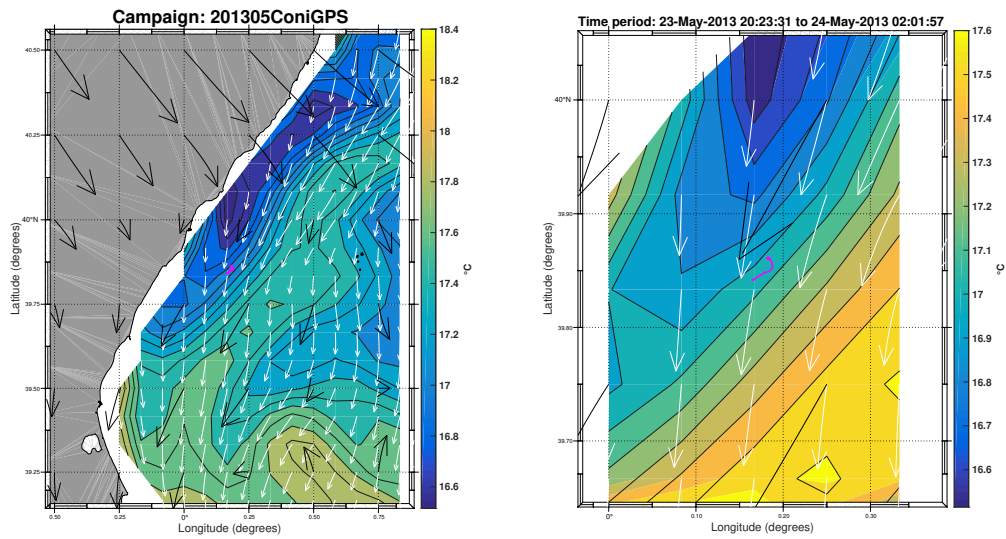


Figure 25: The same as explained in Appendix A.1 Fig: 1, now for this example from ConiGPS201305, trajectory 1, and the surface current, temperature and wind data corresponding to this seabird track analyzed here.

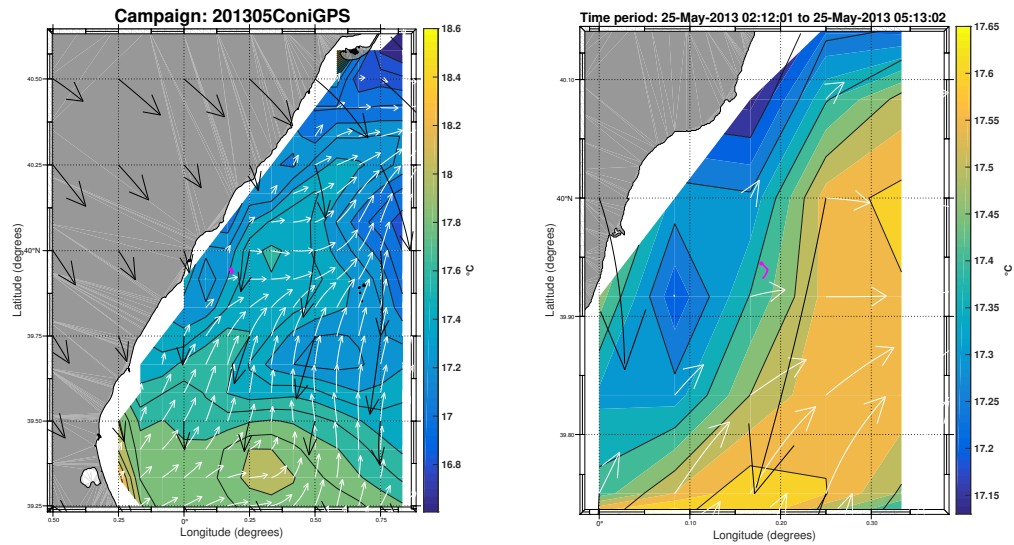


Figure 26: The same as explained in Appendix A.1 Fig: 1, now for this example from ConiGPS201305, trajectory 2, and the surface current, temperature and wind data corresponding to this seabird track analyzed here.

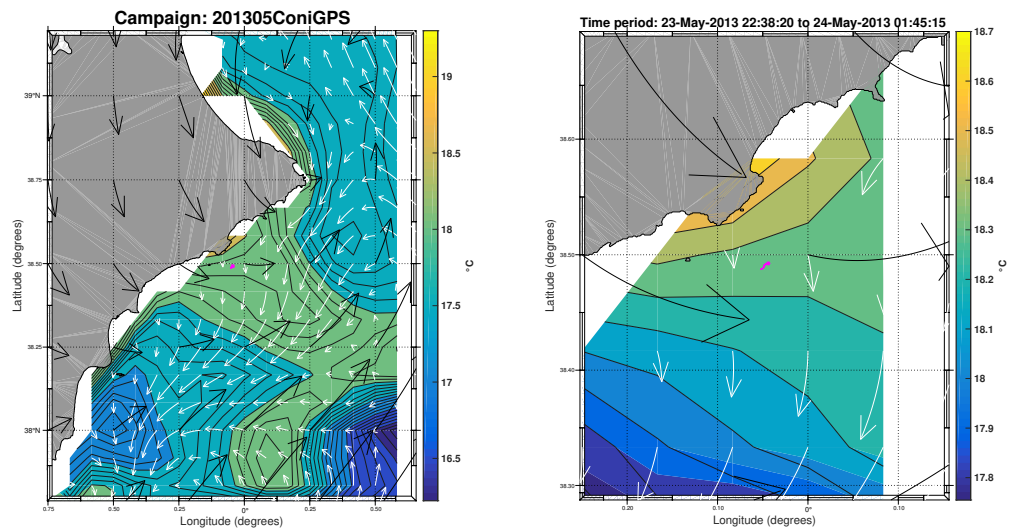


Figure 27: The same as explained in Appendix A.1 Fig: 1, now for this example from ConiGPS201305, trajectory 3, and the surface current, temperature and wind data corresponding to this seabird track analyzed here.

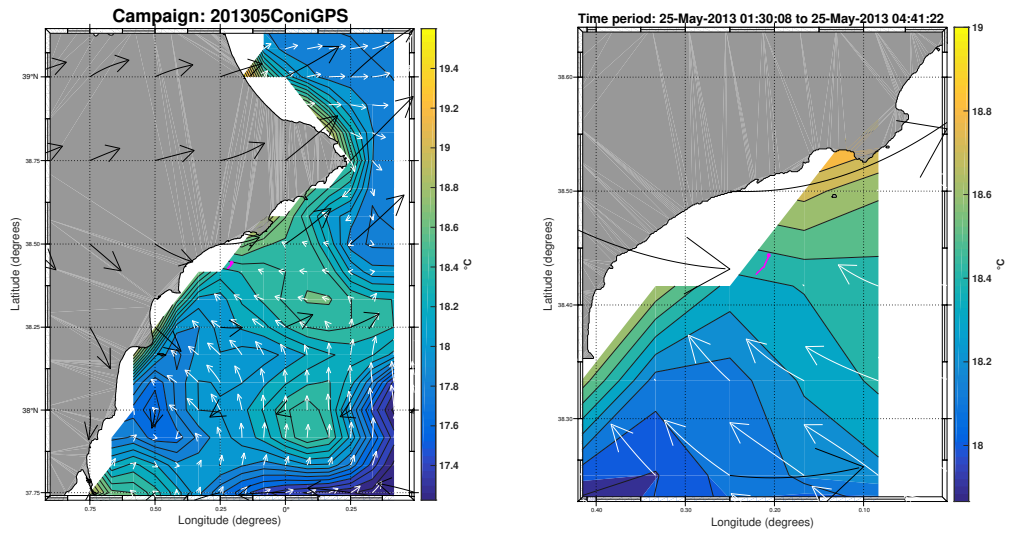


Figure 28: The same as explained in Appendix A.1 Fig: 1, now for this example from ConiGPS201305, trajectory 4, and the surface current, temperature and wind data corresponding to this seabird track analyzed here.

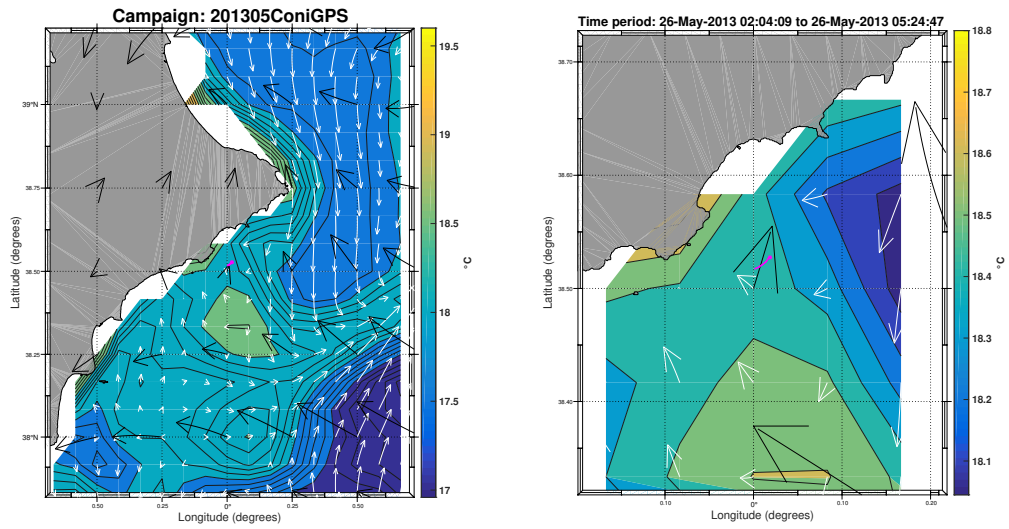


Figure 29: The same as explained in Appendix A.1 Fig: 1, now for this example from ConiGPS201305, trajectory 5, and the surface current, temperature and wind data corresponding to this seabird track analyzed here.

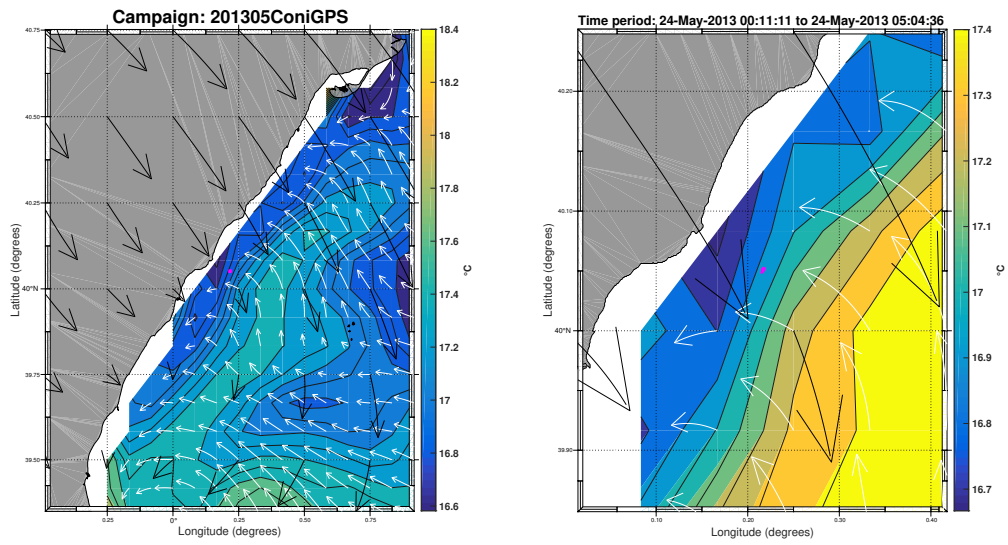


Figure 30: The same as explained in Appendix A.1 Fig: 1, now for this example from ConiGPS201305, trajectory 6, and the surface current, temperature and wind data corresponding to this seabird track analyzed here.

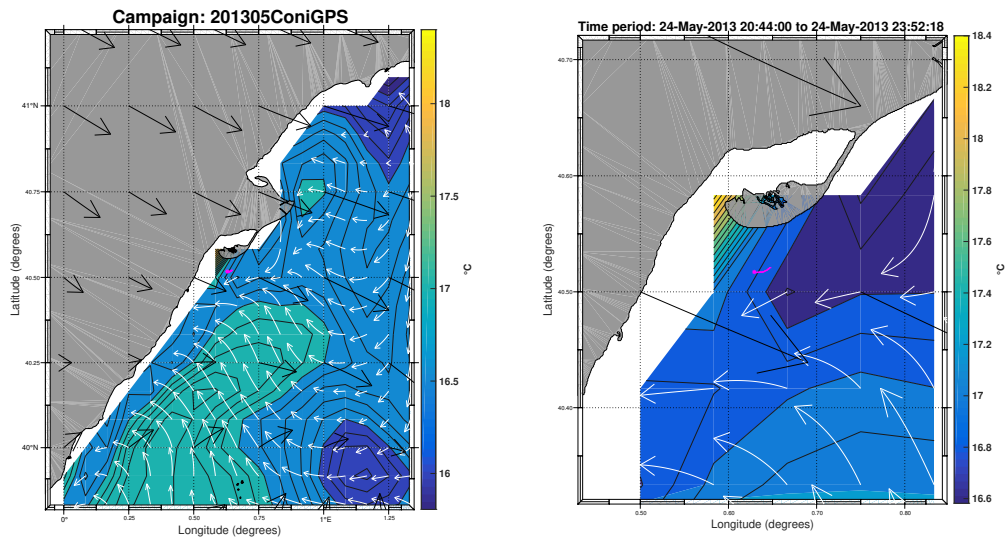


Figure 31: The same as explained in Appendix A.1 Fig: 1, now for this example from ConiGPS201305, trajectory 7, and the surface current, temperature and wind data corresponding to this seabird track analyzed here.

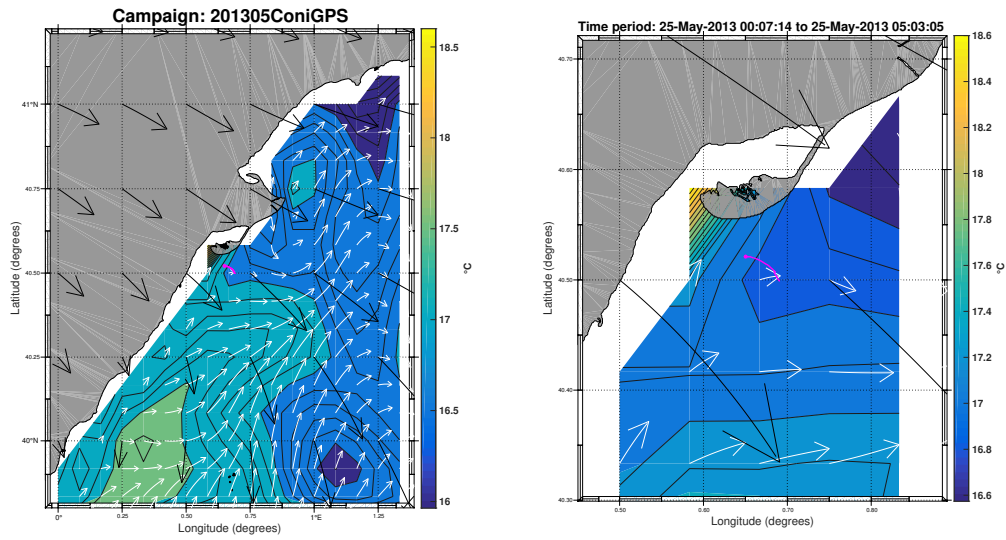


Figure 32: The same as explained in Appendix A.1 Fig: 1, now for this example from ConiGPS201305, trajectory 8, and the surface current, temperature and wind data corresponding to this seabird track analyzed here.

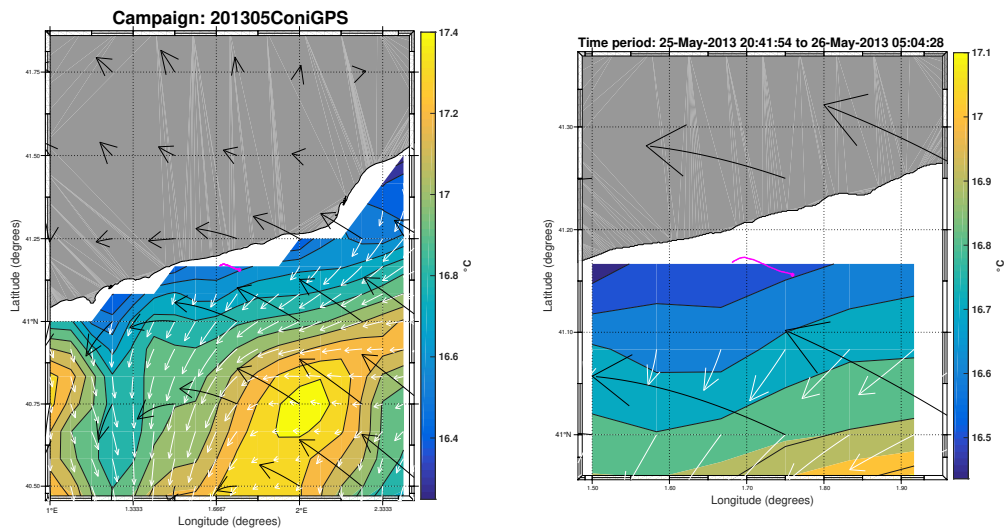


Figure 33: The same as explained in Appendix A.1 Fig: 1, now for this example from ConiGPS201305, trajectory 9, and the surface current, temperature and wind data corresponding to this seabird track analyzed here.

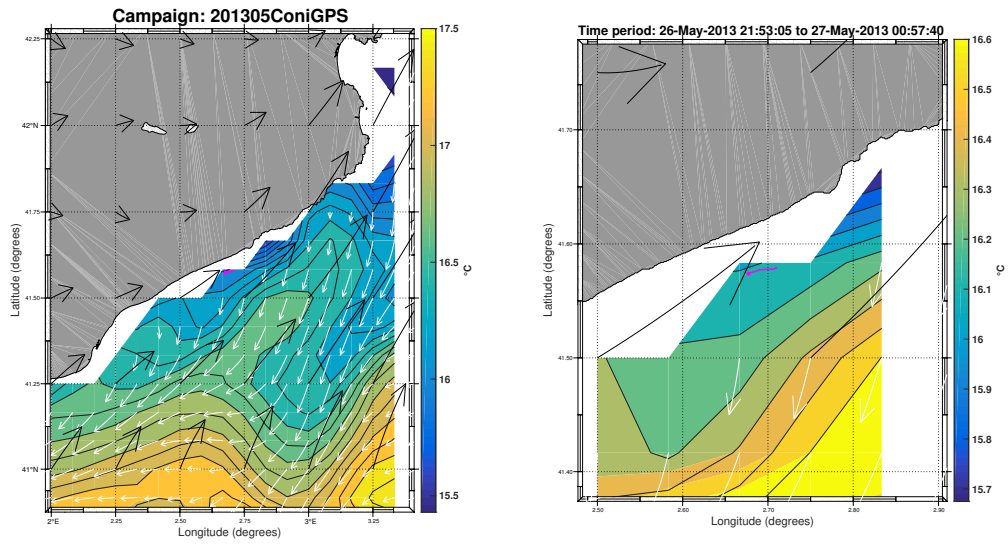


Figure 34: The same as explained in Appendix A.1 Fig: 1, now for this example from ConiGPS201305, trajectory 10, and the surface current, temperature and wind data corresponding to this seabird track analyzed here.

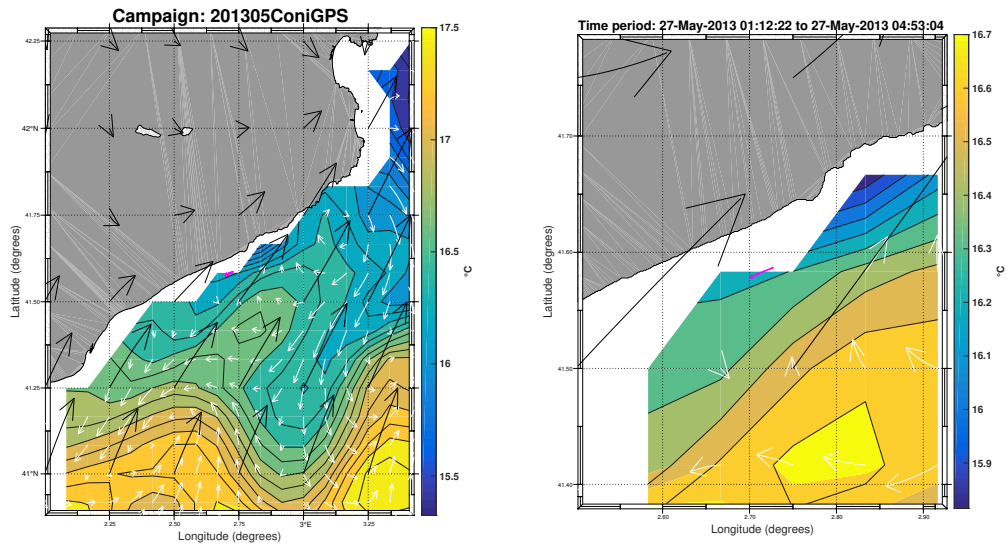


Figure 35: The same as explained in Appendix A.1 Fig: 1, now for this example from ConiGPS201305, trajectory 11, and the surface current, temperature and wind data corresponding to this seabird track analyzed here.

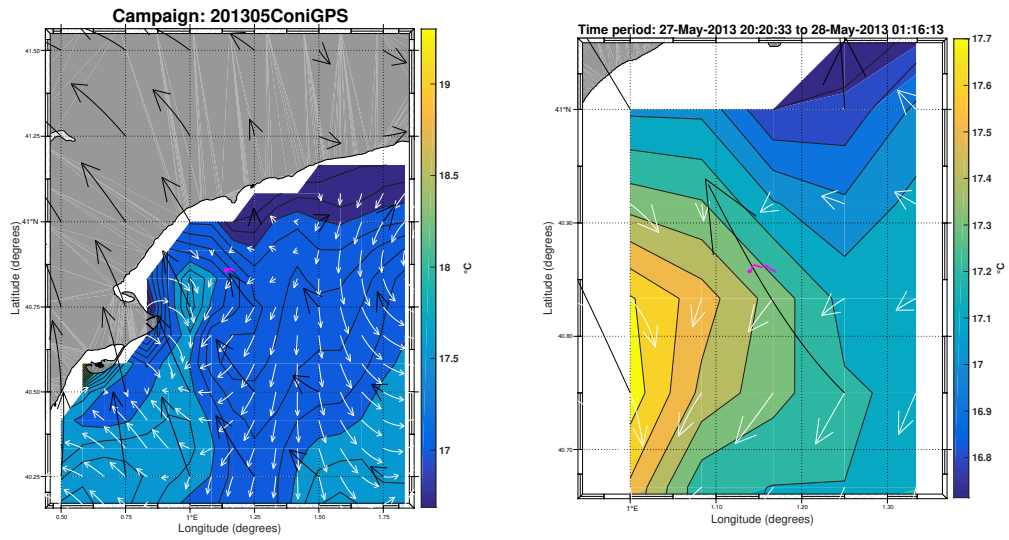


Figure 36: The same as explained in Appendix A.1 Fig: 1, now for this example from ConiGPS201305, trajectory 12, and the surface current, temperature and wind data corresponding to this seabird track analyzed here.

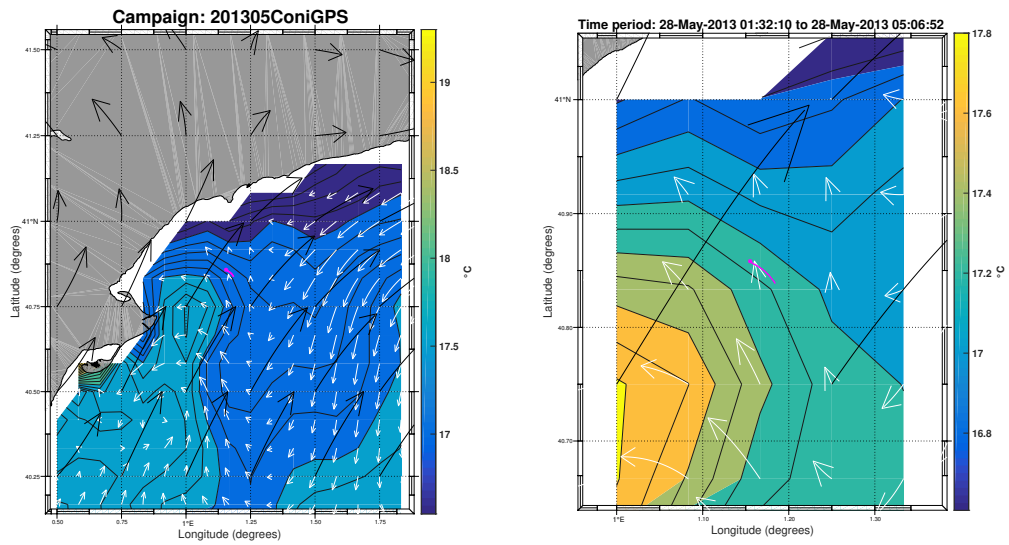


Figure 37: The same as explained in Appendix A.1 Fig: 1, now for this example from ConiGPS201305, trajectory 13, and the surface current, temperature and wind data corresponding to this seabird track analyzed here.

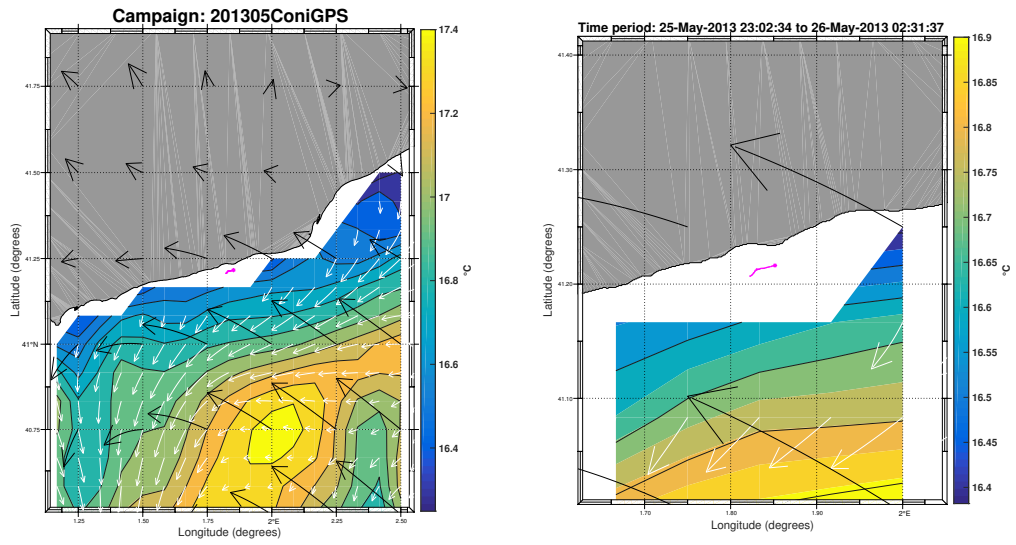


Figure 38: The same as explained in Appendix A.1 Fig: 1, now for this example from ConiGPS201305, trajectory 14, and the surface current, temperature and wind data corresponding to this seabird track analyzed here.

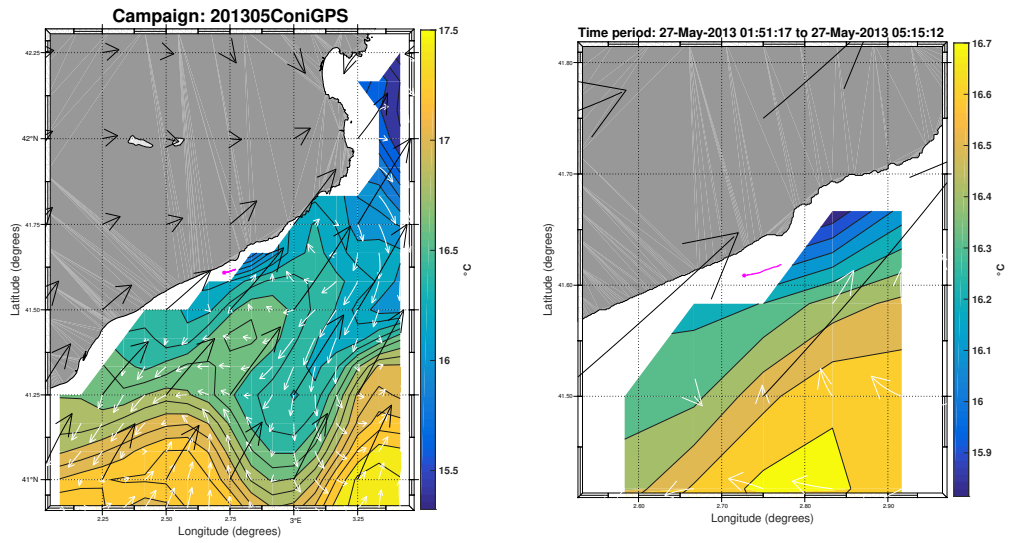


Figure 39: The same as explained in Appendix A.1 Fig: 1, now for this example from ConiGPS201305, trajectory 15, and the surface current, temperature and wind data corresponding to this seabird track analyzed here.

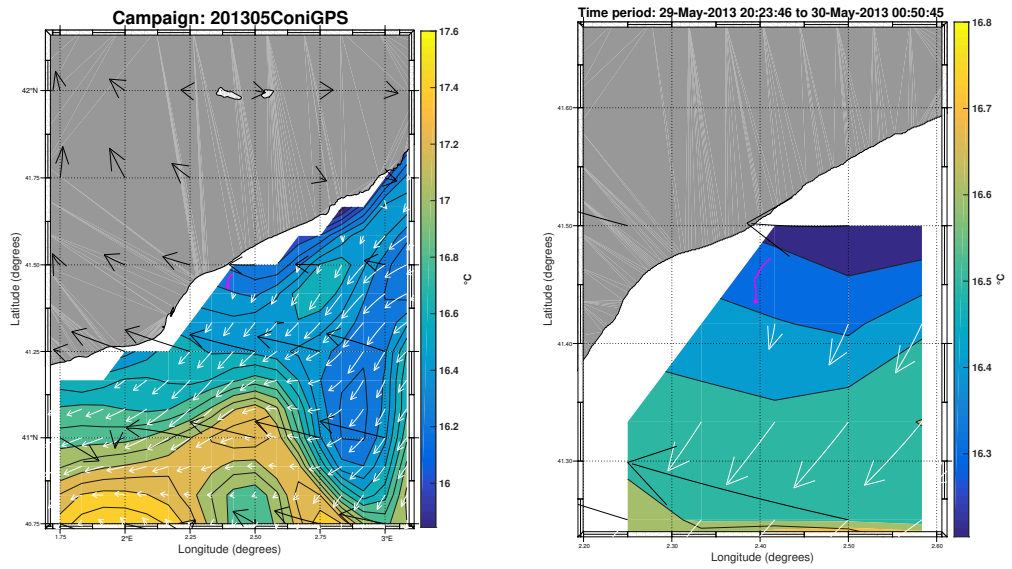


Figure 40: The same as explained in Appendix A.1 Fig: 1, now for this example from ConiGPS201305, trajectory 16, and the surface current, temperature and wind data corresponding to this seabird track analyzed here.

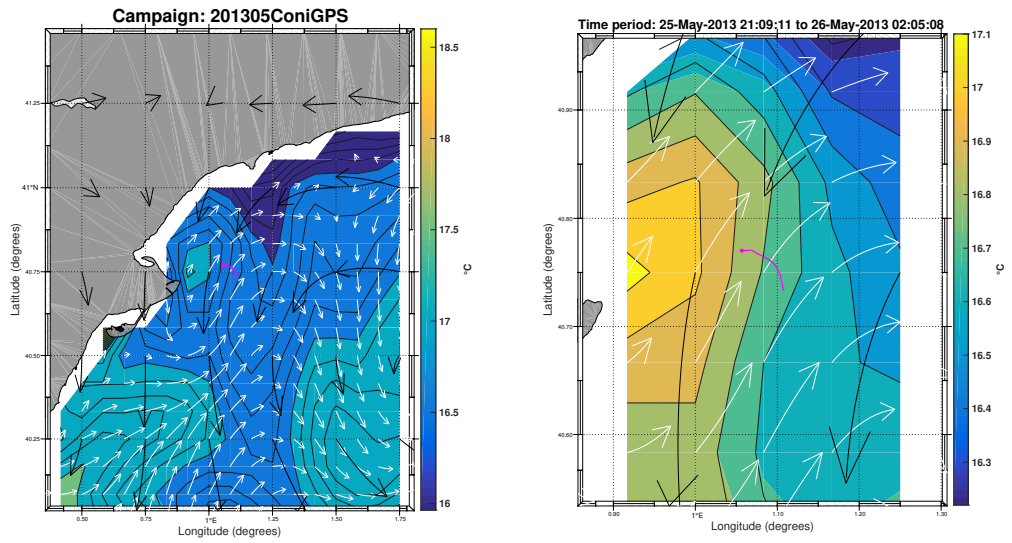


Figure 41: The same as explained in Appendix A.1 Fig: 1, now for this example from ConiGPS201305, trajectory 17, and the surface current, temperature and wind data corresponding to this seabird track analyzed here.

Temporal series

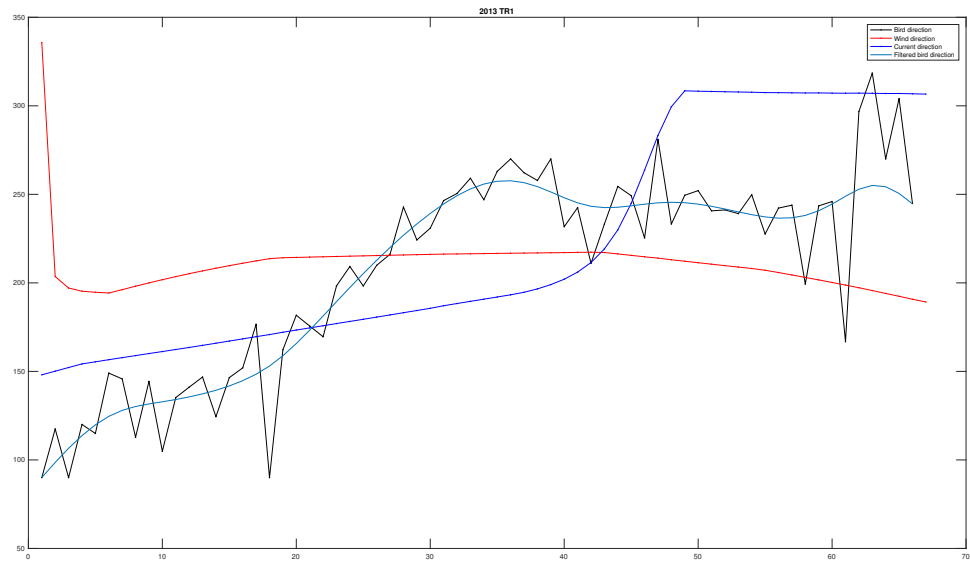


Figure 42: The same as in Appendix A.1 Fig: 14 but for ConiGPS2013 trajectory 1.

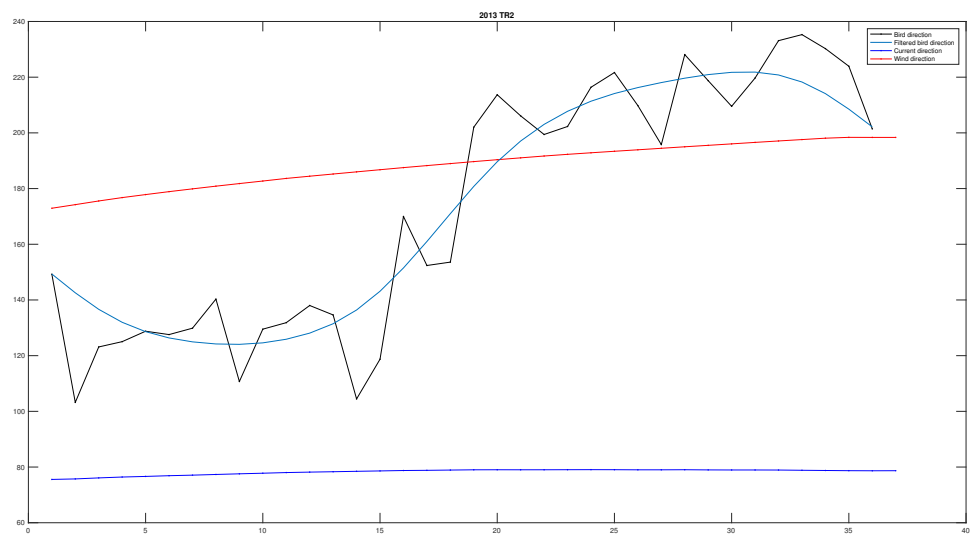


Figure 43: The same as in Appendix A.1 Fig: 14 but for ConiGPS2013 trajectory 2.

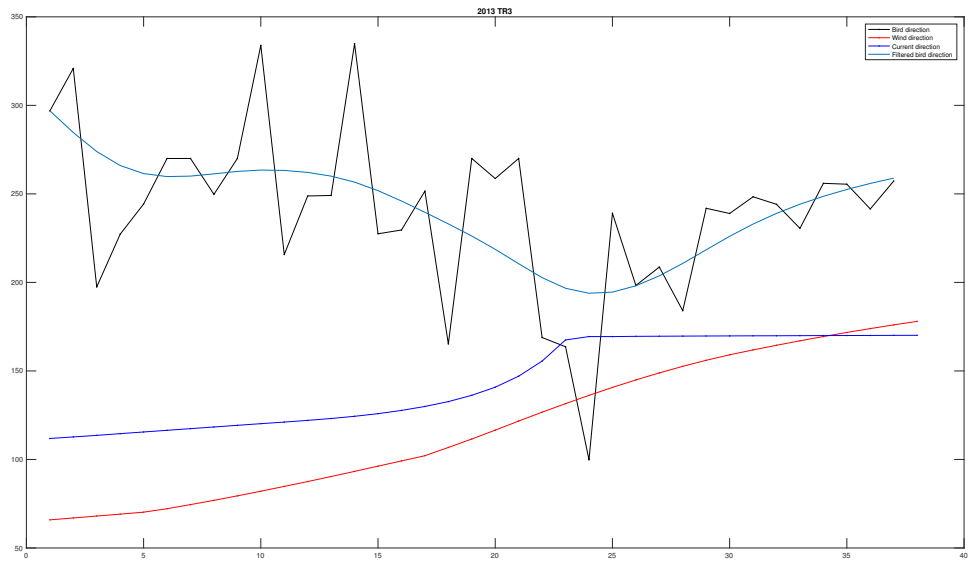


Figure 44: The same as in Appendix A.1 Fig: 14 but for ConiGPS201305 trajectory 3.

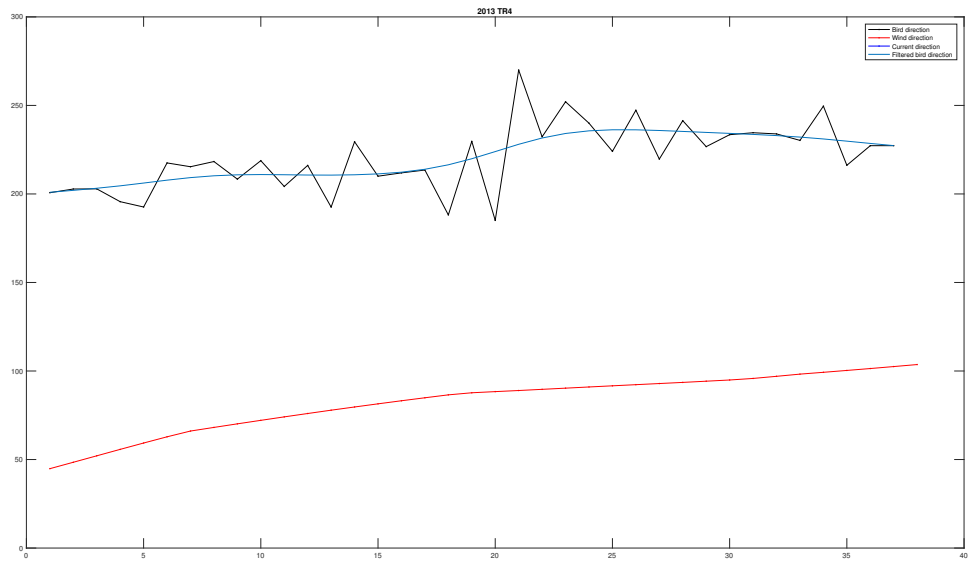


Figure 45: The same as in Appendix A.1 Fig: 14 but for ConiGPS201305 trajectory 4.

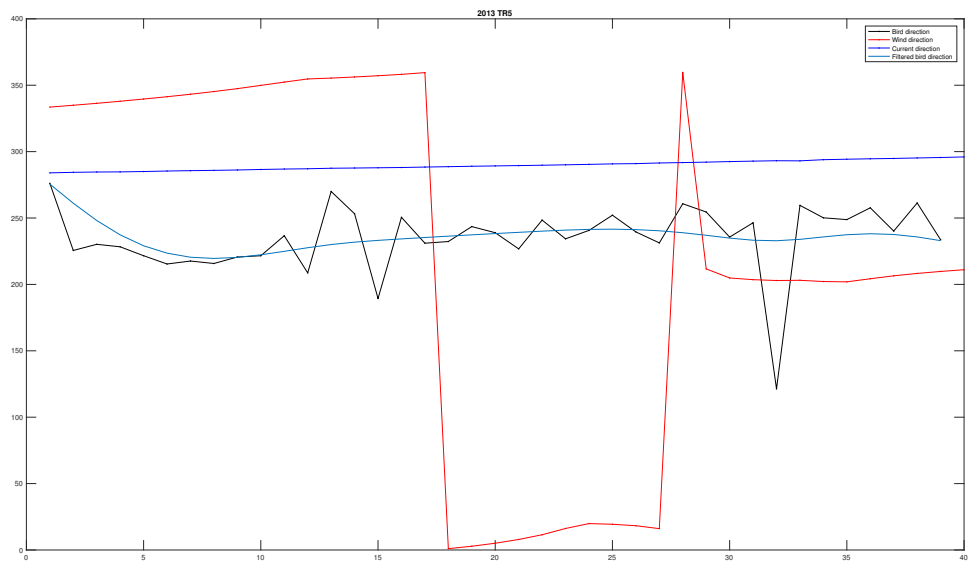


Figure 46: The same as in Appendix A.1 Fig: 14 but for ConiGPS201305 trajectory 5.

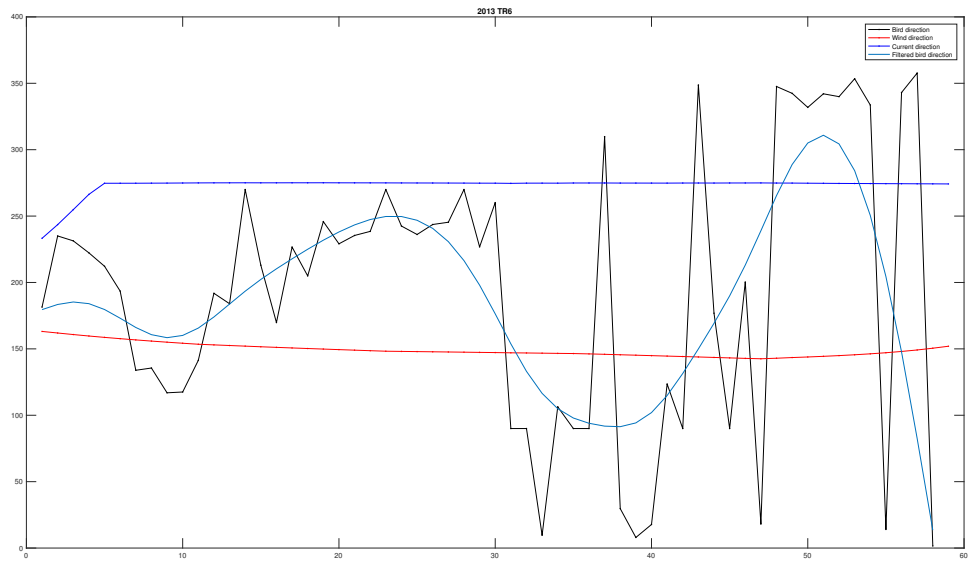


Figure 47: The same as in Appendix A.1 Fig: 14 but for ConiGPS2013 trajectory 6.

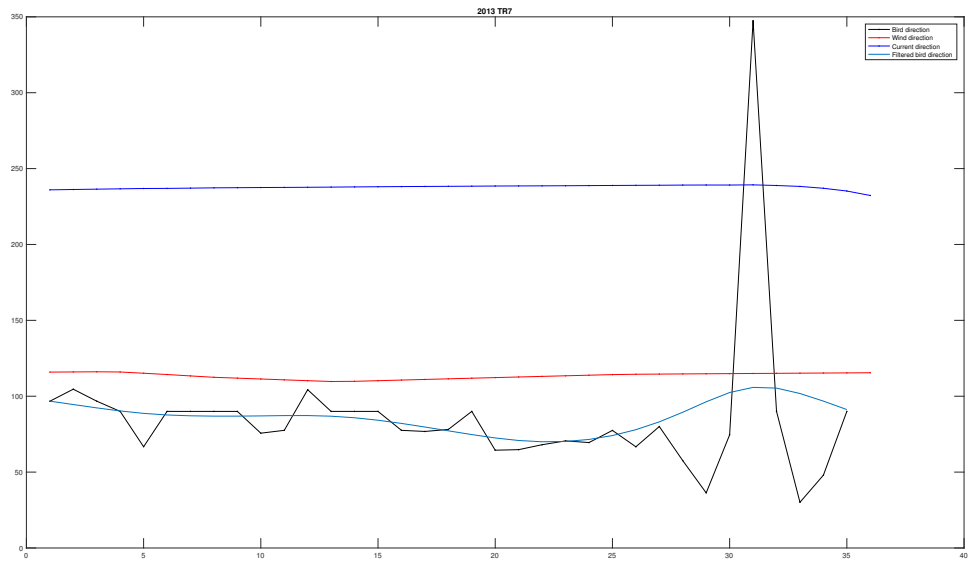


Figure 48: The same as in Appendix A.1 Fig: 14 but for ConiGPS201305 trajectory 7.

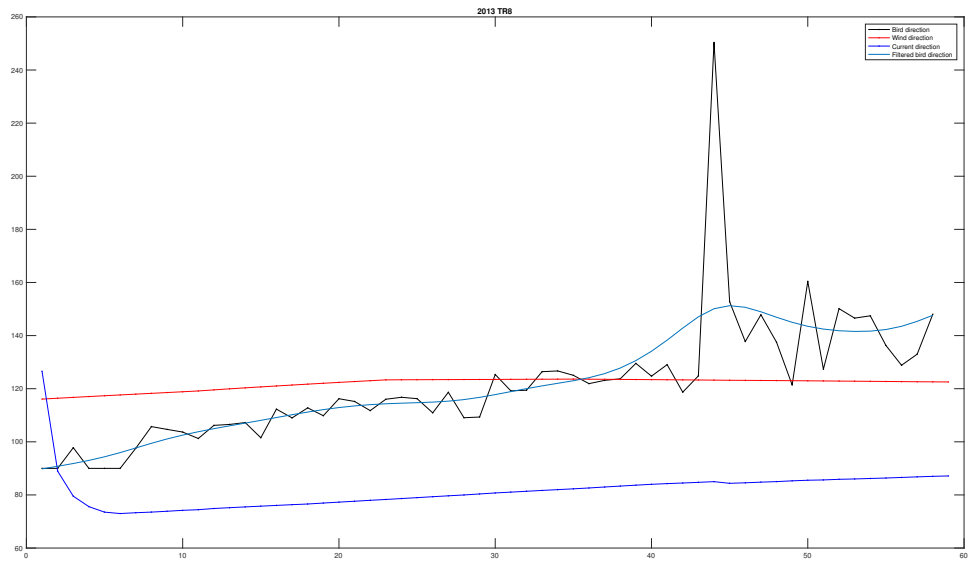


Figure 49: The same as in Appendix A.1 Fig: 14 but for ConiGPS201305 trajectory 8.

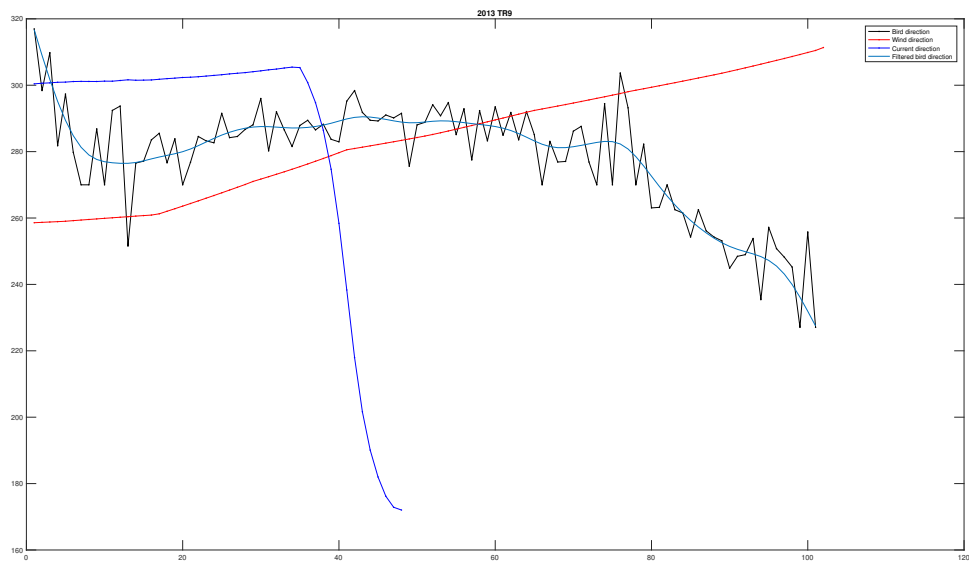


Figure 50: The same as in Appendix A.1 Fig: 14 but for ConiGPS201305 trajectory 9.

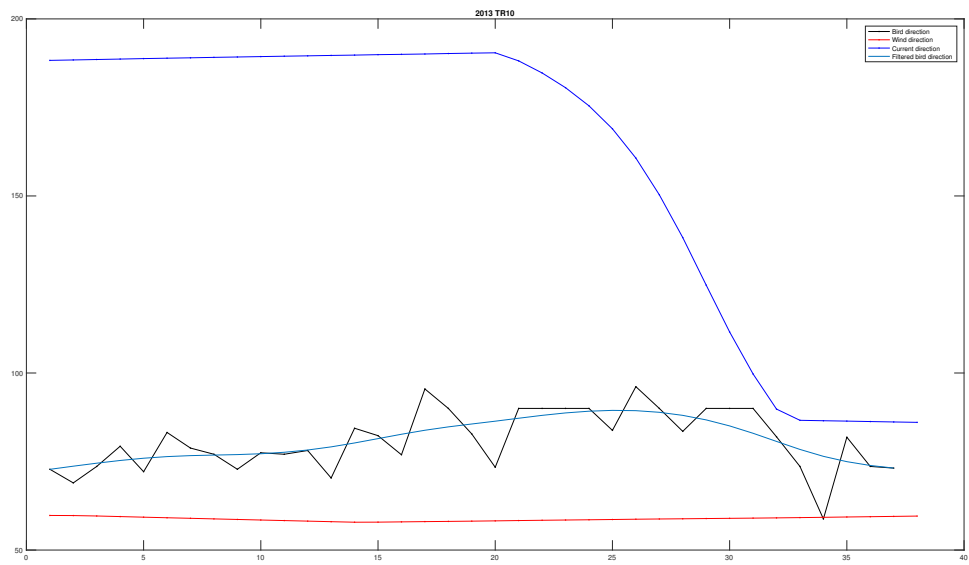


Figure 51: The same as in Appendix A.1 Fig: 14 but for ConiGPS2013 trajectory 10.

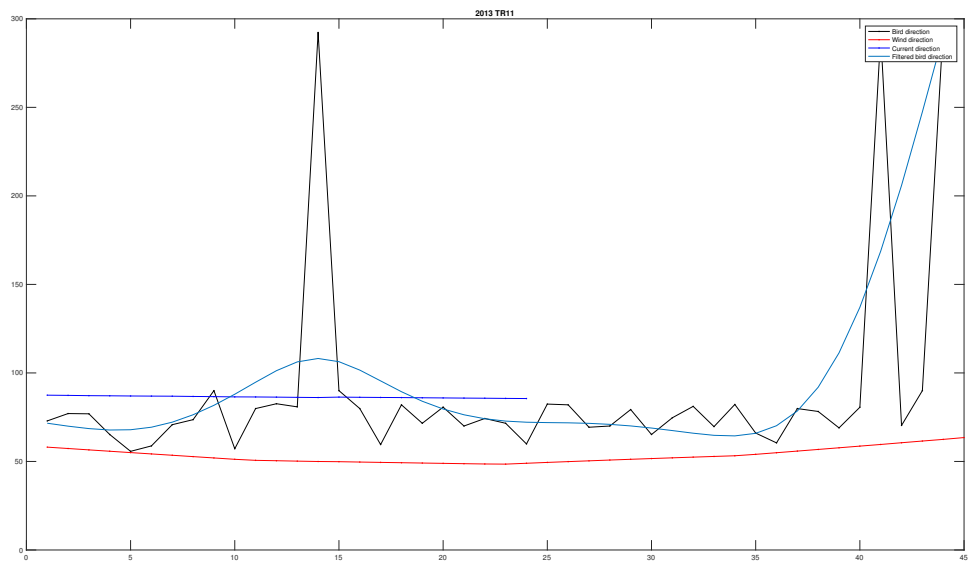


Figure 52: The same as in Appendix A.1 Fig: 14 but for ConiGPS2013 trajectory 11.

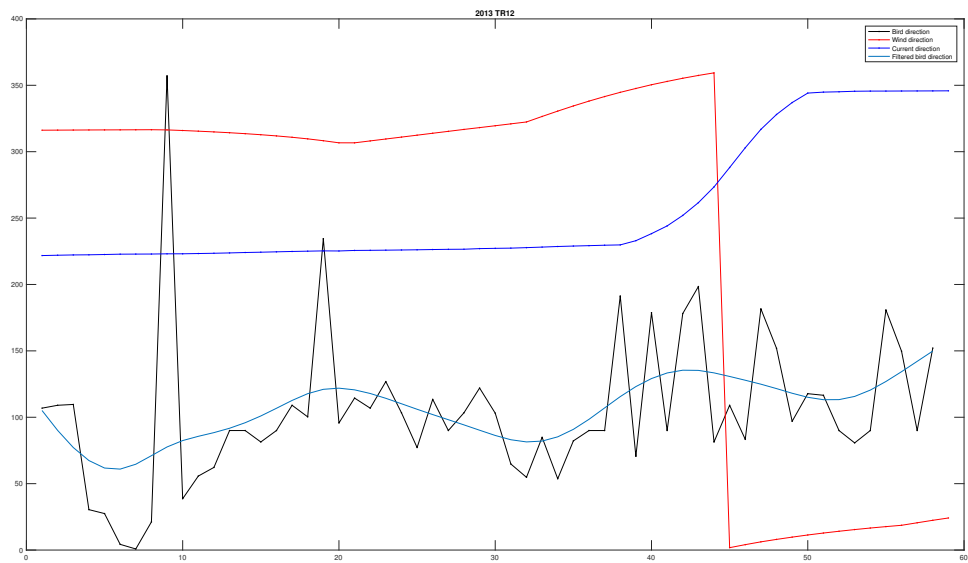


Figure 53: The same as in Appendix A.1 Fig: 14 but for ConiGPS2013 trajectory 12.

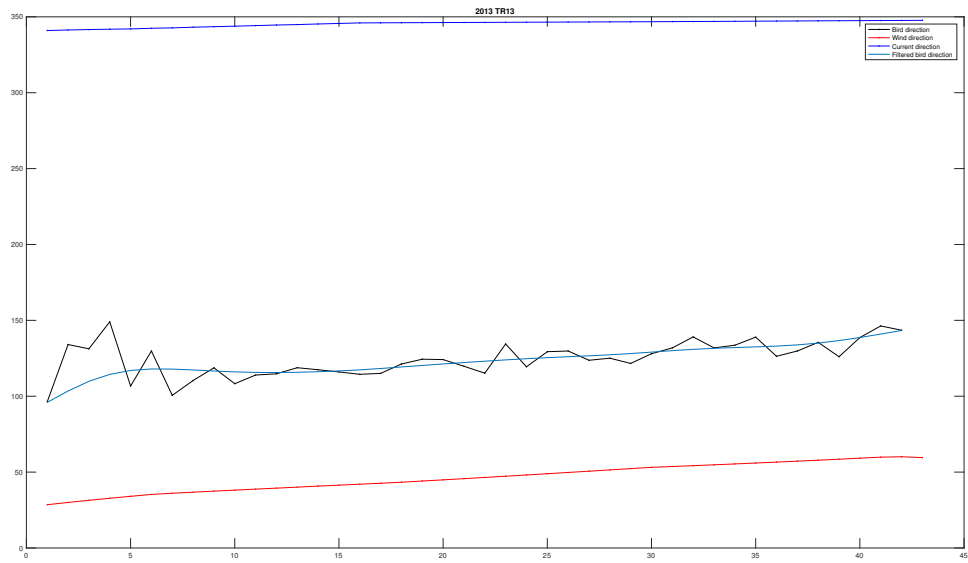


Figure 54: The same as in Appendix A.1 Fig: 14 but for ConiGPS201305 trajectory 13.

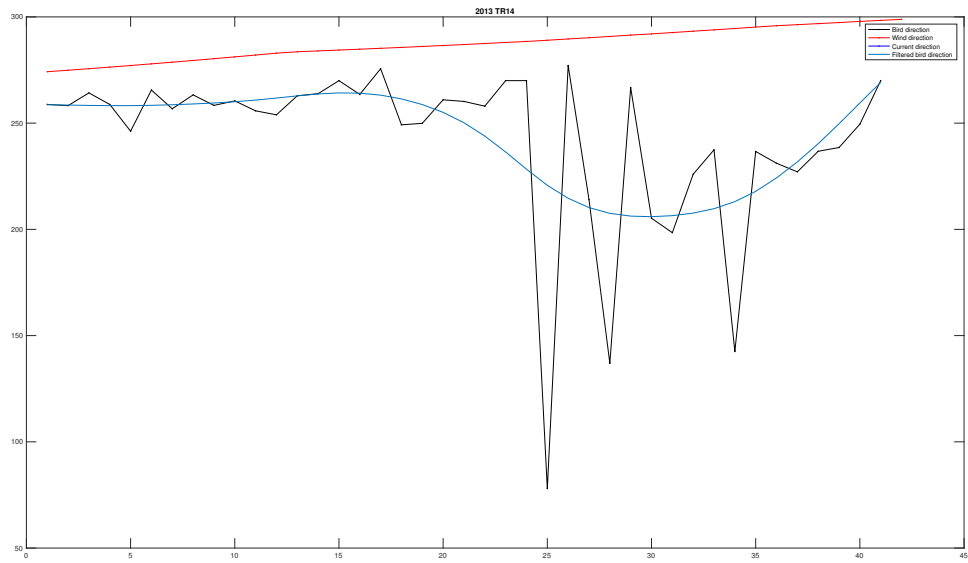


Figure 55: The same as in Appendix A.1 Fig: 14 but for ConiGPS201305 trajectory 14.

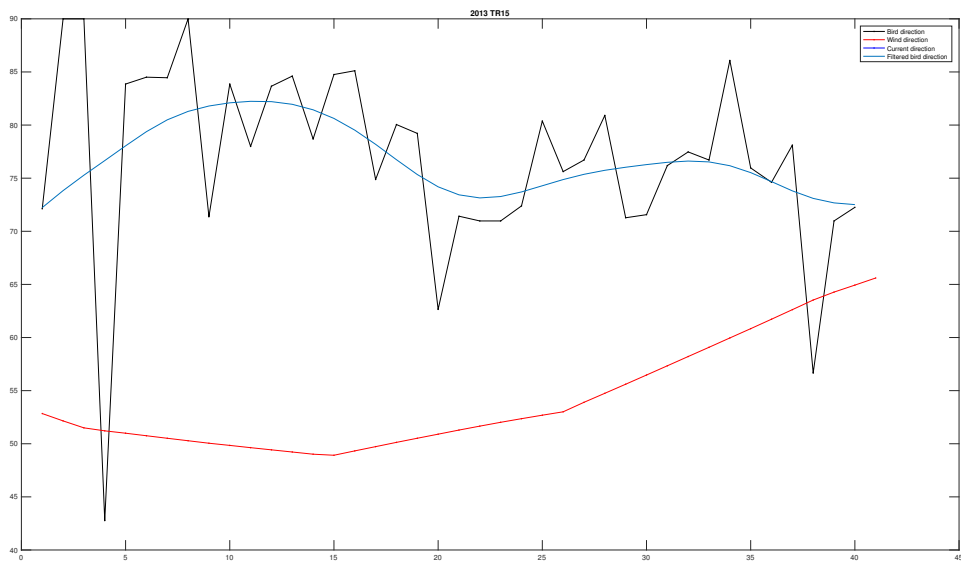


Figure 56: The same as in Appendix A.1 Fig: 14 but for ConiGPS201305 trajectory 15.

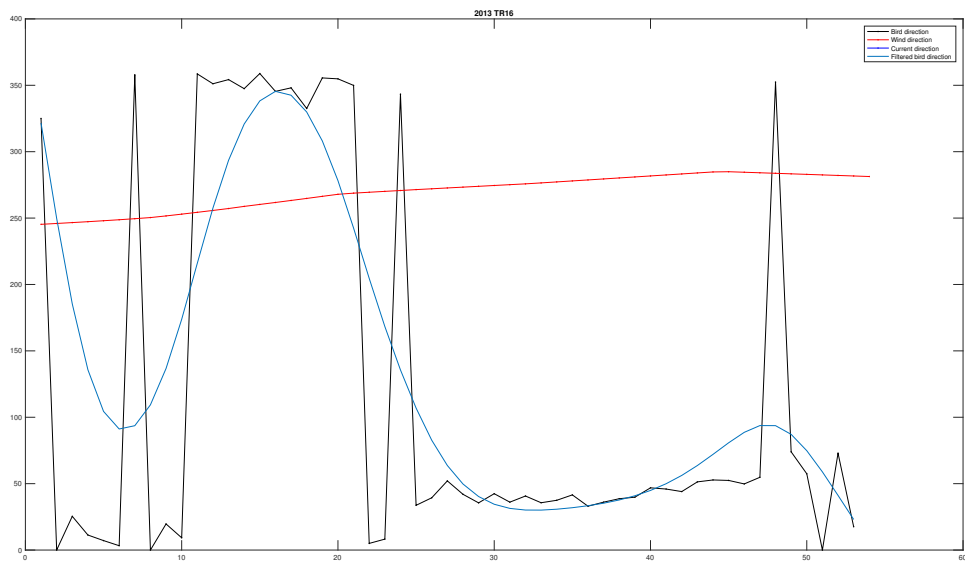


Figure 57: The same as in Appendix A.1 Fig: 14 but for ConiGPS2013 trajectory 16.

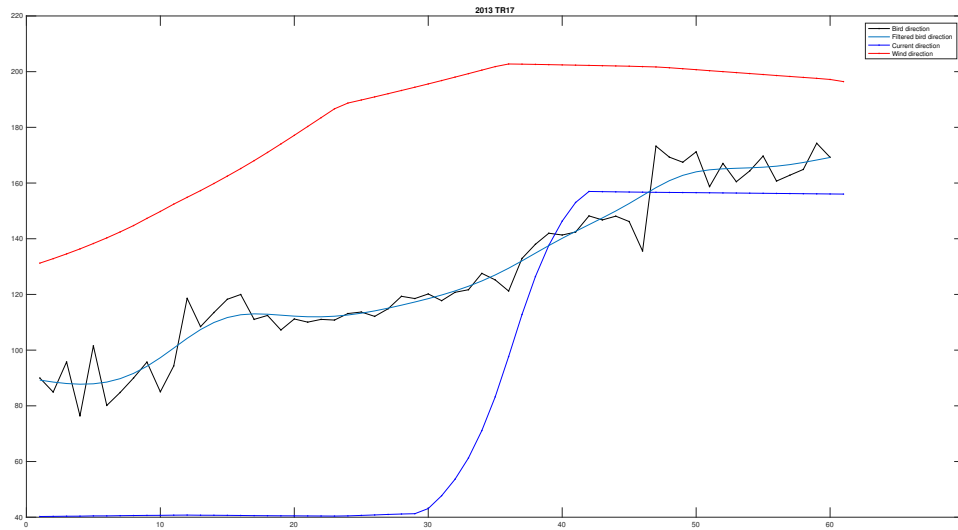


Figure 58: The same as in Appendix A.1 Fig: 14 but for ConiGPS2013 trajectory 17.

Tables

Trajectory	Rw	Pw	RMSEw	meanW	stdW	meanB	stdB	difW
1	-0,09	0,49	56,98	210,81	17,55	205,87	52,95	4,94
2	0,88	0,00	35,57	188,19	7,61	173,55	39,39	49,64
3	-0,57	0,00	137,08	116,66	37,71	241,49	26,96	124,83
4	0,88	4,17E-13	138,87	81,99	15,82	220,66	12,22	138,67
5	-0,24	0,14	140,51	221,53	138,81	235,90	10,22	14,37
6	-0,11	0,41	74,02	149,14	5,13	186,49	63,69	37,35
7	0,44	0,01	28,51	113,35	2,01	86,36	10,02	26,99
8	0,74	3,13E-11	16,77	121,81	2,27	121,59	18,53	0,23
9	-0,64	4,36E-13	29,82	283,55	16,33	286,14	7,92	5,37
10	-0,55	0,00	23,00	58,75	0,55	81,02	5,54	22,26
11	0,62	6,55E-06	60,97	53,06	3,86	83,16	13,88	41,28
12	-0,47	0,0002	202,86	247,84	134,42	105,67	21,85	142,17
13	0,96	2,13E-23	77,26	46,08	9,11	123,28	9,75	77,21
14	-0,57	0,00	51,40	287,00	7,00	242,86	22,02	44,15
15	-0,57	0,00	23,92	53,83	4,82	76,69	3,17	22,86
16	-0,59	2,90E-06	177,42	269,47	12,98	131,90	104,93	137,57
17	0,82	1,88E-75	57,35	182,50	23,68	127,27	26,73	55,23
18	-0,45	0,00	94,39	10,41	3,72	103,87	11,32	93,45

Table 3: Statistical parameters wind-bird. ConiGPS2013

Trajectory	Rc	Pc	RMSEc	meanC	stdC	meanB	sdtB	difC
1	0,69	2,04E-10	47,38	219,07	61,20	205,87	52,95	13,1997
2	0,70	0,00	102,66	78,23	1,06	173,55	39,39	95,3218
3	-0,70	1,34E-06	108,85	143,00	23,97	241,49	26,96	98,4926
4	NaN	NaN	NaN	NaN	NaN	NaN	NaN	NaN
5	-0,02	0,91	54,63	289,47	3,43	235,90	10,22	53,5741
6	0,02	0,87	107,33	273,09	7,26	186,49	63,69	86,6040
7	-0,24	0,17	151,89	237,91	1,03	86,36	10,02	151,5527
8	0,29	0,03	43,82	81,49	7,50	121,59	18,53	40,0974
9	-0,22	0,13	43,91	282,32	41,75	286,14	7,92	3,8197
10	0,10	0,55	90,20	161,97	40,51	81,02	5,54	80,9543
11	-0,35	0,09	14,17	86,42	0,55	83,16	13,88	3,2598
12	0,58	1,50E-06	153,47	254,23	47,32	105,67	21,85	148,5622
13	0,85	6,20E-13	222,36	345,50	1,98	123,28	9,75	222,2188
14	NaN	NaN	NaN	NaN	NaN	NaN	NaN	NaN
15	NaN	NaN	NaN	NaN	NaN	NaN	NaN	NaN
16	NaN	NaN	NaN	NaN	NaN	NaN	NaN	NaN
17	0,93	5,71E-27	49,67	88,09	54,06	127,27	26,73	39,1832
18	-0,52	0,00	118,76	221,95	2,50	103,87	11,32	118,0836

Table 4: Statistical parameters current-bird. ConiGPS2013

A.3 ConiGPS201405

A.3.1 IBI - ERA5

Maps

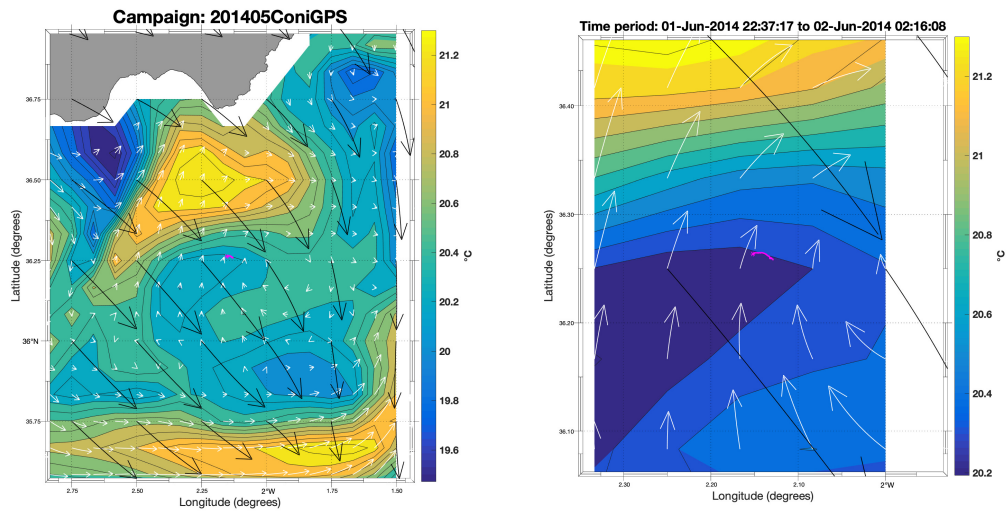


Figure 1: The same as explained in Appendix A.1 Fig:1, now for this example from ConiGPS201405, trajectory 1, and the surface current, temperature and wind data corresponding to this seabird track analyzed here.

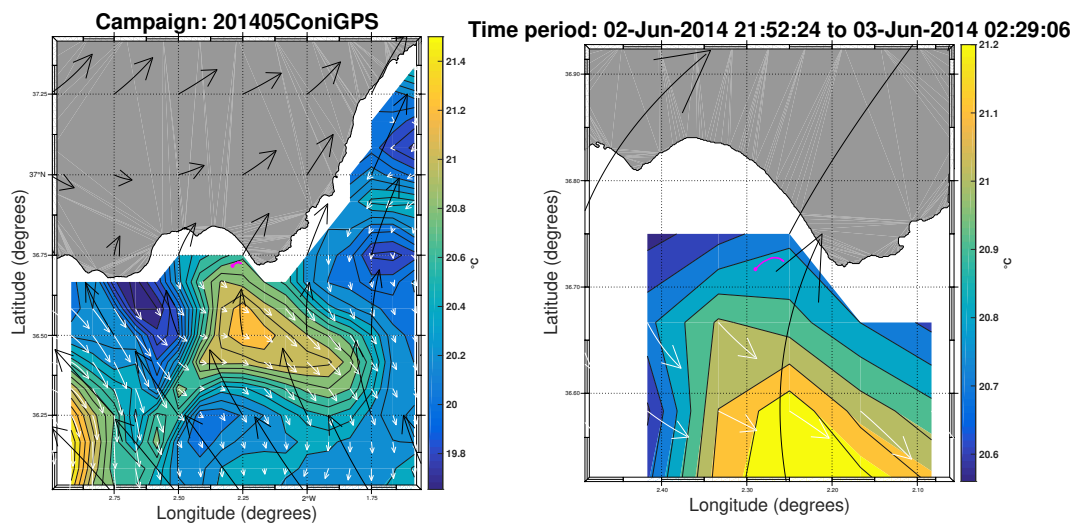


Figure 2: The same as explained in Appendix A.1 Fig:1, now for this example from ConiGPS201405, trajectory 2, and the surface current, temperature and wind data corresponding to this seabird track analyzed here.

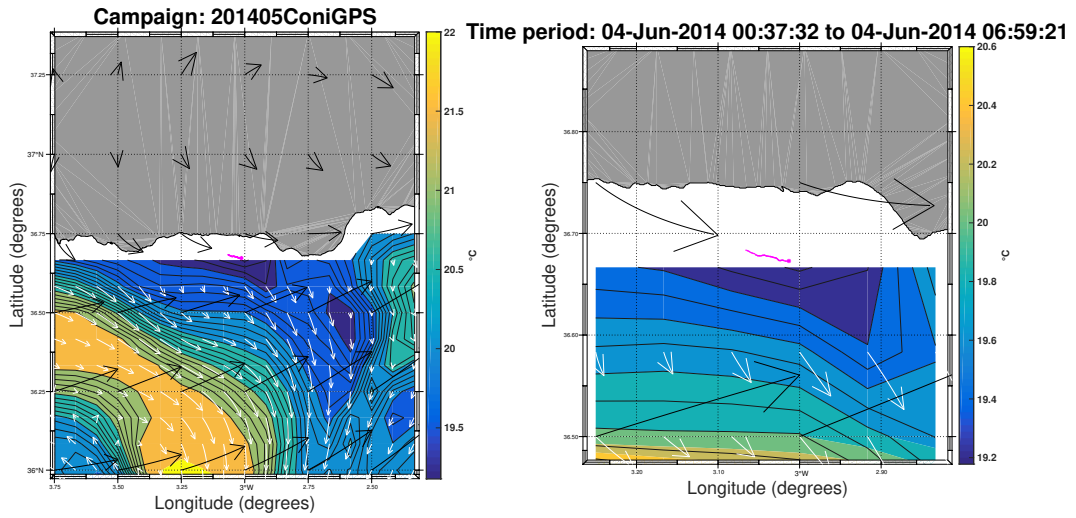


Figure 3: The same as explained in Appendix A.1 Fig:1, now for this example from ConiGPS201405, trajectory 3, and the surface current, temperature and wind data corresponding to this seabird track analyzed here.

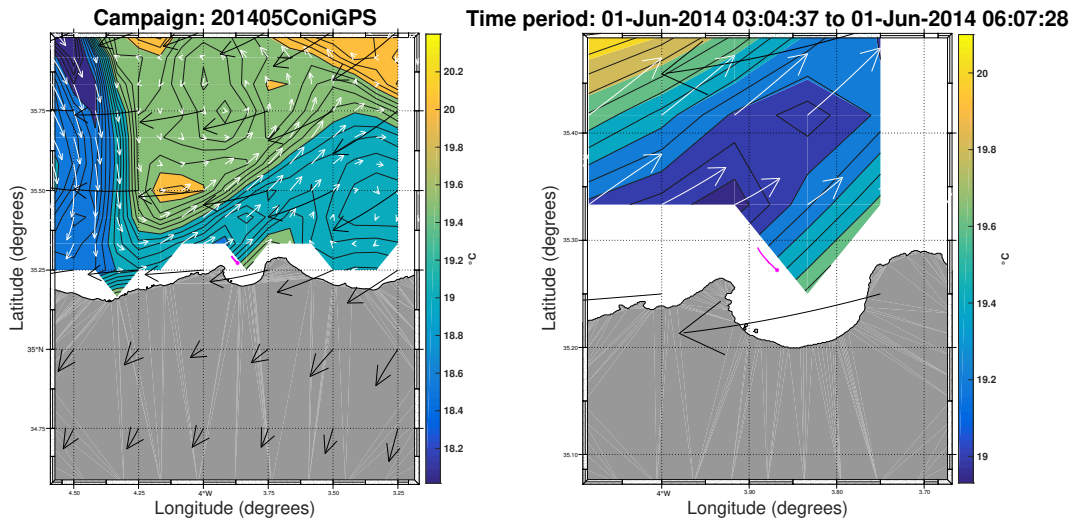


Figure 4: The same as explained in Appendix A.1 Fig:1, now for this example from ConiGPS201405, trajectory 4, and the surface current, temperature and wind data corresponding to this seabird track analyzed here.

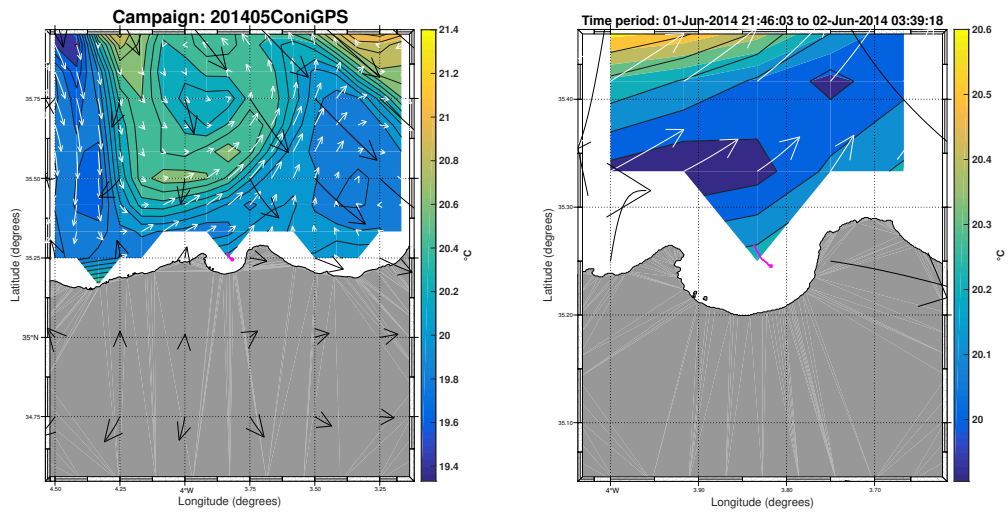


Figure 5: The same as explained in Appendix A.1 Fig:1, now for this example from ConiGPS201405, trajectory 5, and the surface current, temperature and wind data corresponding to this seabird track analyzed here.

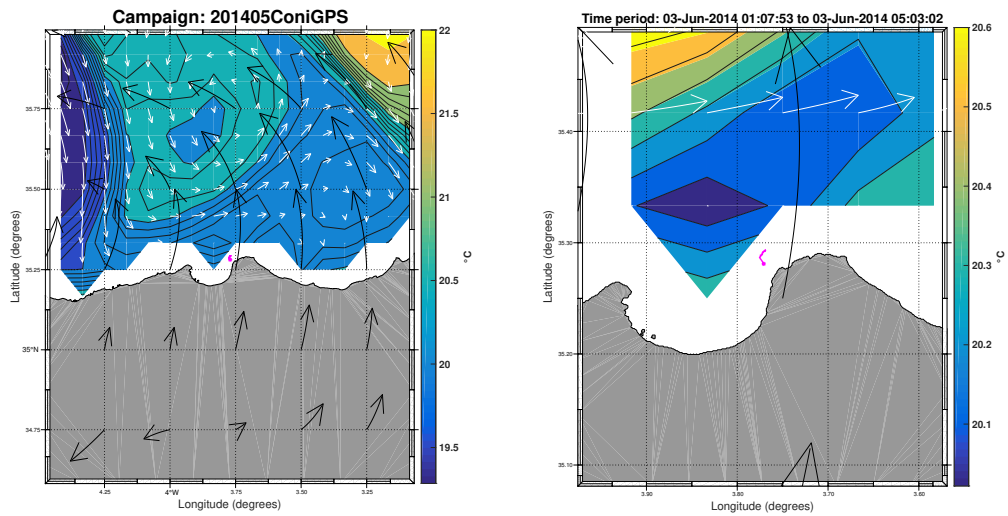


Figure 6: The same as explained in Appendix A.1 Fig:1, now for this example from ConiGPS201405, trajectory 6, and the surface current, temperature and wind data corresponding to this seabird track analyzed here.

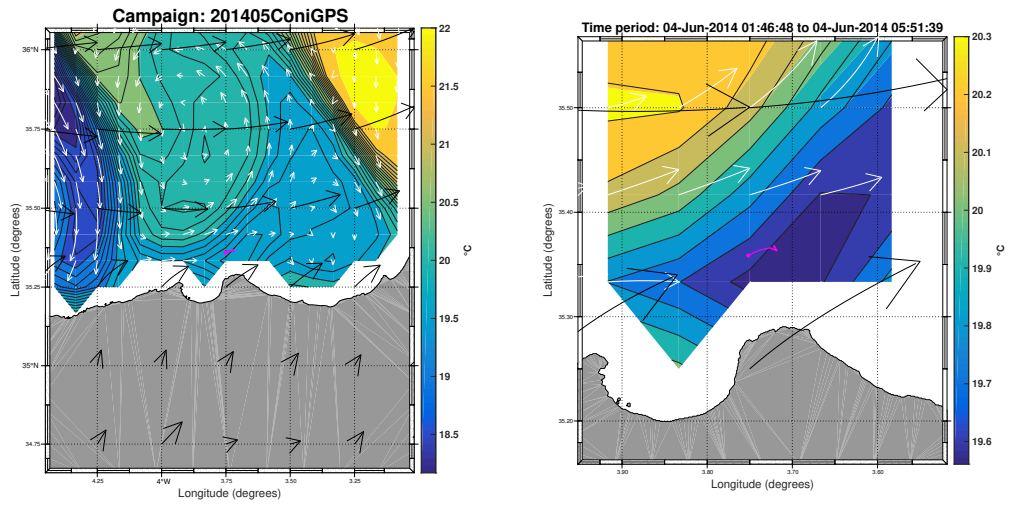


Figure 7: The same as explained in Appendix A.1 Fig:1, now for this example from ConiGPS201405, trajectory 7, and the surface current, temperature and wind data corresponding to this seabird track analyzed here.

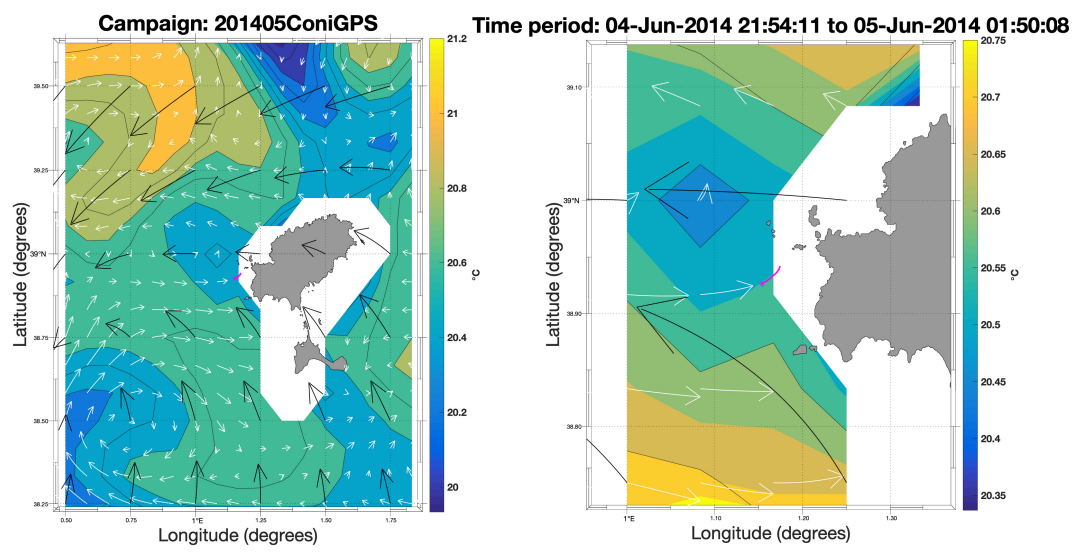


Figure 8: The same as explained in Appendix A.1 Fig:1, now for this example from ConiGPS201405, trajectory 8, and the surface current, temperature and wind data corresponding to this seabird track analyzed here.

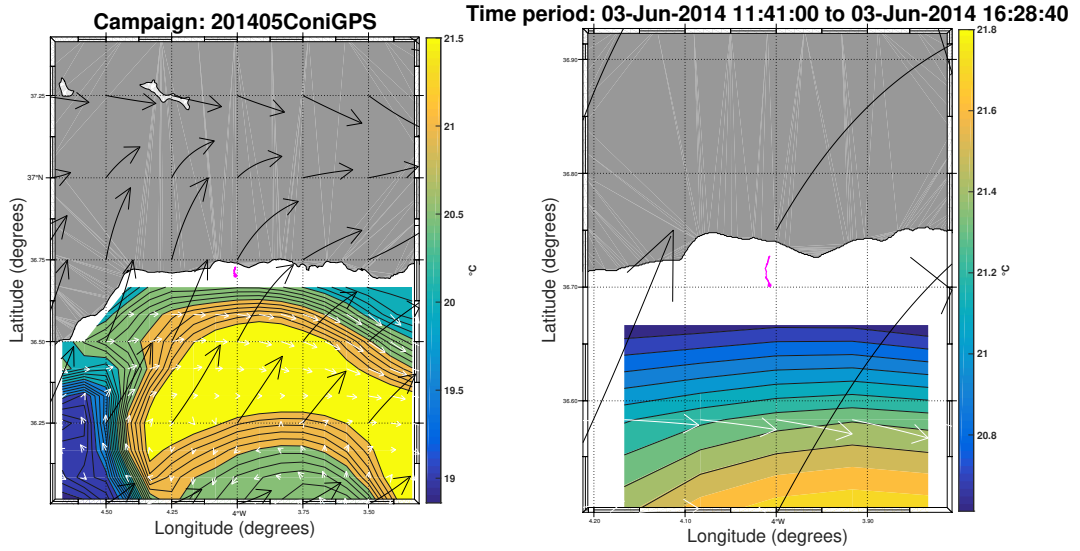


Figure 9: The same as explained in Appendix A.1 Fig:1, now for this example from ConiGPS201405, trajectory 9, and the surface current, temperature and wind data corresponding to this seabird track analyzed here.

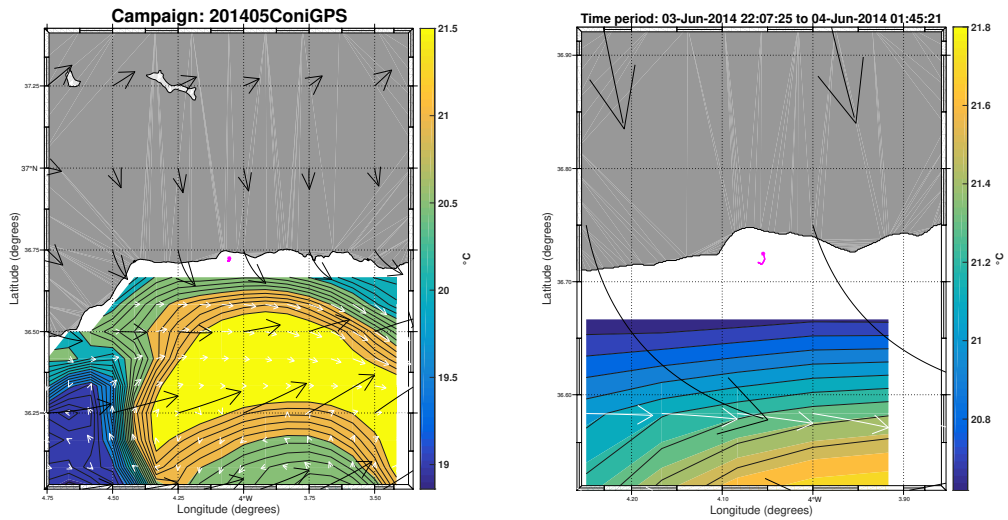


Figure 10: The same as explained in Appendix A.1 Fig:1, now for this example from ConiGPS201405, trajectory 10, and the surface current, temperature and wind data corresponding to this seabird track analyzed here.

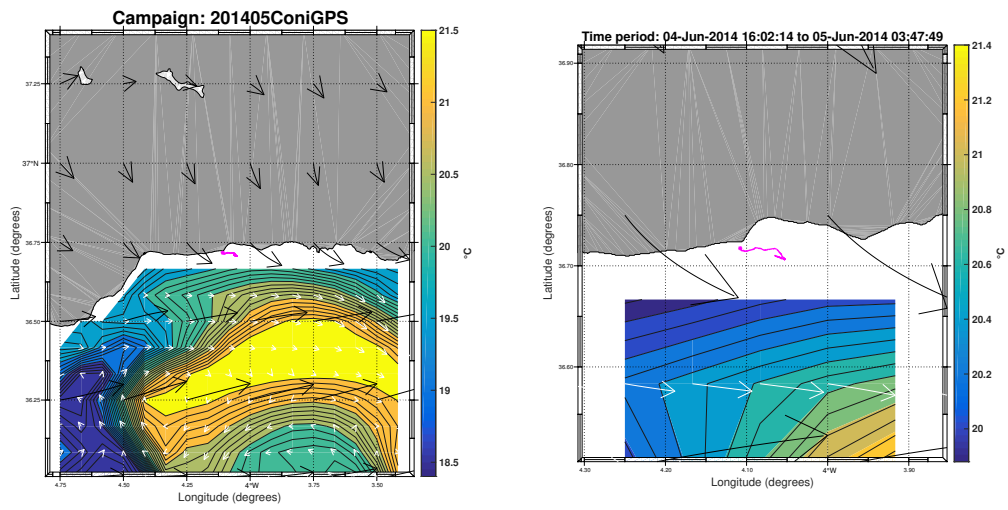


Figure 11: The same as explained in Appendix A.1 Fig:1, now for this example from ConiGPS201405, trajectory 11, and the surface current, temperature and wind data corresponding to this seabird track analyzed here.

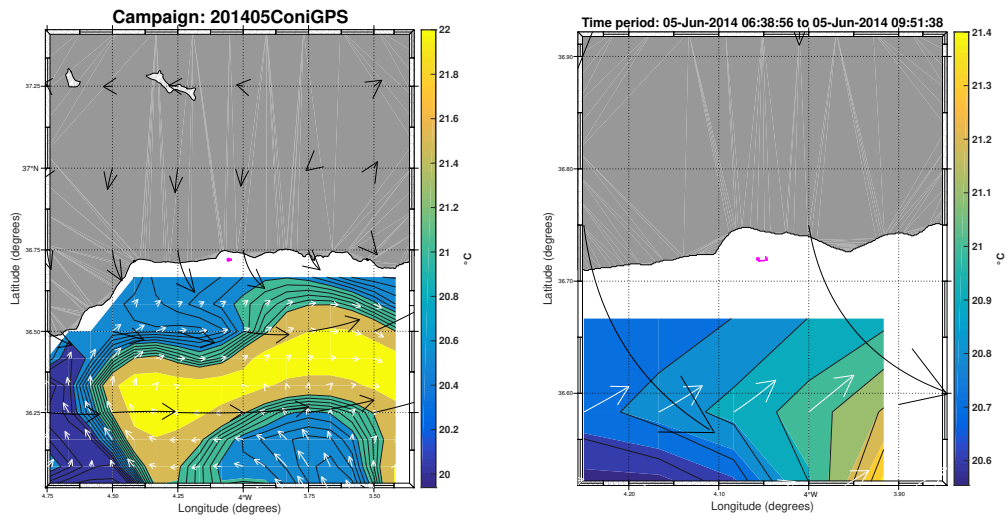


Figure 12: The same as explained in Appendix A.1 Fig:1, now for this example from ConiGPS201405, trajectory 12, and the surface current, temperature and wind data corresponding to this seabird track analyzed here.

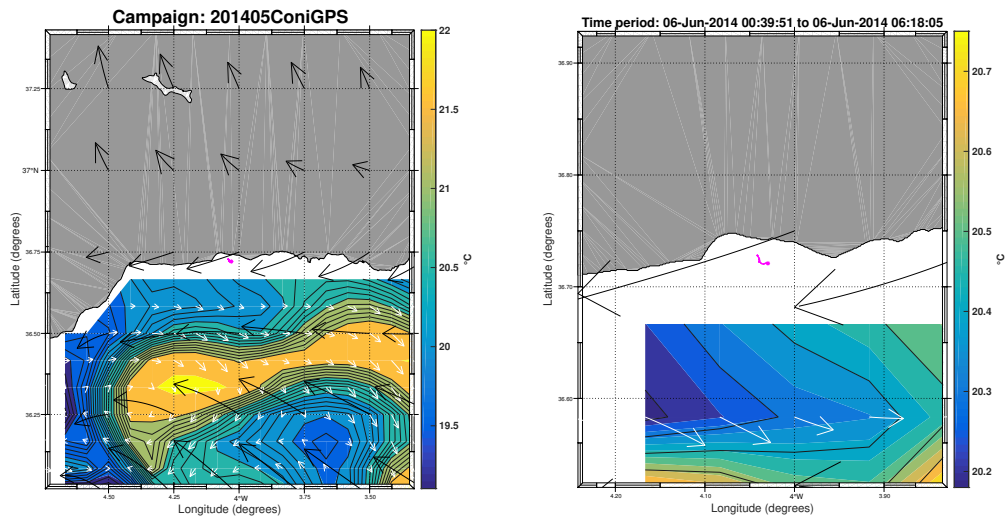


Figure 13: The same as explained in Appendix A.1 Fig:1, now for this example from ConiGPS201405, trajectory 13, and the surface current, temperature and wind data corresponding to this seabird track analyzed here.

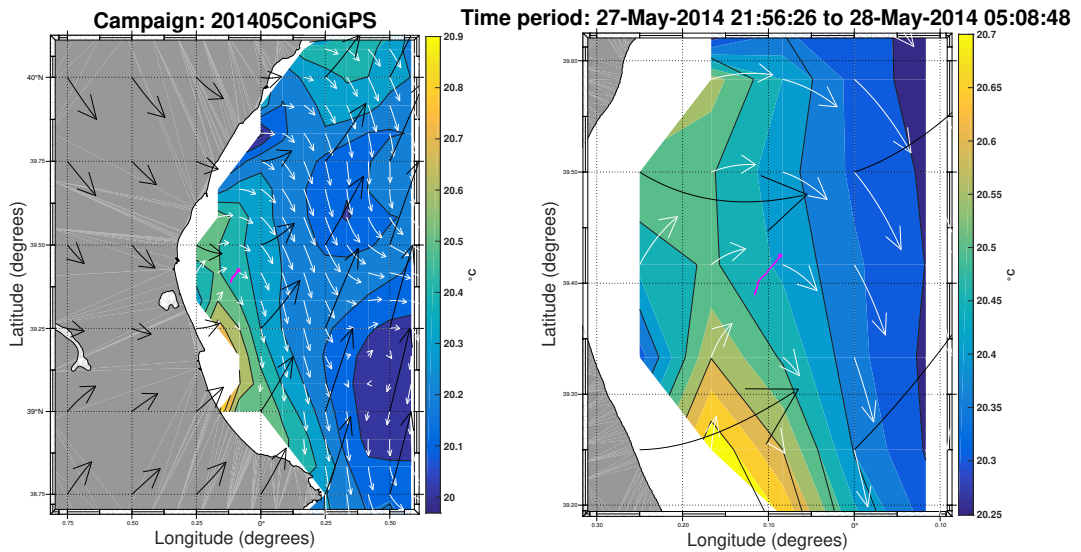


Figure 14: The same as explained in Appendix A.1 Fig:1, now for this example from ConiGPS201405, trajectory 14, and the surface current, temperature and wind data corresponding to this seabird track analyzed here.

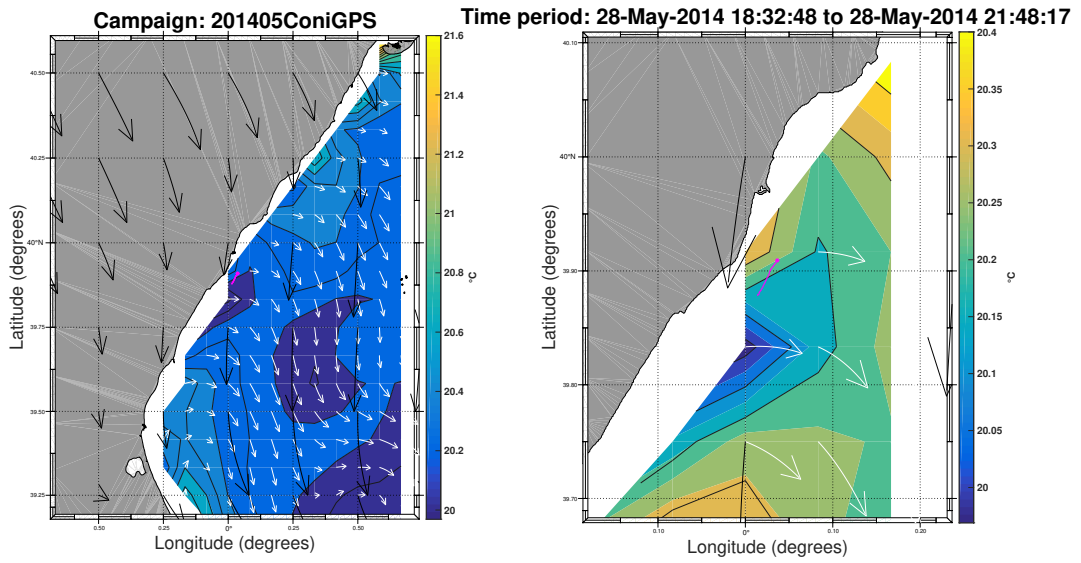


Figure 15: The same as explained in Appendix A.1 Fig:1, now for this example from ConiGPS201405, trajectory 15, and the surface current, temperature and wind data corresponding to this seabird track analyzed here.

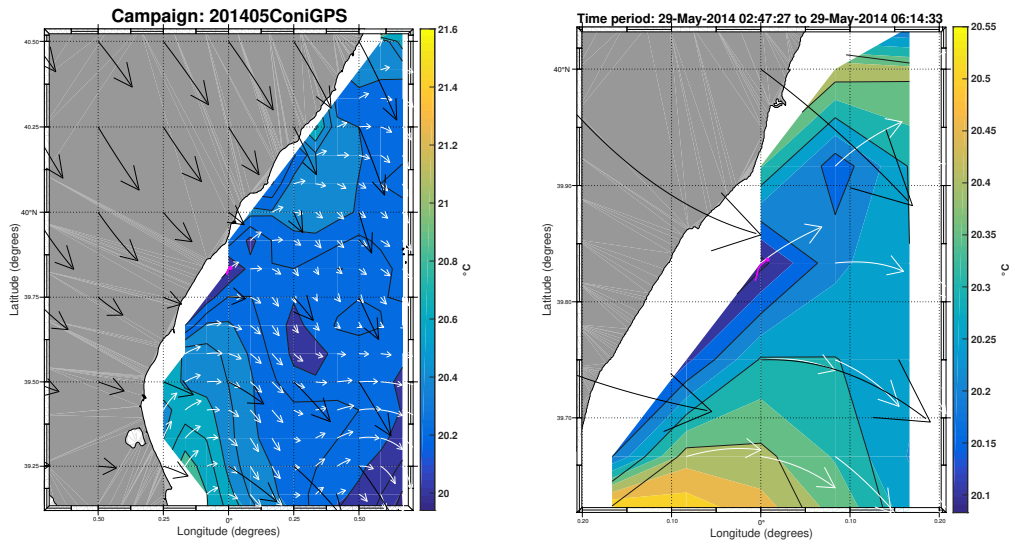


Figure 16: The same as explained in Appendix A.1 Fig:1, now for this example from ConiGPS201405, trajectory 16, and the surface current, temperature and wind data corresponding to this seabird track analyzed here.

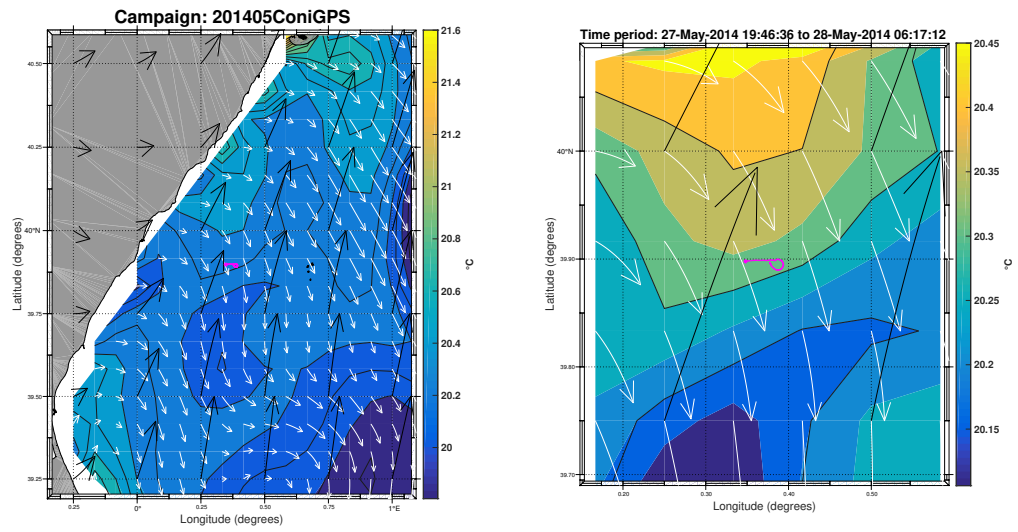


Figure 17: The same as explained in Appendix A.1 Fig:1, now for this example from ConiGPS201405, trajectory 18, and the surface current, temperature and wind data corresponding to this seabird track analyzed here.

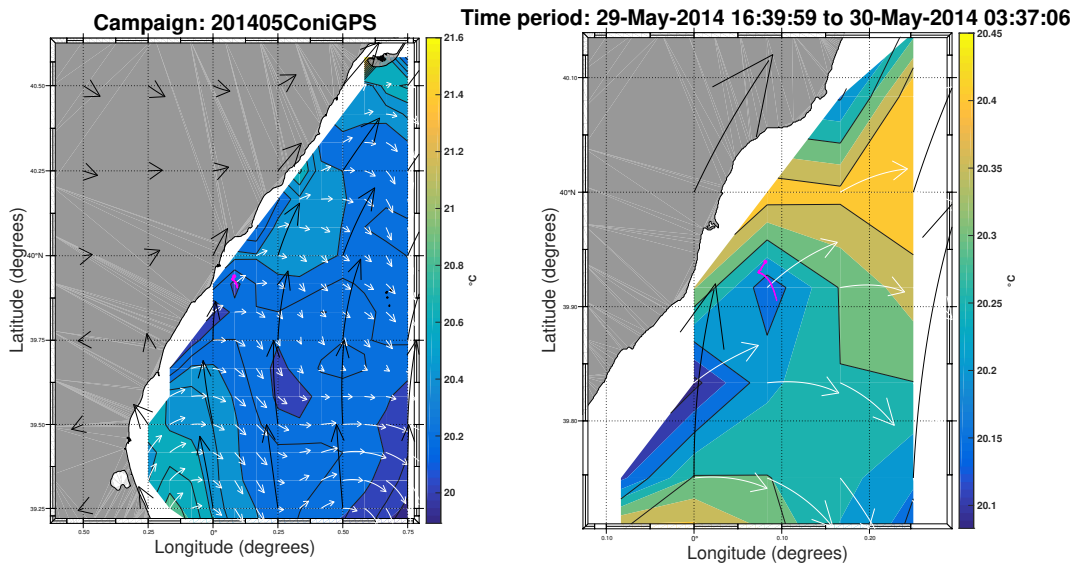


Figure 18: The same as explained in Appendix A.1 Fig:1, now for this example from ConiGPS201405, trajectory 19, and the surface current, temperature and wind data corresponding to this seabird track analyzed here.

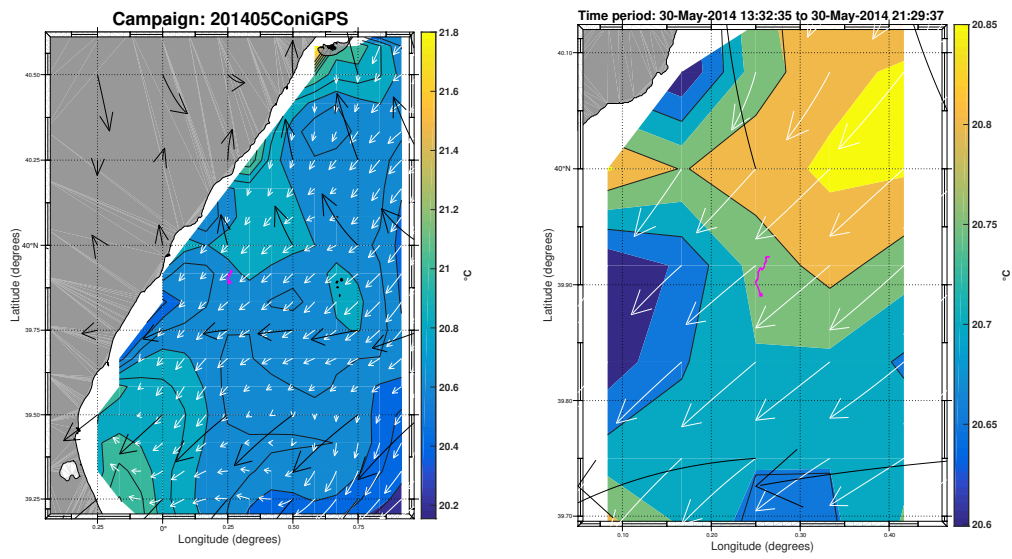


Figure 19: The same as explained in Appendix A.1 Fig:1, now for this example from ConiGPS201405, trajectory 20, and the surface current, temperature and wind data corresponding to this seabird track analyzed here.

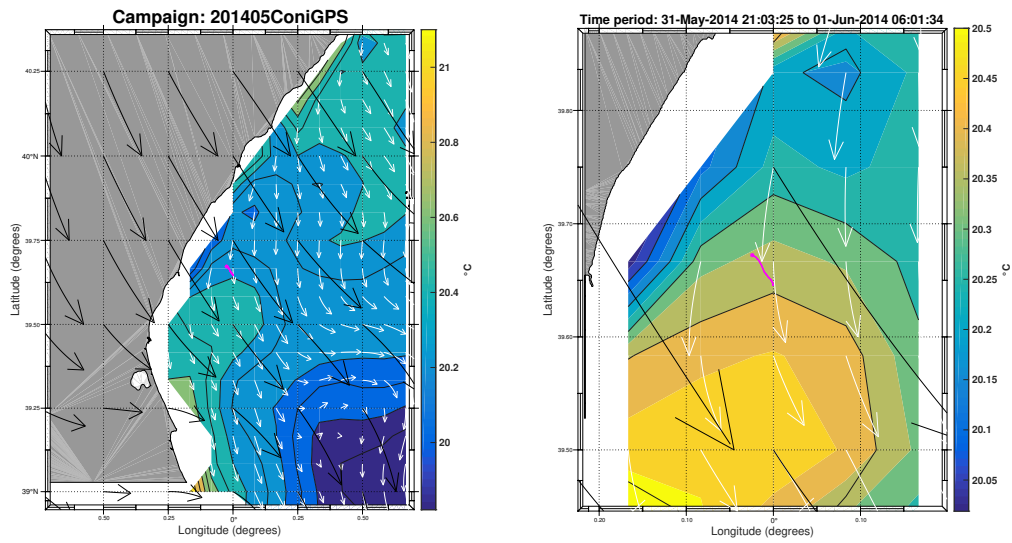


Figure 20: The same as explained in Appendix A.1 Fig:1, now for this example from ConiGPS201405, trajectory 22, and the surface current, temperature and wind data corresponding to this seabird track analyzed here.

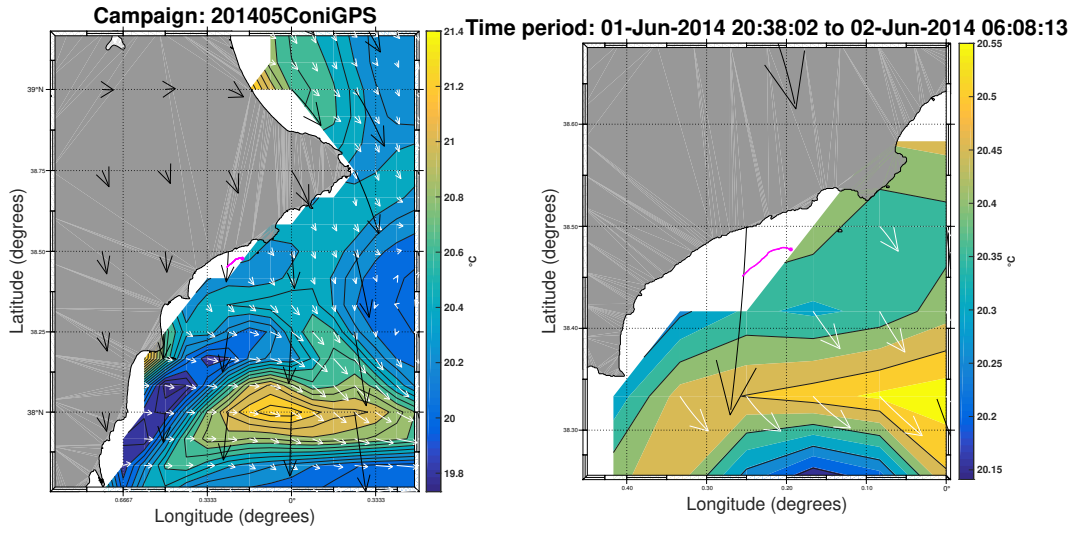


Figure 21: The same as explained in Appendix A.1 Fig:1, now for this example from ConiGPS201405, trajectory 23, and the surface current, temperature and wind data corresponding to this seabird track analyzed here.

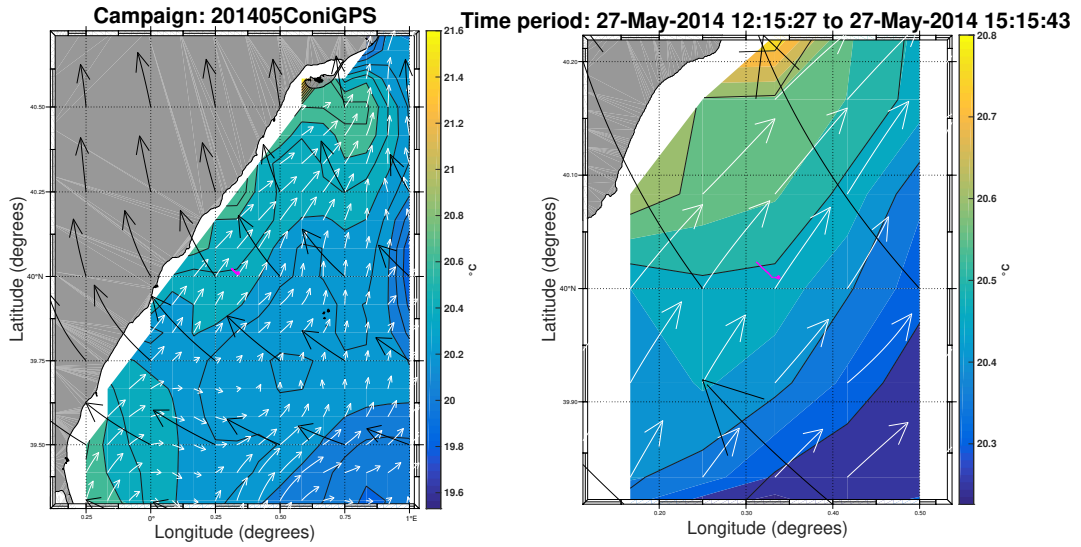


Figure 22: The same as explained in Appendix A.1 Fig:1, now for this example from ConiGPS201405, trajectory 24, and the surface current, temperature and wind data corresponding to this seabird track analyzed here.

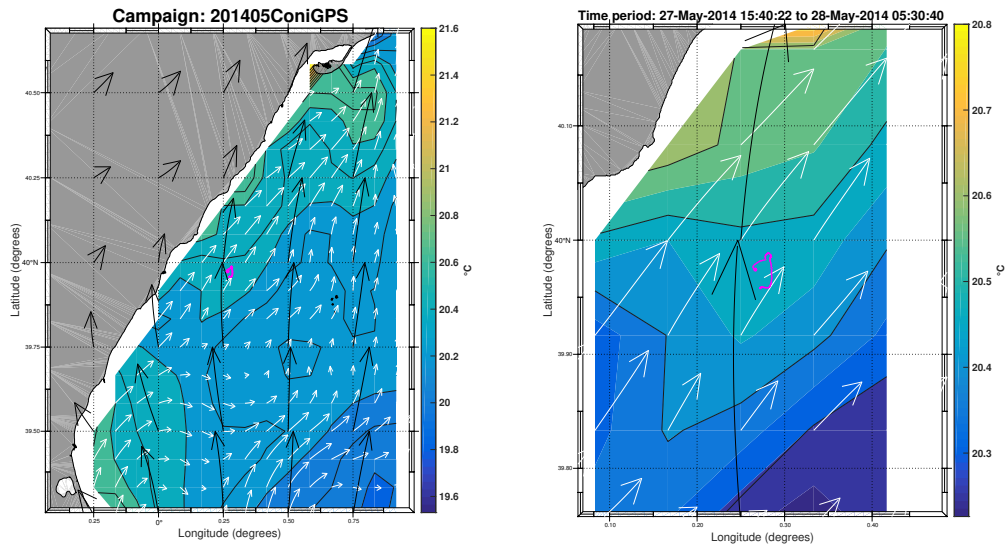


Figure 23: The same as explained in Appendix A.1 Fig:1, now for this example from ConiGPS201405, trajectory 25, and the surface current, temperature and wind data corresponding to this seabird track analyzed here.

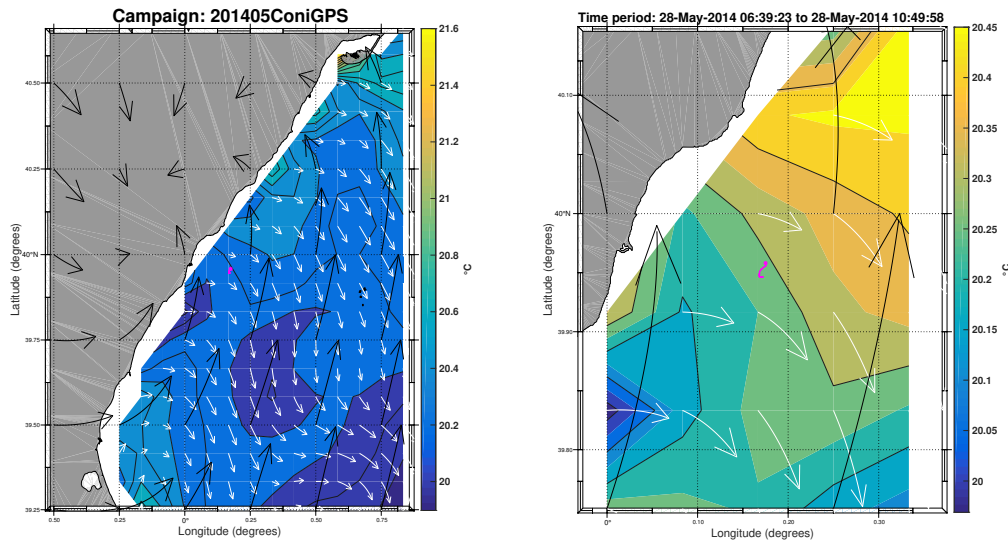


Figure 24: The same as explained in Appendix A.1 Fig:1, now for this example from ConiGPS201405, trajectory 26, and the surface current, temperature and wind data corresponding to this seabird track analyzed here.

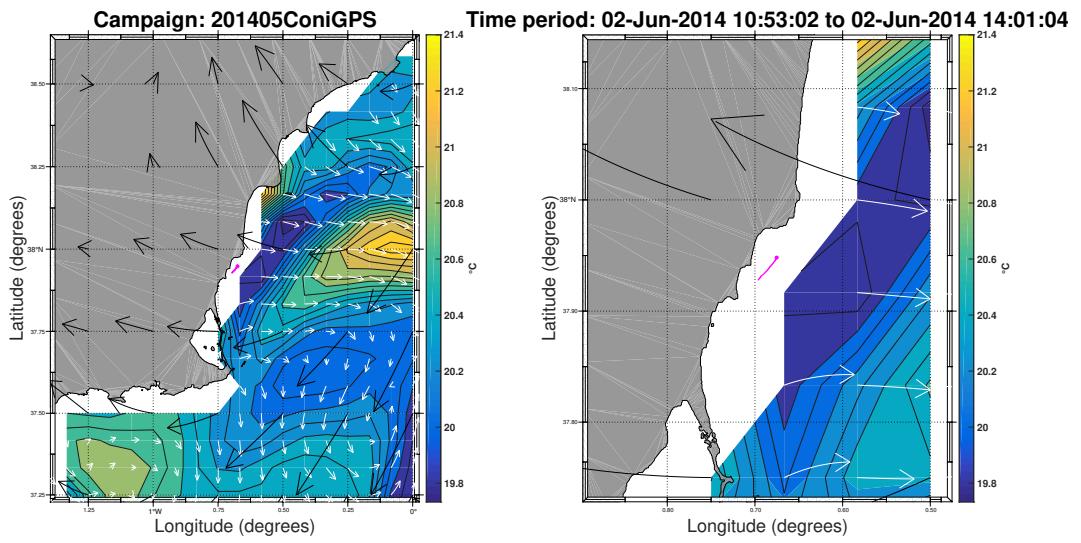


Figure 25: The same as explained in Appendix A.1 Fig:1, now for this example from ConiGPS201405, trajectory 28, and the surface current, temperature and wind data corresponding to this seabird track analyzed here.

Temporal series

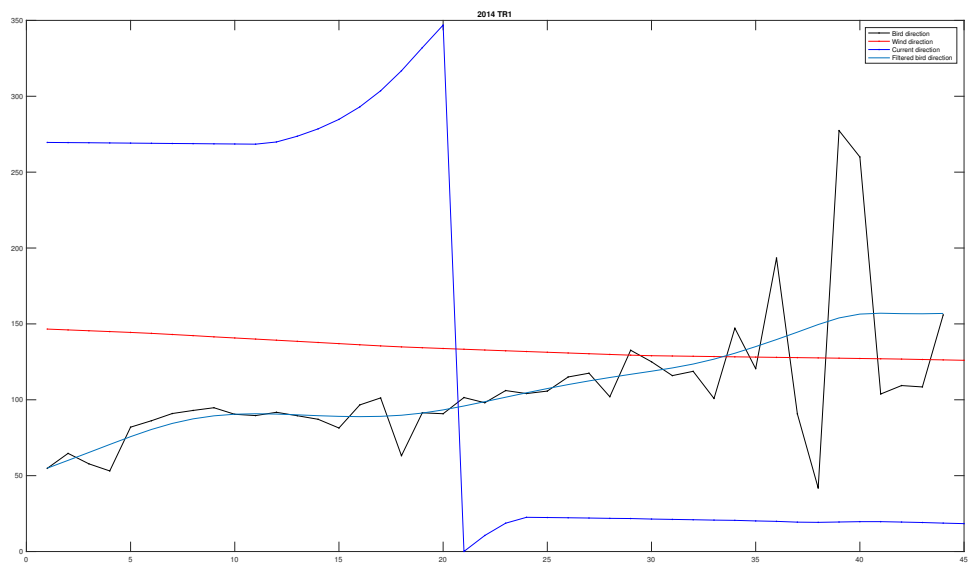


Figure 26: The same as in Appendix A.1 Fig: 14 but for ConiGPS201405 trajectory 1.

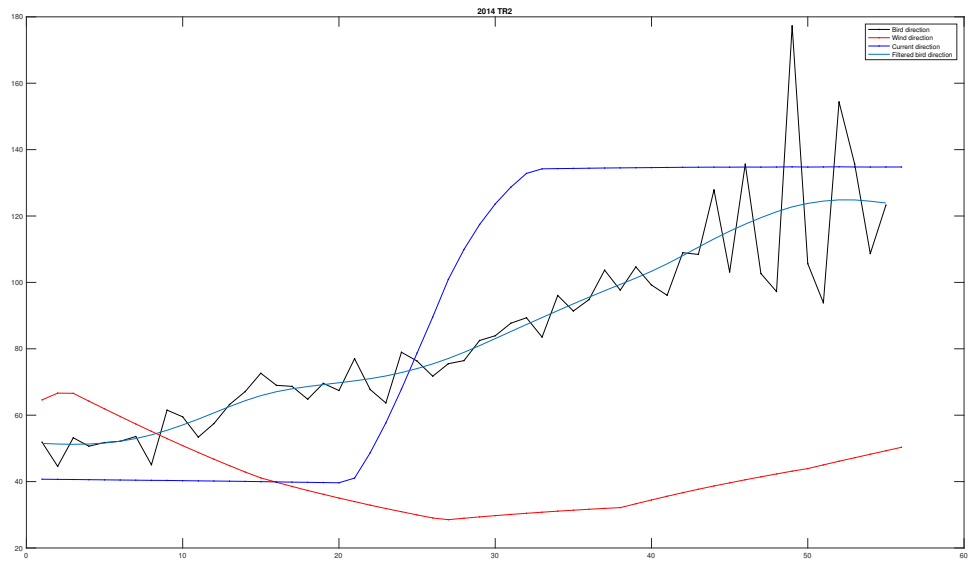


Figure 27: The same as in Appendix A.1 Fig: 14 but for ConiGPS201405 trajectory 2.

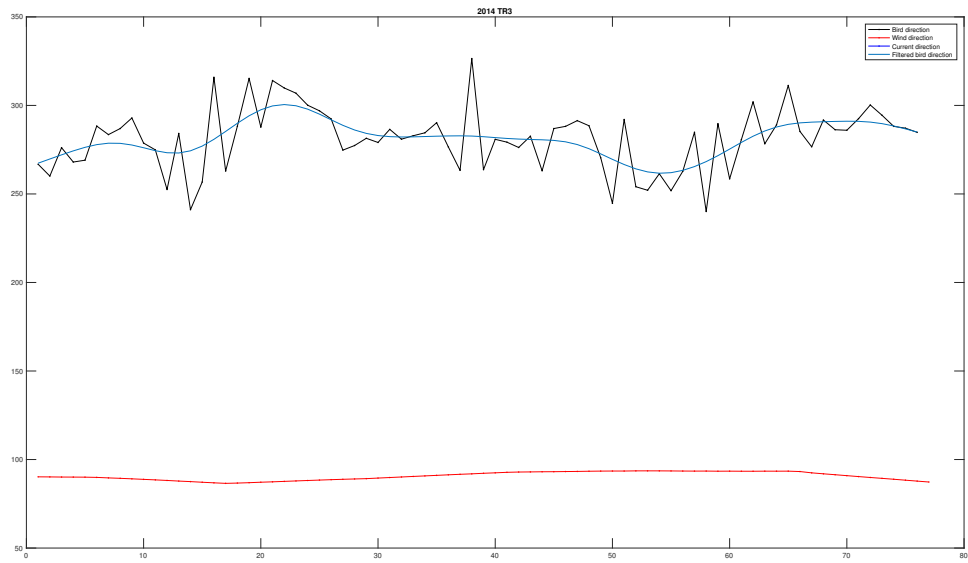


Figure 28: The same as in Appendix A.1 Fig: 14 but for ConiGPS201405 trajectory 3.

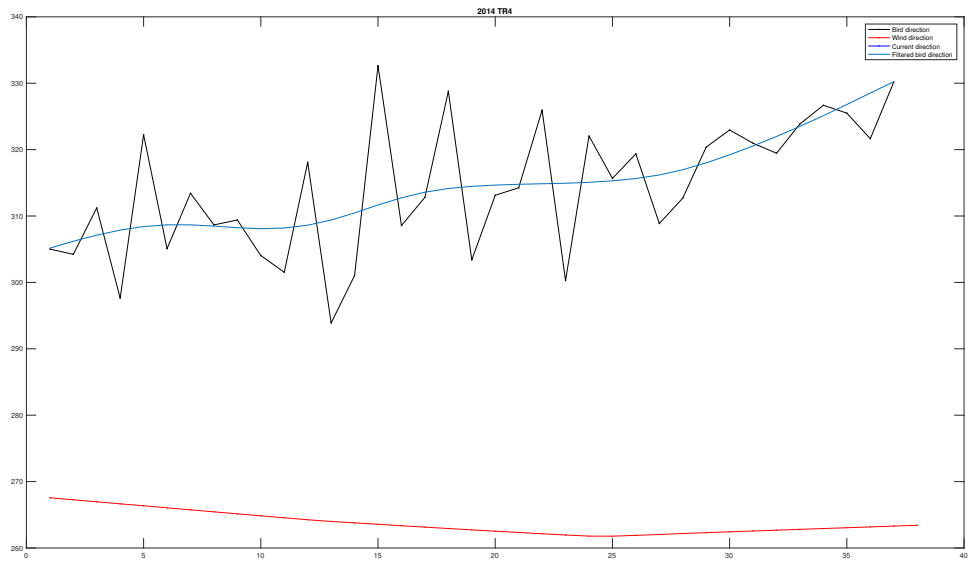


Figure 29: The same as in Appendix A.1 Fig: 14 but for ConiGPS201405 trajectory 4.

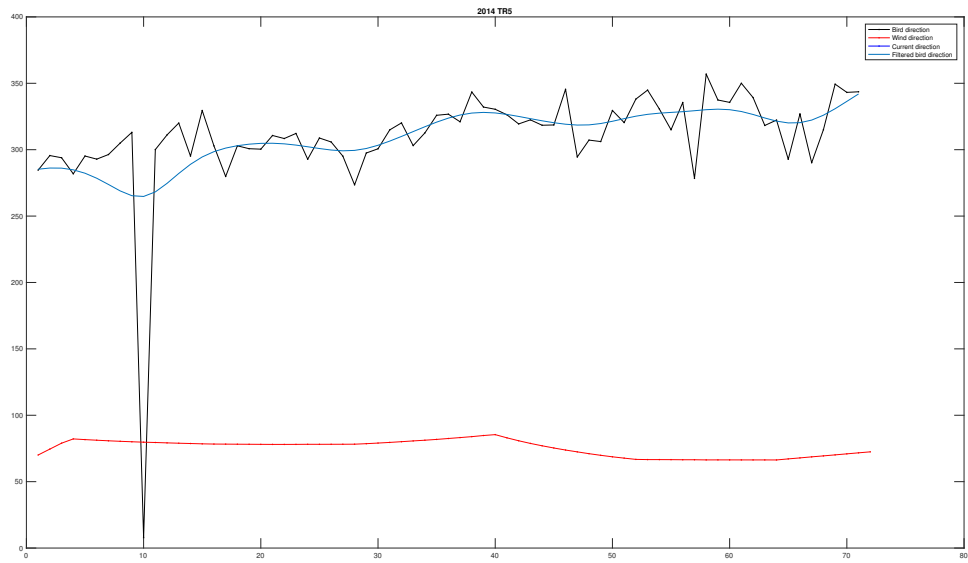


Figure 30: The same as in Appendix A.1 Fig: 14 but for ConiGPS201405 trajectory 5.

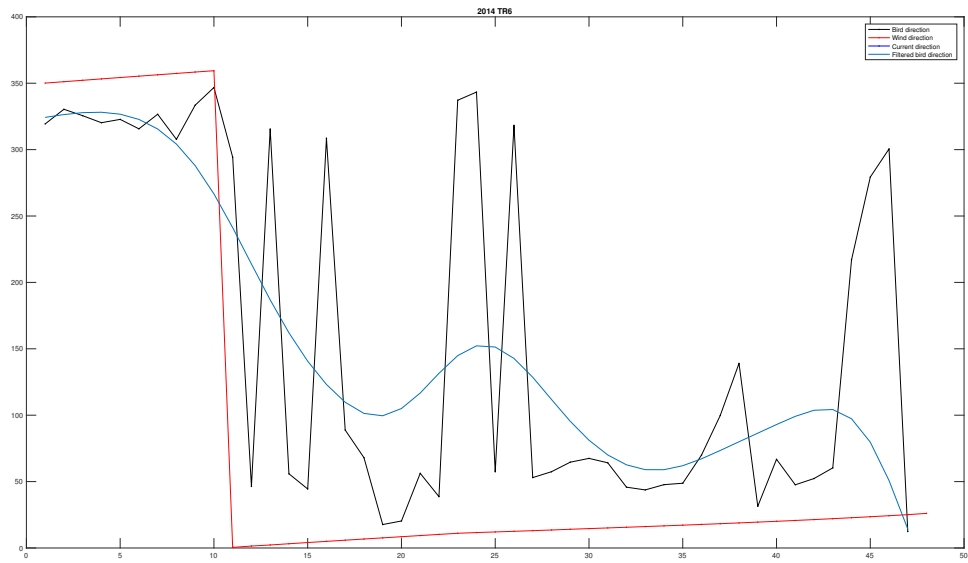


Figure 31: The same as in Appendix A.1 Fig: 14 but for ConiGPS201405 trajectory 6.

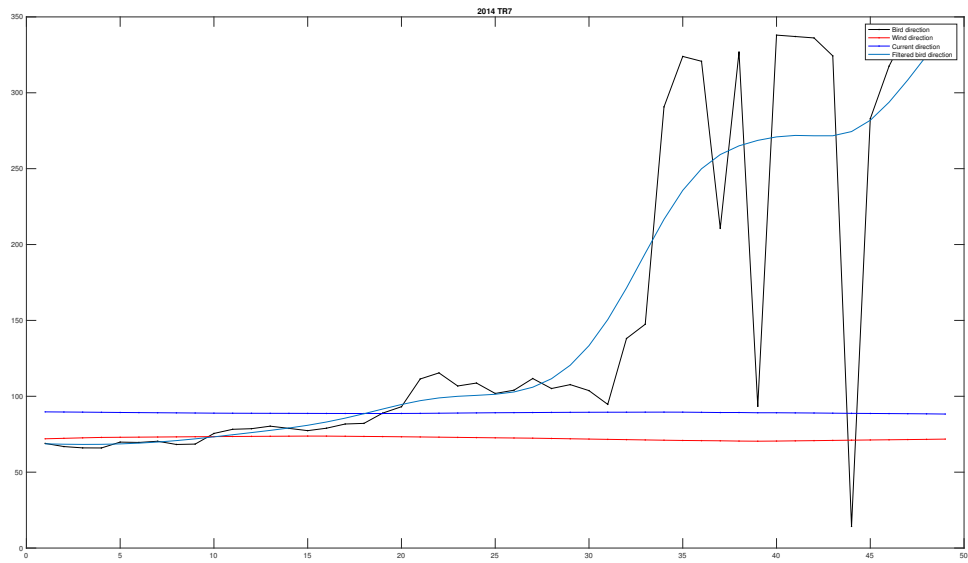


Figure 32: The same as in Appendix A.1 Fig: 14 but for ConiGPS201405 trajectory 7.

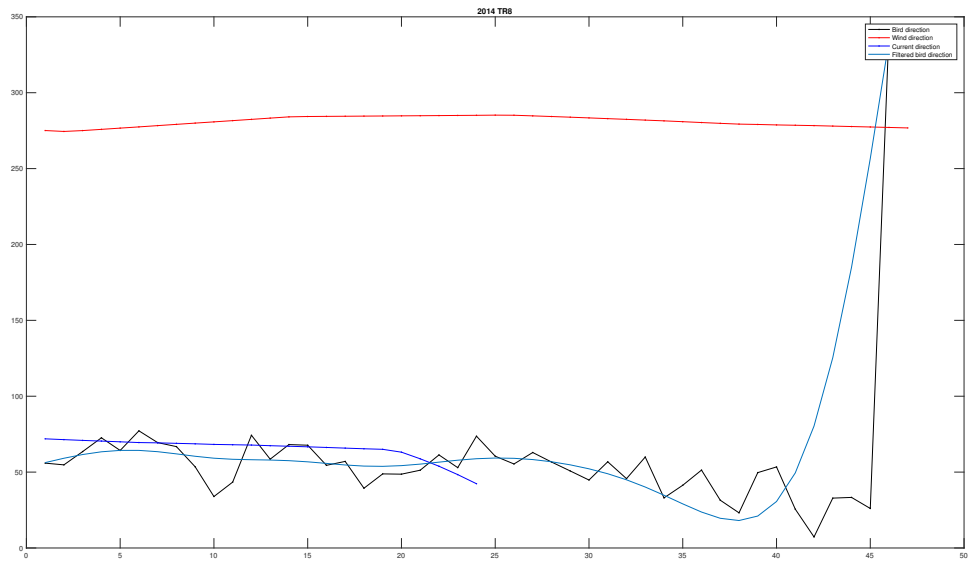


Figure 33: The same as in Appendix A.1 Fig: 14 but for ConiGPS201405 trajectory 8.

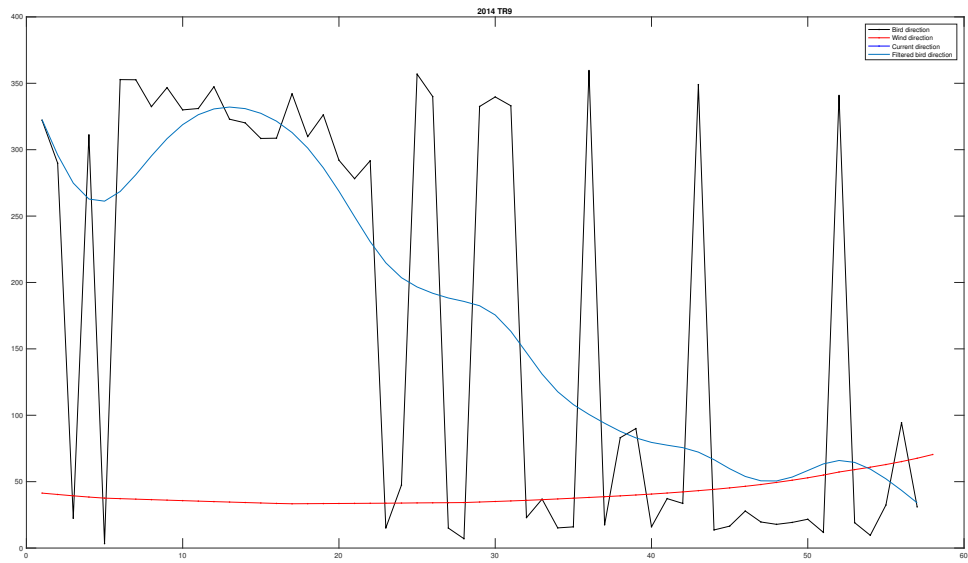


Figure 34: The same as in Appendix A.1 Fig: 14 but for ConiGPS201405 trajectory 9.

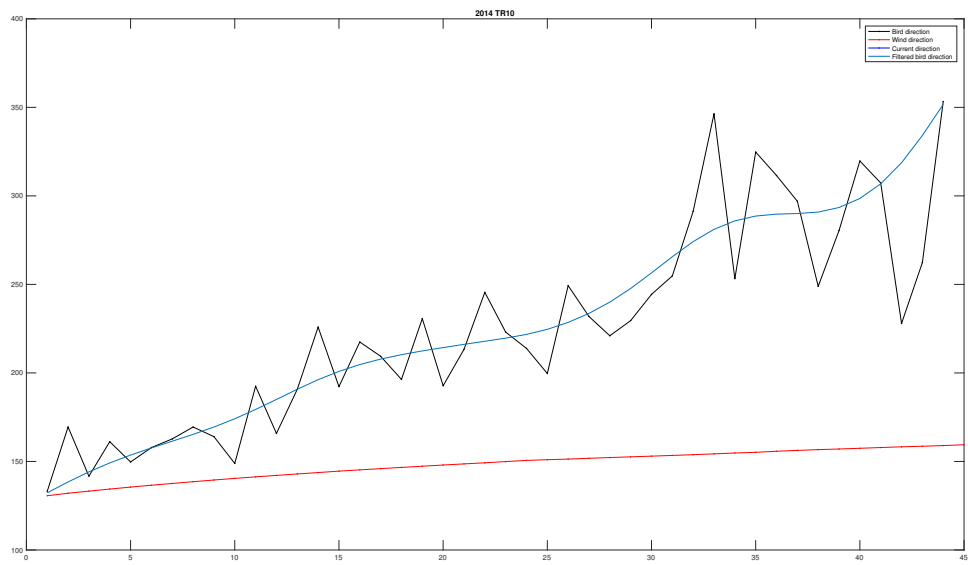


Figure 35: The same as in Appendix A.1 Fig: 14 but for ConiGPS201405 trajectory 10.

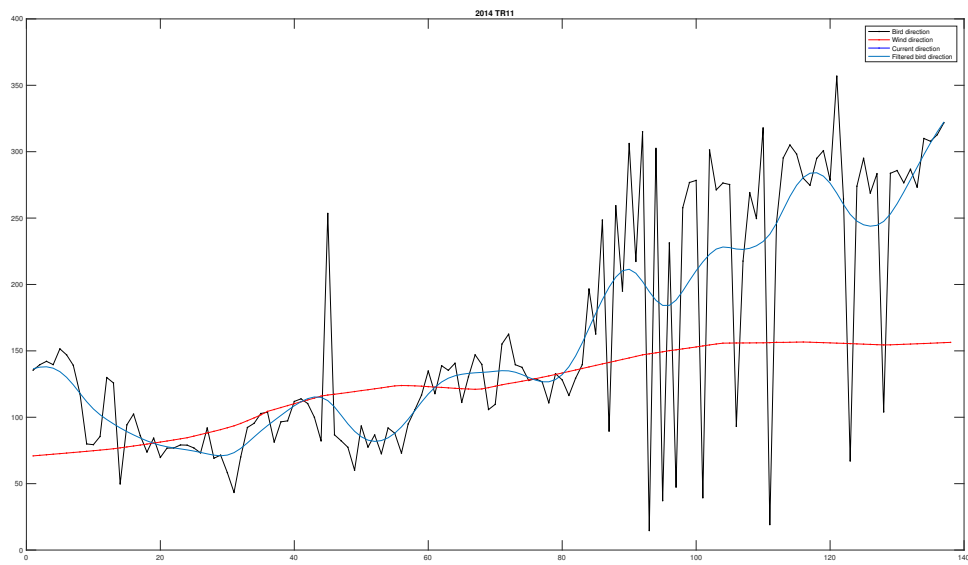


Figure 36: The same as in Appendix A.1 Fig: 14 but for ConiGPS201405 trajectory 11.

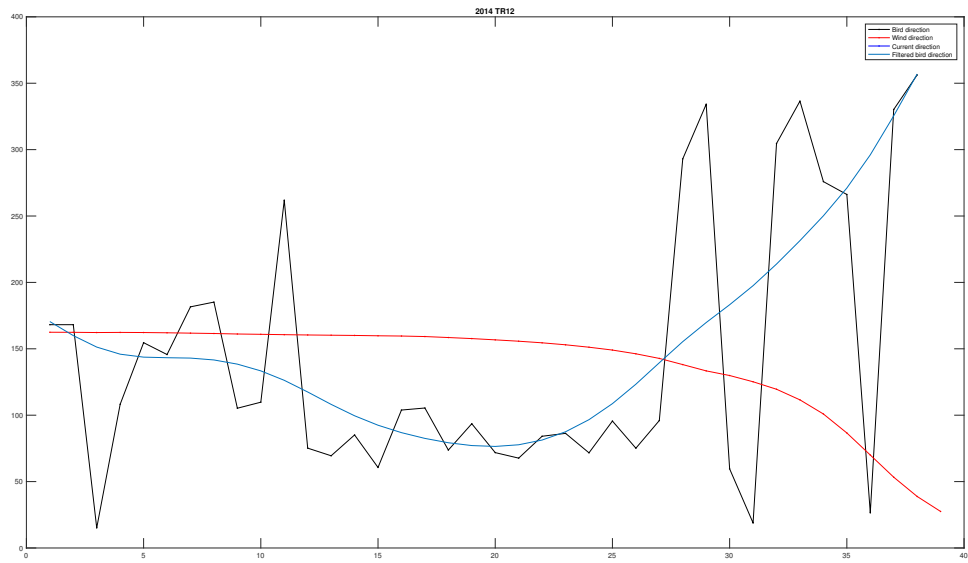


Figure 37: The same as in Appendix A.1 Fig: 14 but for ConiGPS201405 trajectory 12.

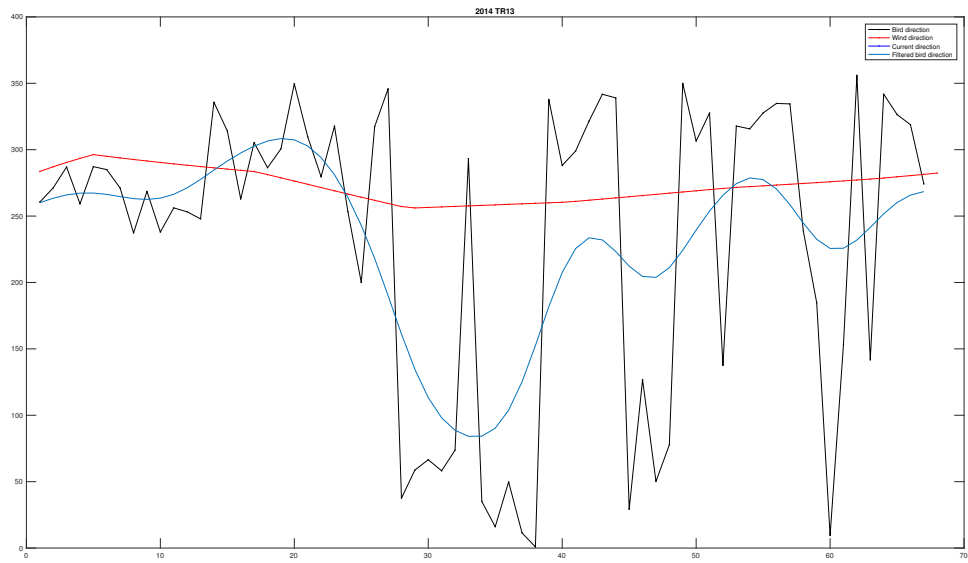


Figure 38: The same as in Appendix A.1 Fig: 14 but for ConiGPS201405 trajectory 13.

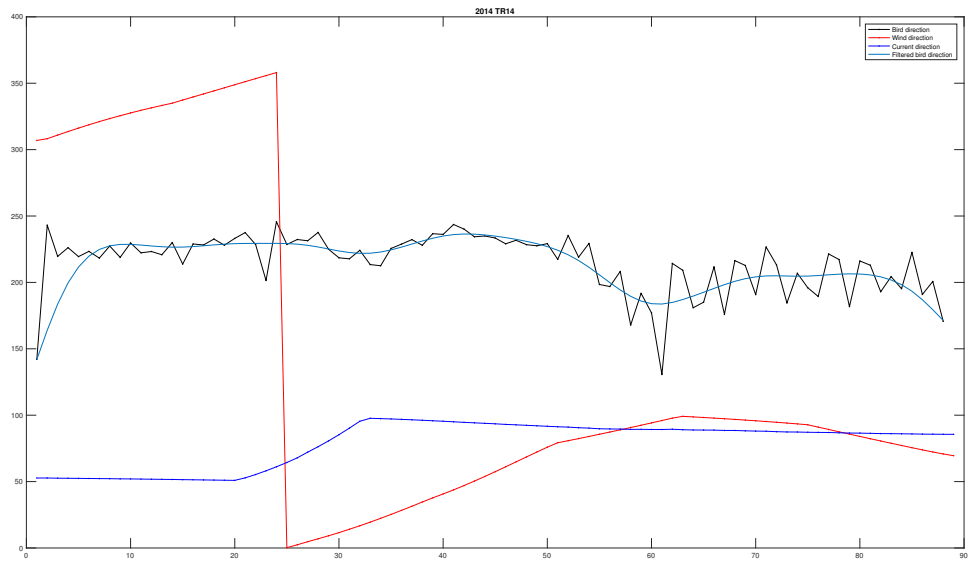


Figure 39: The same as in Appendix A.1 Fig: 14 but for ConiGPS201405 trajectory 14.

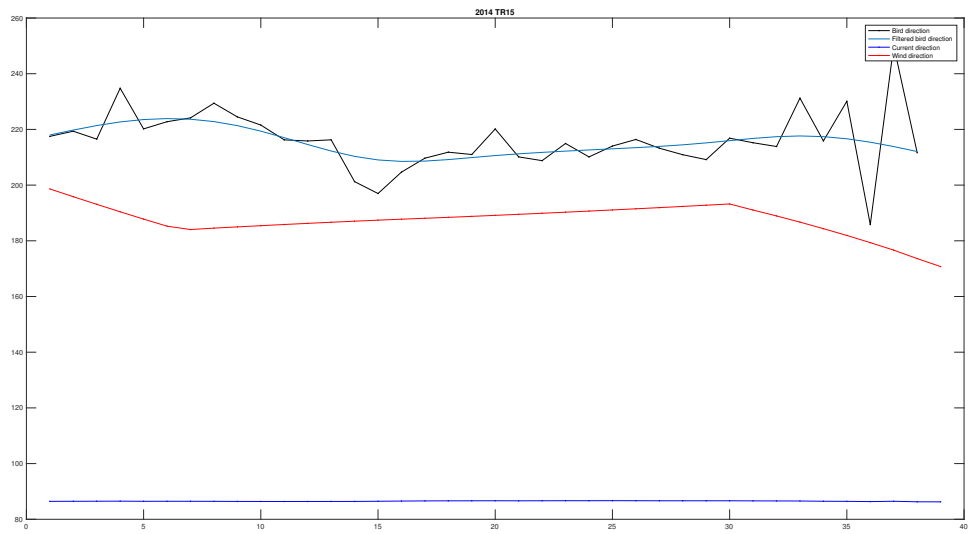


Figure 40: The same as in Appendix A.1 Fig: 14 but for ConiGPS201405 trajectory 15.

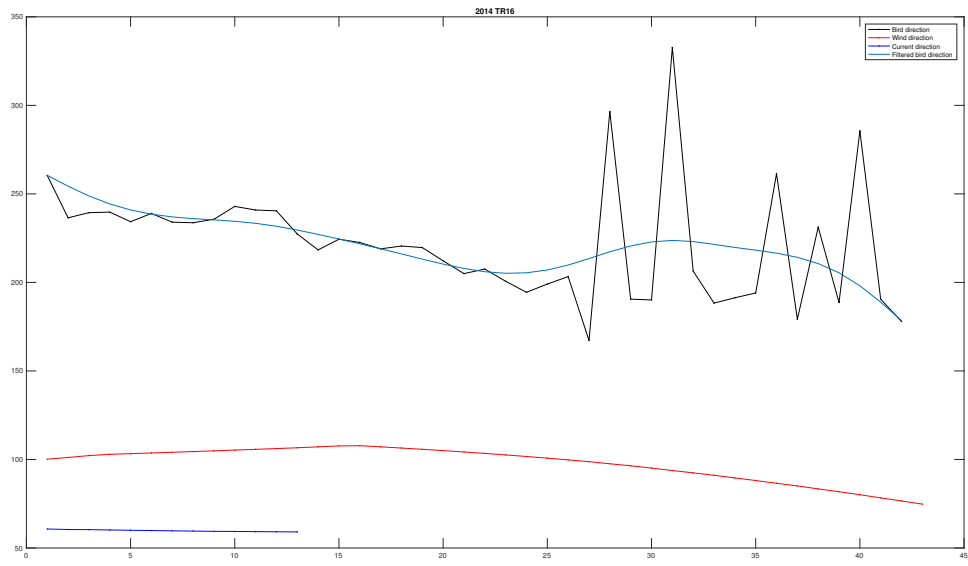


Figure 41: The same as in Appendix A.1 Fig: 14 but for ConiGPS201405 trajectory 16.

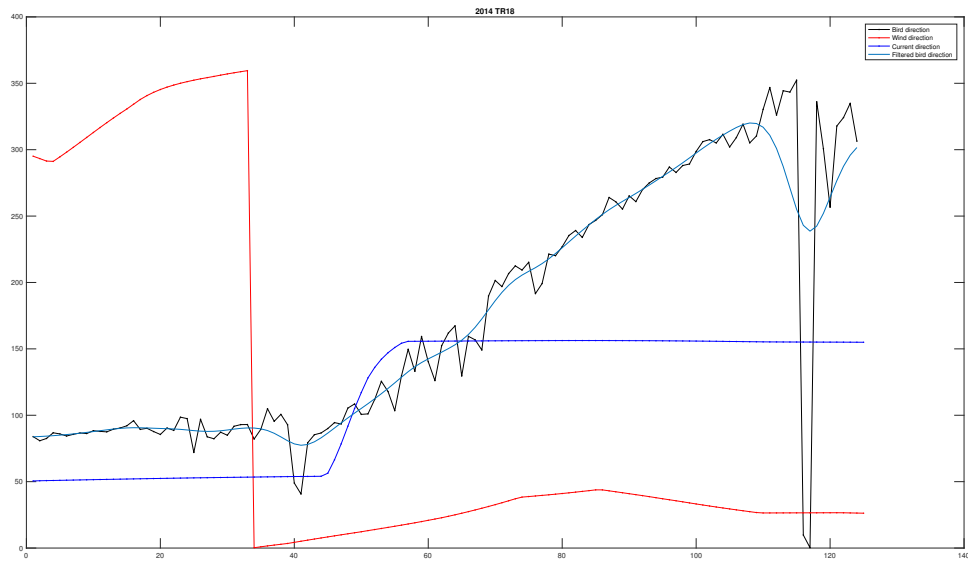


Figure 42: The same as in Appendix A.1 Fig: 14 but for ConiGPS201405 trajectory 18.

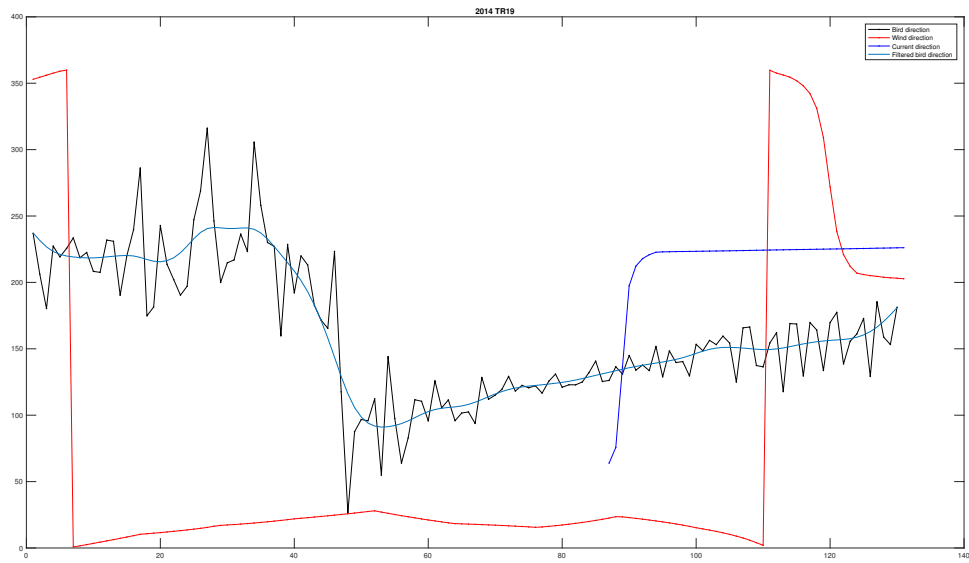


Figure 43: The same as in Appendix A.1 Fig: 14 but for ConiGPS201405 trajectory 19.

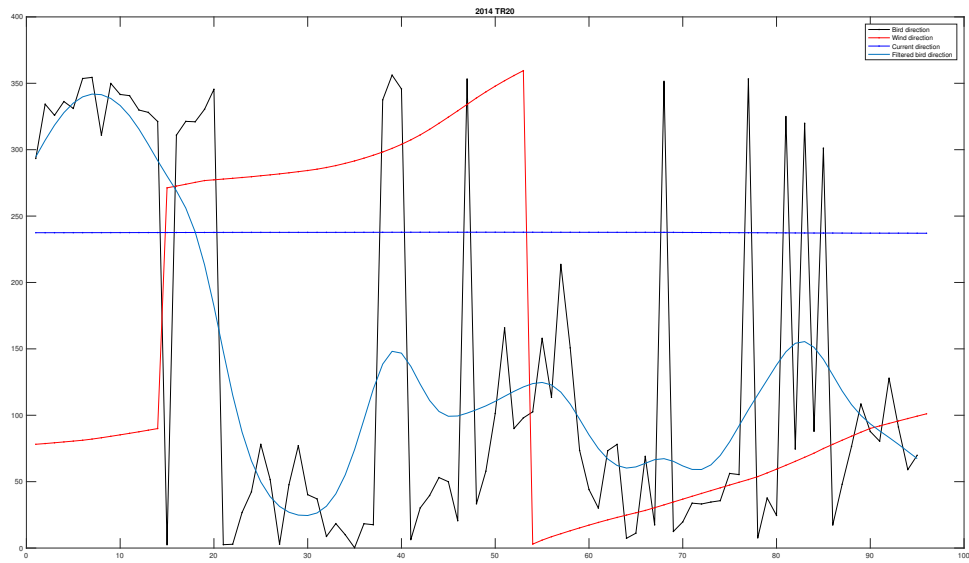


Figure 44: The same as in Appendix A.1 Fig: 14 but for ConiGPS201405 trajectory 20.

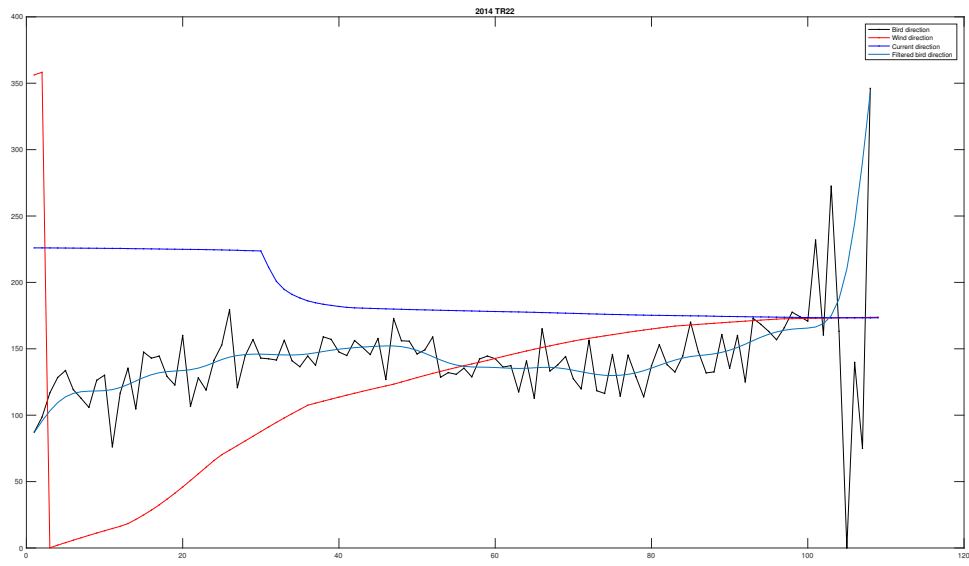


Figure 45: The same as in Appendix A.1 Fig: 14 but for ConiGPS201405 trajectory 22.

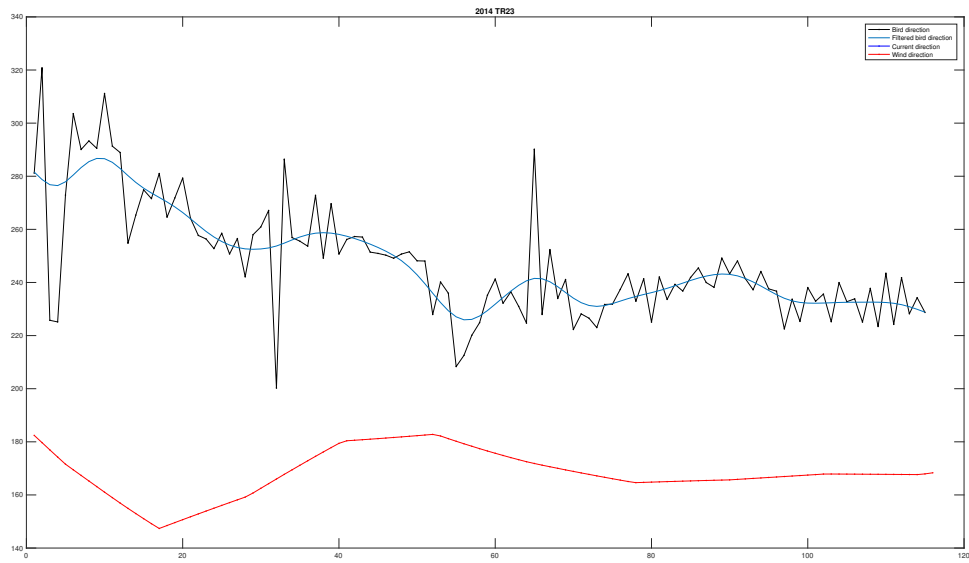


Figure 46: The same as in Appendix A.1 Fig: 14 but for ConiGPS201405 trajectory 23.

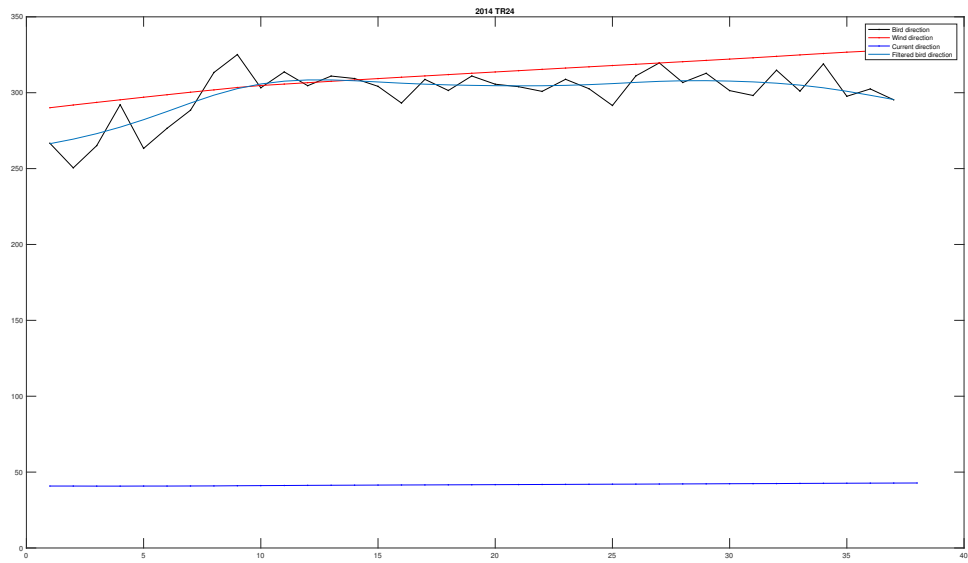


Figure 47: The same as in Appendix A.1 Fig: 14 but for ConiGPS201405 trajectory 24.

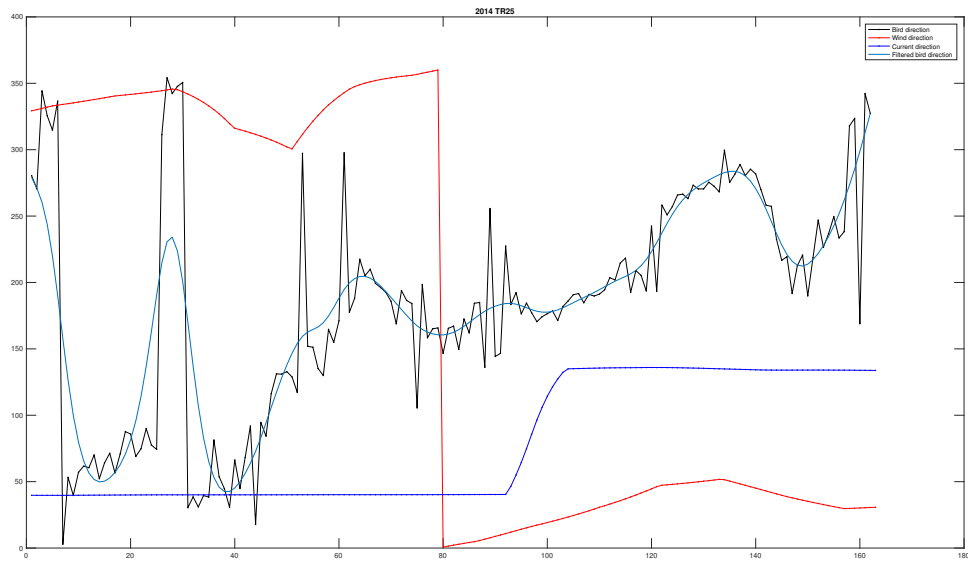


Figure 48: The same as in Appendix A.1 Fig: 14 but for ConiGPS201405 trajectory 25.

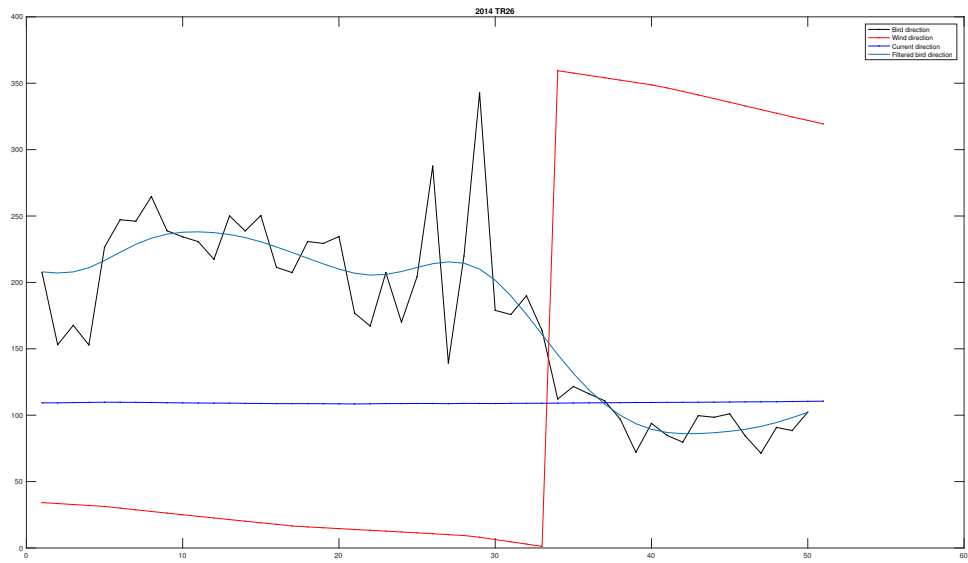


Figure 49: The same as in Appendix A.1 Fig: 14 but for ConiGPS201405 trajectory 26.

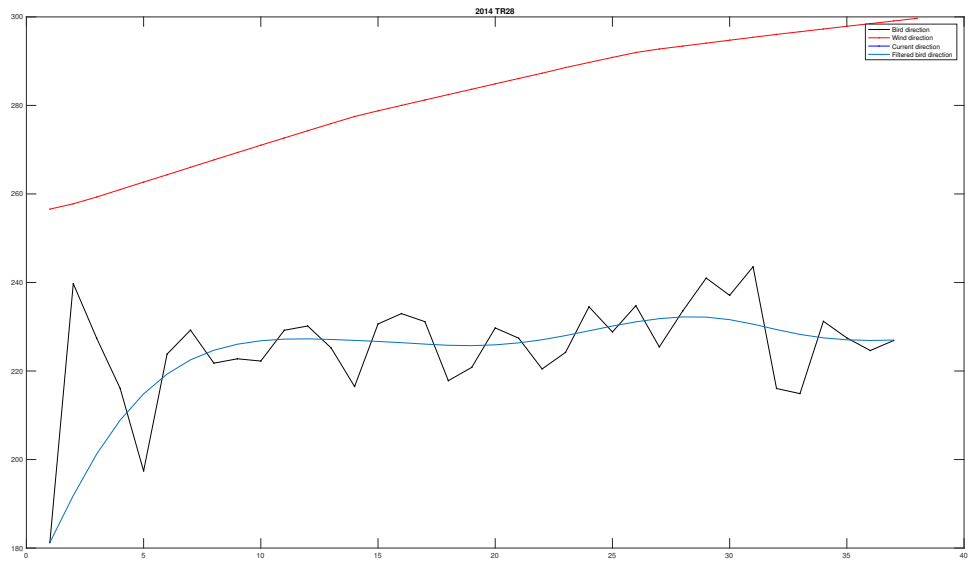


Figure 50: The same as in Appendix A.1 Fig: 14 but for ConiGPS201405 trajectory 28.

Tables

Trajectory	Rw	Pw	RMSEw	meanW	stdW	meanB	sdtB	difW
1,00	-0,91	1,33E-17	43,21	134,18	6,47	107,97	28,76	26,21
2,00	-0,35	0,01	53,12	41,26	10,86	84,79	25,17	43,53
3,00	-0,47	1,90E-05	190,74	90,73	2,31	281,18	9,47	190,44
4,00	-0,65	1,17E-05	51,23	263,73	1,71	314,39	6,52	50,66
5,00	-0,49	1,25E-05	235,75	75,35	6,00	309,98	19,50	234,63
6,00	0,88	2,78E-16	97,67	86,18	141,30	151,75	94,42	65,57
7,00	-0,87	4,393E-16	116,89	72,27	1,11	149,62	87,59	77,35
8,00	-0,30	0,04	221,40	281,13	3,31	67,09	56,15	214,04
9,00	-0,69	2,25E-09	176,52	40,92	9,05	178,26	105,40	137,34
10,00	0,96	1,41E-25	93,80	147,84	8,13	227,80	57,39	79,96
11,00	0,82	2,53E-34	61,07	123,73	28,88	158,68	71,09	34,95
12,00	-0,91	2,30E-15	100,53	141,37	32,04	152,18	71,25	10,82
13,00	0,73	2,66E-12	67,29	273,29	11,82	231,55	61,17	41,74
14,00	0,06	0,61	142,71	139,07	122,25	213,11	19,22	74,04
15,00	0,03	0,99	28,31	187,93	4,84	215,46	4,60	27,53
16,00	0,54	0,00	123,79	98,19	9,06	221,22	16,57	123,02
17,00	0,22	0,02	127,61	157,38	98,96	159,61	106,04	2,24
18,00	-0,55	3,61E-11	207,98	107,24	136,11	174,54	86,73	67,30
19,00	0,12	0,18	149,52	72,26	115,26	163,04	47,30	90,77
20,00	0,30	0,00	137,90	184,15	123,81	136,01	91,98	48,13
21,00	0,97	2,04E-37	42,44	181,28	5,95	220,04	23,16	38,76
22,00	0,25	0,01	66,74	122,93	63,46	145,00	30,85	22,07
23,00	-0,04	0,64	120,79	143,14	57,57	247,68	17,13	104,53
24,00	0,69	2,50E-06	14,70	311,83	10,78	300,04	11,65	11,79
25,00	-0,55	2,36E-14	198,11	179,41	153,37	183,09	67,34	3,69
26,00	-0,94	2,26E-24	213,91	128,53	155,43	175,88	57,75	47,35
27,00	0,12	0,26	56,70	147,74	4,24	186,03	42,34	38,29
28,00	0,73	2,65E-07	58,50	281,55	13,29	223,75	10,95	57,80
29,00	0,90	6,66E-25	16,85	64,10	5,00	78,00	13,85	13,91

Table 1: Statistical parameters wind-bird. ConiGPS2014

Trajectory	Rc	Pc	RMSEc	meanC	stdC	meanB	sdtB	difC
1	-0,78	5,23E-10	158,48	139,09	133,78	107,97	28,76	31,12
2	0,90	2,21E-20	25,11	90,87	44,48	84,80	25,17	6,08
3	NaN	NaN	NaN	NaN	NaN	281,18	9,47	NaN
4	NaN	NaN	NaN	NaN	NaN	314,39	6,52	NaN
5	NaN	NaN	NaN	NaN	NaN	309,98	19,50	NaN
6	NaN	NaN	NaN	NaN	NaN	151,75	94,42	NaN
7	-0,11	0,45	105,76	89,08	0,35	149,62	87,59	60,54
8	0,31	0,15	9,65	65,21	7,35	67,09	56,15	1,88
9	NaN	NaN	NaN	NaN	NaN	178,26	105,40	NaN
10	NaN	NaN	NaN	NaN	NaN	227,80	57,40	NaN
11	NaN	NaN	NaN	NaN	NaN	158,68	71,09	NaN
12	NaN	NaN	NaN	NaN	NaN	152,18	71,25	NaN
13	NaN	NaN	NaN	NaN	NaN	231,55	61,17	NaN
14	-0,09	0,38	136,77	78,98	17,05	213,11	19,23	134,14
15	-0,37	0,02	129,02	86,53	0,11	215,46	4,60	128,94
16	0,97	1,01E-07	180,82	59,77	0,54	221,22	16,57	161,45
17	0,17	0,08	126,67	152,32	89,70	159,61	106,04	7,29
18	0,83	1,17E-32	79,79	115,15	49,22	174,54	86,73	59,39
19	0,49	0,00	70,72	214,29	34,81	163,04	47,30	51,25
20	-0,18	0,09	136,75	237,61	0,23	136,01	91,98	101,60
21	0,93	1,53E-25	38,61	252,93	3,02	220,04	23,16	32,88
22	-0,41	9,95E-06	64,01	191,24	21,77	145,00	30,85	46,24
23	NaN	NaN	NaN	NaN	NaN	247,68	17,13	NaN
24	0,55	0,00	258,60	41,68	0,65	300,04	11,65	258,37
25	0,65	8,25E-21	116,66	78,20	45,59	183,09	67,34	104,90
26	-0,65	3,078E-07	87,11	109,26	0,51	175,88	57,75	66,62
27	0,88	3,462E-31	74,56	120,87	6,89	186,03	42,34	65,17
28	NaN	NaN	NaN	NaN	NaN	223,7515	10,95	NaN
29	-0,91	1,04E-25	31,32	79,11	18,43	78,01	13,85	1,11

Table 2: Statitical parameters current-bird. ConiGPS2014

Bibliography

- Allen, J. T., E. Alou-Font, G. Aulicino, B. Barceló-Llull, A. Cabornero, N. Calafat, E. Capó, B. Casas, Y. Cotroneo, E. Cutolo, F. Cyr, F. D'Ovidio, A. M. Doglioli, F. Dumas, L. Día-Barroso, J. G. Fernández, G. Gregori, L. Gómez Navarro, J. Hernández-Lasheras, A. Mahadevan, E. Mason, A. Miralles, B. Mourre, C. Muñoz, A. Pascual, D. Roque, M. Rubio, I. Ruiz, S. Ruiz, E. Ser-Giacomi, A. Sánchez-Román, T. Toomey, and M. Torner (2018), Pre-swot cruise report. mesoscale and sub-mesoscale vertical exchanges from multi-platform experiments and supporting modeling simulations: anticipating swot launch (ctm2016-78607-p).
- Aulicino, G., A. Sanchez-Roman, Y. Cotroneo, S. Ruiz, A. Pascual, G. Fusco, J. Tintoré, and G. Budillon (2017), Monitoring of the algerian basin circulation through glider observations, numerical simulations and altimetry during fall 2014-2016, in *Journal of Mar.Sys.*, vol. 179, pp. 55–71.
- Belmonte Rivas, M., and A. Stoffelen (2019), Characterizing era-interim and era5 surface wind biases using ascats, *Ocean Sci.*, 15(3), 831–852, doi:10.5194/os-15-831-2019.
- Birol, F., M. Cancet, and C. Estournel (2010), Aspects of the seasonal variability of the northern current (nw mediterranean sea) observed by altimetry, *Journal of Marine Systems*, 81, 297–311, doi:10.1016/j.jmarsys.2010.01.005.
- Bouffard, J., L. Renault, S. Ruiz, A. Pascual, C. Dufau, and J. Tintoré (2012), Sub-surface small-scale eddy dynamics from multi-sensor observations and modeling, *Progress in Oceanography*, 106, 62 – 79, doi:https://doi.org/10.1016/j.pocean.2012.06.007.
- Carter, M. I. D., S. L. Cox, K. L. Scales, A. W. J. Bicknell, M. D. Nicholson, K. M. Atkins, G. Morgan, L. Morgan, W. J. Grecian, S. C. Patrick, and S. C. Votier (2016), Gps tracking reveals rafting behaviour of northern gannets (*morus bassanus*): implications for foraging ecology and conservation, *Bird Study*, 63(1), 83–95, doi:10.1080/00063657.2015.1134441.
- Carton, J. A., and B. S. Giese (2008), A reanalysis of ocean climate using simple ocean data assimilation (soda), *Monthly Weather Review*, 136(8), 2999–3017, doi:10.1175/2007MWR1978.1.
- Castellón, A., J. Font, and E. García-Ladona (1990), The liguro-provençal-catalan current (nw mediterranean) observed by doppler profiling in the balearic sea, *Scientia Marina*, 54, 269–276.
- Chronis, T., V. Papadopoulos, and E. I. Nikolopoulos (2011), Quikscat observations of extreme wind events over the mediterranean and black seas during 2000–2008, *International Journal of Climatology*, 31(14), 2068–2077, doi:10.1002/joc.2213.
- Conti, D., Á. Galán, C. López, A. Orfila, L. Renault, J. M. Sayol, and G. Simarro (2013), Sea surface transport in the western mediterranean sea : A lagrangian perspective.
- Dorman, C. E., R. C. Beardsley, and R. Limeburner (1995), Winds in the strait of gibraltar, *Quarterly Journal of the Royal Meteorological Society*, 121(528), 1903–1921, doi:10.1002/qj.49712152807.
- Font, J., J. Salat, and J. Tintoré (1988), Permanent features of the circulation in the catalan sea, *Oceanol. Acta*, 9, 51–57.
- García, M. L., C. Millot, J. Font, and E. GarcíaâLadona (1994), Surface circulation variability in the balearic basin, *Journal of Geophysical Research: Oceans*, 99(C2), 3285–3296.
- Heslop, E. E., S. Ruiz, J. Allen, J. L. López-Jurado, L. Renault, and J. Tintoré (2012), Autonomous underwater gliders monitoring variability at “choke points” in our ocean system: A case study in the western mediterranean sea, *Geophysical Research Letters*, 39(20), doi:10.1029/2012GL053717.
- Heslop, E. E., A. Sánchez-Román, A. Pascual, D. Rodríguez, K. A. Reeve, Y. Faugère, and M. Raynal (2017), Sentinel-3a views ocean variability more accurately at finer resolution, *Geophysical Research Letters*, 44(24), 12,367–12,374, doi:10.1002/2017GL076244.
- Hoffmann, L., G. Günther, D. Li, O. Stein, X. Wu, S. Griessbach, Y. Heng, P. Konopka, R. Müller, B. Vogel, and J. Wright (2019), From era-interim to era5: The considerable impact of ecmwf’s next-generation reanalysis on lagrangian transport simulations, *Atmospheric Chemistry and Physics*, 19, 3097–3124, doi:10.5194/acp-19-3097-2019.

- Jansa, A. (1987), Distribution of the mistral: A satellite observation, *Meteorol. Atmos. Phys.*, *36*, 201–214, doi:10.1007/BF01045149.
- Juzà, M., L. Renault, S. Ruiz, and J. Tintoré (2013), Origin and pathways of winter intermediate water in the northwestern mediterranean sea using observations and numerical simulation.
- Lana, A., J. Marmain, V. Fernandez, J. Tintoré, and A. Orfila (2016), Wind influence on surface current variability in the ibiza channel from hf radar, *Ocean Dynamics*, *66*, doi:10.1007/s10236-016-0929-z.
- LaViolette, P. E. (1990), Interannual and seasonal variation in the western mediterranean circulation, *Eos, Transactions American Geophysical Union*, *71*(32), 1021–1021, doi:10.1029/90EO00258.
- Le Traon, P. Y. (2013), From satellite altimetry to argo and operational oceanography: three revolutions in oceanography, *Ocean Sci.*
- Le Traon, P. Y., F. Nadal, and N. Ducet (1998), An improved mapping method of multisatellite altimeter data, *Journal of Atmospheric and Oceanic Technology*, *15*(2), 522–534, doi:10.1175/1520-0426(1998)015<0522:AIMMOM>2.0.CO;2.
- Liu, W. T., and X. Xie (2014), *Sea Surface Wind/Stress Vector*, pp. 759–767, Springer New York, New York, NY, doi:10.1007/978-0-387-36699-9_168.
- Louzano, M. (2016), *Conservación Integral de la Pardela Balear Puffinus mauretanicus en Pitiüses: uniendo puentes entre los ecosistemas marino y terrestre*, SEO/BidLife.
- Louzao, M., J. Bécares, B. Rodríguez, D. Hyrenbach, A. Ruiz, and J. Arcos (2009), Combining vessel-based surveys and tracking data to identify key marine areas for seabirds, *Marine Ecology Progress Series*, Vol. *391*, 183–197, doi:10.3354/meps08124.
- Lumpkin, R., and M. Pazos (2007), *Measuring surface currents with Surface Velocity Program drifters: The instrument, its data, and some recent results*, doi:10.1017/CBO9780511535901.003.
- March, D., L. Boehme, J. Tintoré, P. VélezâBelchi, and B. Godley (2019), Towards the integration of animalâborne instruments into global ocean observing systems, *Global Change Biology*, *26*, doi:10.1111/gcb.14902.
- Mason, E., and A. Pascual (2013), Multiscale variability in the balearic sea: An altimetric perspective, *Journal of Geophysical Research: Oceans*, *118*(6), 3007–3025, doi:10.1002/jgrc.20234.
- Monserrat, S., J. López-Jurado, and M. Marcos (2008), A mesoscale index to describe the regional circulation around the balearic islands, *Journal of Marine Systems*, *71*(3-4), 413–420.
- Palomares Losada, A. (2001), Análisis de las situaciones meteorológicas que afectan al estrecho de gibraltar y su influencia sobre el viento superficial.
- Pascual, A., J. Bouffard, S. Ruiz, B. Buongiorno Nardelli, E. Vidal-Vijande, R. Escudier, J. Sayol, and A. Orfila (2013), Recent improvements in mesoscale characterization of the western mediterranean sea: synergy between satellite altimetry and other observational approaches, *Scientia Marina*, *77*, 19–36, doi:10.3989/scimar.03740.15A.
- Pinot, J.-M., A. Álvarez, V. Fernández, and M. Riera (1999), The role of winter intermediate waters in the spring-summer circulation of the balearic sea: 2. a sensitivity numerical study, *Journal of Geophysical Research: Oceans*, *104*(C12), 29,865–29,884, doi:10.1029/1999JC900071.
- Pinot, J.-M., J. López-Jurado, and M. Riera (2002), The canales experiment (1996-1998). interannual, seasonal, and mesoscale variability of the circulation in the balearic channels, *Progress in Oceanography*, *55*(3), 335 – 370, doi:https://doi.org/10.1016/S0079-6611(02)00139-8.
- Poulain, P.-M., R. Gerin, E. Mauri, and R. Pennel (2009), Wind effects on drogued and undrogued drifters in the eastern mediterranean, *Journal of Atmospheric and Oceanic Technology - J ATMOS OCEAN TECHNOL*, *26*, doi:10.1175/2008JTECH0618.1.

- Poulain, P.-M., M. Menna, and E. Mauri (2012), Surface geostrophic circulation of the mediterranean sea derived from drifter and satellite altimeter data, *Journal of Physical Oceanography*, *42*(6), 973–990, doi:10.1175/JPO-D-11-0159.1.
- Pujol, M. I. (2013), *A 20-year reference period for SSALTO/DUACS products*, OSTST.
- Pujol, M.-I., Y. Faugère, G. Taburet, S. Dupuy, C. Pelloquin, M. Ablain, and N. Picot (2016), Duacs dt2014: the new multi-mission altimeter data set reprocessed over 20 years, *Ocean Science*, *12*(5), 1067–1090, doi: 10.5194/os-12-1067-2016.
- Renault, L., T. Oguz, A. Pascual, G. Vizoso, and J. Tintore (2012), Surface circulation in the alborán sea (western mediterranean) inferred from remotely sensed data, *Journal of Geophysical Research: Oceans*, *117*(C8), doi: 10.1029/2011JC007659.
- Ribic, C. A., R. Davis, N. Hess, and D. Peake (1997), Distribution of seabirds in the northern Gulf of Mexico in relation to mesoscale features: initial observations, *ICES Journal of Marine Science*, *54*(4), 545–551, doi: 10.1006/jmsc.1997.0251.
- Rio, M.-H., A. Pascual, P.-M. Poulain, M. Menna, B. Barceló-Llull, and J. Tintoré (2014), Computation of a new mean dynamic topography for the mediterranean sea from model outputs, altimeter measurements and oceanographic in situ data, *Ocean Science (OS)*, *10*, doi:10.5194/os-10-731-2014.
- Ruffino, L., K. Bourgeois, E. Vidal, J. Icard, F. Torre, and J. Legrand (2008), Introduced predators and cavity-nesting seabirds: unexpected low level of interaction at breeding sites, *Canadian Journal of Zoology*, *86*(9), 1068–1073, doi:10.1139/Z08-070.
- Ruiz, S., A. Pascual, B. Garau, F. Yannice, A. Alvarez, and J. Tintoré (2009), Mesoscale dynamics of the balearic front, integrating glider, ship and satellite data, *Journal of Marine Systems*, *78*, doi: 10.1016/j.jmarsys.2009.01.007.
- Sánchez-Román, A., L. Gómez-Navarro, R. Fablet, D. Oro, E. Mason, J. M. Arcos, S. Ruiz, and A. Pascual (2019), Rafting behaviour of seabirds as a proxy to describe surface ocean currents in the balearic sea, *Scientific Reports*, *9*(1), 17,775, doi:10.1038/s41598-018-36819-w.
- Taburet, G., A. Sanchez-Roman, M. Ballarotta, I. Pujol, J.-F. Legeais, F. Fournier, F. Yannice, and D. Gerald (2019), Duacs dt-2018: 25 years of reprocessed sea level altimeter products, *Ocean Science Discussions*, pp. 1–30, doi:10.5194/os-2018-150.
- Testor, P., U. Send, J.-C. Gascard, C. Millot, I. Taupier-Letage, and K. Béranger (2005), The mean circulation of the southwestern mediterranean sea: Algerian gyres, *Journal of Geophysical Research: Oceans*, *110*(C11), doi:10.1029/2004JC002861.
- Tew Kai, E., V. Rossi, J. Sudre, H. Weimerskirch, C. Lopez, E. Hernandez-Garcia, F. Marsac, and V. Garçon (2009), Top marine predators track lagrangian coherent structures, *Proceedings of the National Academy of Sciences*, p. pnas.0811034106, doi:10.1073/pnas.0811034106.
- Troupin, C., A. Pascual, G. Valladeau, I. Pujol, A. Lana, E. Heslop, S. Ruiz, M. Torner, N. Picot, and J. Tintoré (2015), Illustration of the emerging capabilities of saral/altika in the coastal zone using a multi-platform approach, *Advances in Space Research*, *55*(1), 51–59.
- Yoda, K., K. Shiomi, and K. Sato (2014), Foraging spots of streaked shearwaters in relation to ocean surface currents as identified using their drift movements, *Progress in Oceanography*, *122*, 54 – 64, doi: https://doi.org/10.1016/j.pocean.2013.12.002.
- Zavatorielli, M., and G. L. Mellor (1995), A numerical study of the mediterranean sea circulation, *Journal of Physical Oceanography*, *25*(6), 1384–1414, doi:10.1175/1520-0485(1995)025<1384:ANSOTM>2.0.CO;2.
- Zecchetto, S., and F. De Biasio (2007), Sea surface winds over the mediterranean basin from satellite data (2000–04): Meso and local-scale features on annual and seasonal time scales, *Journal of Applied Meteorology and Climatology - J APPL METEOROL CLIMATOL*, *46*, 814–827, doi:10.1175/JAM2498.1.